Particle Simulation of Lower Hybrid Heating in Magnetized Plasmas

by

KANADE VASUPRAD VIJAY

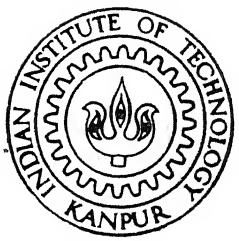

NUCLEAR ENGINEERING AND TECHNOLOGY PROGRAM

INDIAN INSTITUTE OF TECHNOLOGY KANPUR

MARCH, 1997

Particle Simulation of Lower Hybrid Heating in Magnetized Plasmas

A thesis Submitted
in Partial Fulfillment of the Requirements
for the Degree of

Master of Technology

by

KANADE VASUPRAD VIJAY

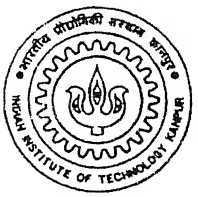

to the

NUCLEAR EENGINEERING AND TECHNOLOGY PROGRAM
INDIAN INSTITUTE OF TECHNOLOGY, KANPUR

March, 1997

ETP-1997-M-VIJ-PAR

Certificate

This is to certify that the work contained in the thesis entitled Particle Simulation of Lower Hybrid Heating in Magnetized Plasmas by KANADE VASUPRAD VIJAY has been carried out under my supervision and that this work has not been submitted elsewhere for a degree.

MSKalra

Dr. M. S. Kalra
Professor,
Nuclear Engineering & Technology Program
and, Department of Mechanical Engineering,
Indian Institute of Technology Kanpur.
March, 1997.

Abstract

A particle simulation study of the propagation and absorption of electromagnetic waves and the associated plasma heating is presented. A plasma slab with nonuniform density profile, with positive gradient of density along the x -axis, is modeled with a two and one-half dimensional electrostatic particle simulation code. A finite length electrostatic single wave exciter is considered. The exciter frequency is chosen to be higher than but close to the lower hybrid frequency. Deceleration of the incident electromagnetic wave along the magnetic field is necessary for its propagation. As the wave penetrates the plasma slab, its phase velocity reduces and at certain plasma density it transforms into a plasma wave. The conditions of this transformation, which have been derived theoretically using the hydrodynamic and the geometric optics approximation are demonstrated computationally. The absorption of the waves by both ions and electrons is observed. Surface electron heating is also apparent in the simulations presented. Small sheaths are found near the exciter. As predicted by the cold plasma theory, the resonance cones are observed in the phase-space plots.

Dedicated to everlasting memories of
Dhananjay and Shree

Acknowledgement

With profound sense of gratitude, I take this opportunity to thank Dr. M. S. Kalra for introducing me to the Particle Simulation method and giving me the oppourtunity to work in the area of Plasma Physics and Fusion Technology. It was his kind concern, constant encouragement and invaluable guidence which led to the sucessful completion of this work.

I also want to take this opportunity to thank Dr. V. Eswaran whose guidence during the course on Numerical Fluid Flow Analysis had been the basic foundation of my work.

Working as a Chairman of the Cultural Committee gave me some of the best experiences in my life. During my tenure I recived constant help and appreciation from the Wardens as well as the DOSA. In this regard I am really greatfull to Dr. N. S. Gajbhiye, Warden In-charge, the Committee Of Wardens (COW), and Dr. Kripashankar (Dean Of Students Affairs). I also want to express my sincere thanks to the Hall-office staff. It was because of their help I was able to organize and conduct large functions and programs. Taking this as a opportunity I thank the NET staff who always took care of all my departmental formalities and left me free to think about my work.

Happy memories of the time I spent with my music group will reside in my mind forever. I dont have words to express my feelings. They not only shared

music with me but also extended their Love and affection towards me. Being far from home I never felt of being away from the dear ones. Specially to mention Mr. Girish Gupte, Dr. & Mrs. Govind Sharma, Dr. & Mrs. Bishwas, Dr. & Mrs. Karnic, Mr. & Mrs. Marathe and Dr. Prabhu.

Finally I would like to thank all my friends at Hall IV, Ghat Mandal, the junior NET gang and ofcourse UGs who made my stay here at I.I.T. Kanpur, comfortable and enjoyable.

This institute gave me the opportunity to work in such a advanced field, contribute a little to science; I learned here new ragas, I was exposed to different kind of people, and many more. It really pinches my heart a lot to leave from here.

March, 1997

Kanade Vasuprad Vijay

Contents

Abstract i

Acknowledgements ii

Contents iv

List of Figures viii

Nomenclature xii

1 Introduction 1

1.1 Role of Numerical Simulation in Understanding the Physics of Fusion Plasmas 2

1.2 Radio Frequency Wave Heating of Fusion Plasma 4

1.2.1 The Lower Hybrid Frequency Range 5

1.2.2 The Lower Hybrid Resonance 7

1.3 Theories of Lower Hybrid Heating 10

1.3.1 Collisional Heating 10

1.3.2 Collisionless Absorption 10

1.3.3 Nonlinear Processes 10

1.4 State of the Art 12

1.5 Outline of the Work 15

2 Linear Theory of Lower Hybrid Waves in Maxwellian Plasma 17

2.1 Introduction 17

2.2 Wave Propagation in Cold Plasma 19

2.2.1 Electrostatic Approximation [*Bonoli*,(1983)] 19

2.2.2 Electromagnetic Case [*Bonoli*,(1983)] 23

2.3 Thermal Corrrection to 'Cold' Plasma Dispersion Relation . . . 26

2.3.1 Electron Vlasov Analysis [*Bonoli*,(1983)] 27

2.3.2 Ion Vlasov Analysis [*Bonoli*,(1983)] 31

2.4 Plasma Heating Via Mode Conversion 33

2.5 Summary 36

3 Overview of the Algorithm and Structure of the Program 39

3.1 Introduction 39

3.2 Validity of The Algorithm 40

3.3 Overview of the Program 42

3.4 Particle Weighting 43

3.4.1 The Particle-In-Cell Method 43

3.5 Integration of Field Equations 46

3.6 Integration of Equations of Motion 47

3.7 Initial Particle Loading 52

3.7.1 Position Loading 53

3.7.2 Velocity Loading 53

3.8 Organization of the Program 55

3.9 About the Program 58

4 Discussion of Results **59**

4.1 Computer Model 59

4.2 Organization of the Results 61

4.3 Simulation Results 61

4.3.1 Set I 62

4.3.2 Set II 63

4.3.3 Set III 63

4.3.4 Set IV 64

4.3.5 Set V 64

5 Conclusions **81**

A Algorithms Used in the Code to Solve the Poisson's Equations 83

A.1 Thomas Algorithm 84

A.2 Gauss-Seidel Iterative Technique 85

Bibliography 88

List of Figures

1.1 The dispersion curves (n_x^2 vs. ω) near the plasma resonance. . . 9

2.1 Cartesian geometry for slab analysis of wave propagation 20

2.2 Dependence of n^2 on x-coordinate in case of transformation of the wave into a plasma wave 34

2.3 Dependence of n^2 on x-coordinate in absence of transformation into a plasma wave 34

3.1 A typical time cycle run. 42

3.2 (a) Bi-linear weighting for 2D, and (b) linear weighting for 1D according to PIC scheme 44

3.3 The two and one-half dimensional simulation model for the lower hybrid heating in linear regime 49

3.4 Normalized thermal velocity distribution 54

3.5 A schematic diagram showing a typical run. 57

4.1 Time evolution of the electron parallel kinetic energy ($W_{\|}^{e}$) for $m_i/m_e = 10.0$. 66

4.2 Time evolution of the ion perpendicular kinetic energy ($W_{\perp}^{i}$) for $m_i/m_e = 10.0$. 66

4.3 Time evolution of the electron parallel kinetic energy ($W_{\|}^{e}$) for $m_i/m_e = 100.0$. 67

4.4 Time evolution of the ion perpendicular kinetic energy ($W_{\perp}^{i}$) for $m_i/m_e = 100.0$. 67

4.5 Time evolution of the electron parallel kinetic energy ($W_{\|}^{e}$) for $\omega_0/\omega_g = 1.0$. 68

4.6 Time evolution of the ion perpendicular kinetic energy ($W_{\perp}^{i}$) for $\omega_0/\omega_g = 1.0$. 68

4.7 Time evolution of the electron parallel kinetic energy ($W_{\|}^{e}$) for $\omega_0/\omega_g = 2.0$. 69

4.8 Time evolution of the ion perpendicular kinetic energy ($W_{\perp}^{i}$) for $\omega_0/\omega_g = 2.0$. 69

4.9 Time evolution of the electron parallel kinetic energy ($W_{\|}^{e}$) for $T_e/T_i = 16.0$. 70

4.10 Time evolution of the ion perpendicular kinetic energy ($W_{\perp}^{i}$) for $T_e/T_i = 10$. 70

4.11 Time evolution of the electron parallel kinetic energy ($W_{\|}^{e}$) for $T_e/T_i = 100.0$. 71

4.12 Time evolution of the ion perpendicular kinetic energy ($W_{\perp}^{i}$) for $T_e/T_i = 100.0$. 71

4.13 Time evolution of the electron parallel kinetic energy for a small external static magnetic field. 72

4.14 Time evolution of the ion perpendicular kinetic energy for a small external static magnetic field. 72

4.15 Spatial dependence of ion kinetic energy perpendicular to magnetic field at $\Pi_e t = 400$ 73

4.16 Spatial dependence of ion kinetic energy perpendicular to magnetic field at $\Pi_e t = 600$ 73

4.17 Spatial dependence of ion kinetic energy perpendicular to magnetic field at $\Pi_e t = 1000$ 74

4.18 Spatial dependence of electron kinetic energy parallel to magnetic field at $\Pi_e t = 400$ 74

4.19 Spatial dependence of ion kinetic energy perpendicular to magnetic field at $\Pi_e t = 600$ 75

4.20 Spatial dependence of electron kinetic energy parallel to magnetic field at $\Pi_e t = 1000$ 75

4.21 Phase-space plots (isometric projection) for parallel velocity component of electrons at $t\Pi_e = 400$ 76

4.22 Phase-space plots (orthographic projecion) for parallel velocity component of electrons at $t\Pi_e = 400$ 76

4.23 Phase-space plots (isometric projection) for parallel velocity component of electrons at $t\Pi_e = 400$ 77

4.24 Phase-space plots (orthographic projecion) for parallel velocity component of electrons at $t\Pi_e = 400$ 77

4.25 Phase-space plots (isometric projecion) for perpendicular velocity component of ions at $t\Pi_e = 400$ 78

4.26 Phase-space plots (orthographic projecion) for perpendicular velocity component of ions at $t\Pi_e = 400$ 78

4.27 Phase-space plots (isometric projecion) for perpendicular velocity component of ions at $t\Pi_e = 400$ 79

4.28 Phase-space plots (orthographic projecion) for perpendicular velocity component of ions at $t\Pi_e = 400$ 79

4.29 $Y - V_y$ phase-space plot for perpendicular velocity component of ions at $t\Pi_e = 600$ 80

Nomenclature

A list of symbols is given below. Some symbols which are specific to a section and whose meaning may be different in different sections are not included. Standard mathematical symbols also do not appear in this list.

Symbol	Description
Operation	
$\frac{\partial}{\partial \mathbf{k}}$	Vector derivative
Latin Alphabet	
$\mathbf{B}_o$	External static magnetic field
c	Velocity of light
$\mathbf{D}$	Displacement vector
$\mathbf{E}$	Electric field strength
$f_{k_o}(v)$	Zeroth order velocity distribution for particle of type k
$F_j(v_j)$	Reduced velocity distribution
$H\left(\frac{\omega}{k}, k\right)$	Dispersion function
$\mathbf{J}$	Current density
$\mathbf{k}$	Wave propagation vector
$\mathbf{K}$	Dielectric tensor

m_k	Mass of particle of type k
n	Refractive index, $\mid \mathbf{n} \mid$
n_k	Density of particle of type 'k'
n_0	Initial density
q	charge of a species
$\mathbf{r}$	Position vector
$S(\eta)$	Shape factor
t	Time
T_k	Temperature of particles of type k
$\mathbf{v}$	Macroscopic particle velocity
v_g	Group velocity
v_ϕ	Phase velocity
v_{thk}	Thermal velocity for particle of type k
W_o	Average value of energy density in wave motion
$\hat{\mathbf{x}}, \hat{\mathbf{y}}, \hat{\mathbf{z}}$	Unit vectors
Z_k	Charge number for particles of type k

Greek Alphabet

$\delta\phi$	A perturbation in quantity ϕ
δ_k	damping length for k^{th} species.
ϵ or ϵ_k	Sign of charge for particles of type k
$\epsilon_\perp$, ϵ_{xy}, $\epsilon_\parallel$	Dilectric tensor components
ζ	k_x/k_z
κ	Boltzmann's constant
θ	Angle betweenthe direction of static magnetic field and z-axis, in xz plane
λ	wavelength of incident electromagnetic radiation
λ_{D_k}	Debye shielding distance for particle of type k
ν	Collision frequency
Π_o	Plasma frequency
Π_k	Plasma frequency for particles of type k
ρ	Charge density

ρ_L	Larmor radius
τ	Nondimensional time
ϕ	Plasma potential
ω_0	Angular frequency of incident radiation
Ω_k	Cyclotron frequency for particles of type k
ω_{LH}	Frequency for lower hybrid resonance
ω_{UH}	Frequency for upper hybrid resonance
χ_k	Succeptability of particle of type k

Subscripts

i	Ion
e	Electron
$\perp$	Perpendicular to external static magnetic field
$\parallel$	Parallel to external static magnetic field
$k,\ \alpha$	Particle type, either ion or electron

Accents

$\hat{}$	Unit vector
$\tilde{}$	Averaged value

Chapter 1

Introduction

The failure of fission to provide an environmentally clean energy source has motivated considerable interest towards nuclear fusion. The available information suggests that fusion energy can be a practically inexhaustible and cheap source of energy. After a long research that took place in various organizations worldwide, it was concluded that the nuclei of light elements can be fused efficiently if the plasma of such elements is confined in a magnetic chamber and heated to its ignition temperature. Considerable amount of effort has been directed in the research of the magnetic confinement devices and the heating of plasma in such devices. Although the physics of plasmas was known well before the study of fusion reactions began, a different approach was required to attack the problems encountered in the development of fusion reactors. This lead to the evolution of a new branch of physics the *Physics of Fusion Plasmas.*

1.1 Role of Numerical Simulation in Understanding the Physics of Fusion Plasmas

At present plasma physics widely employs the numerical simulation techniques, particularly in the area of *Heating*. Plasma physics is based on sound mathematical foundation. The equations describing the dynamics of the plasma were known before the fusion research began. However, fusion applications of a plasmas require an analytic investigation of a *mixed* system, combining the equations of hydrodynamics, the kinetic equations, the Maxwell's equations, and other auxiliary equations. The solutions of such a complex system can be approached analytically provided these equations are simplified to a large extent. On the other hand, the modern level of computers and achievements in numerical methods make it possible to analyze the given problem more realistically, considering the structural features of the experimental device, the complex geometry of the magnetic field etc. Computers can be used to carry out the detailed quantitative analysis of a process in order to estimate the role of specific factors, reveal new properties and regularities, and consider complex cooperative phenomena.

The numerical methods are very important in comparing the theoretical and experimental results. A quantitative relation between them is difficult to establish, as many quantities appearing in the theoretical model/results may not be observed or measured directly. The following lines are quoted by Dnestrovskii [*Dnestrovskii and Kostomarov*(1982)],

The theory and experiment use different languages and need an interpreter *to communicate: this role is played by computers.*

Another role played by the computer simulation in fusion research is to make *predictions*. If a model has a reliable theoretical basis and is successfully tested

in practice, the accuracy of the predictions can be very high. Such predictions then become very important in planning the experiments.

The complex nature of the problems that are encountered in the study of fusion plasmas has motivated large amount of interest in computer simulation, which has played an essential role in the development of the theory of fusion plasma. Computer simulation of plasmas comprises two general areas, based on either the *kinetic description* or the *fluid description* Fluid simulation is done by numerically solving the magnetohydrodynamic (MHD) equations of plasmas assuming approximate transport coefficients,while the kinetic simulation considers a more detailed model involving the particle interactions through electromagnetic fields. This is achieved either by solving numerically the plasma kinetic equations as the Vlasov or Fokker-Plank equations, or by the newly developed *Particle Simulation* technique, which simply computes the motion of a collection of charged particles, interacting with each other and with the externally applied fields.

MHD simulations have generally been applied to large-scale problems directly related to the behavior of the experimental devices, whereas, the kinetic simulations are particularly successful in dealing with the basic problems related to fusion physics in which the particle distributions deviate significantly from a local Maxwellian distribution, such as in the wave-particle resonance, trapping, stochastic heating, etc. The *Hybrid Codes* developed recently have been the bridge between the above two algorithms referred above.In the hybrid codes either the fluid or the particle treatment is applied to different components of a plasma.

1.2 Radio Frequency Wave Heating of Fusion Plasma

Radio frequency wave heating has been proved to be very attractive method for bringing the plasma to its ignition temperature in a magnetic fusion device from both the physics and the technological stand-points. In a hot magnetised plasma there exists a wide range of energy absorbing mechanisms for an electromagnetic wave offered by the plasma dielectric properties. Each mechanism is characterized by a perticular range of frequencies of the incident electromagetic wave. Depending upon these frequencies, several schemes have been proposed to heat the plasma. Each RF heating scheme selectively couples energy to a particular species of charged particles (ions or electrons) with a desired spatial deposition profile, to certain velocity distribution (Maxwellian or non-Maxwellian), and in either the perpendicular or the parallel degree of freedom relative to the state magnetic field.

Besides plasma heating, RF waves offer many other advantages which become potentially important considerations in a magnetic fusion device, such as assisting initial discharge breakdown, driving a plasma current, controlling the temperature or current profiles, decreasing unwanted impurities, etc. To date there are three major accepted frequency ranges where plasma wave interaction is found to be strong. The Ion-Cyclotron Range of Frequencies(ICRF[1]), the Lower Hybrid Range of Frequencies(LHRF) and the Electron Cyclotron Range of Frequencies (ECRF) . Both the ICRF and LHRF are below 10GHz, so generators as well as the transmission systems for such high powerm system are available commercially. The ECRF range for future magnetic fusion devices, however, is between 100-200GHz, where high powered sources are still to be developed.

[1]here RF refers Range of Frequencies

The main advantages of using a RF system in a reactor environment is that the wave launchers are thermally shielded from the plasma and the RF sources can be placed well behind the radiation shields to avoid direct neutron streaming. This makes maintaining and operating of high power systems very convenient. Furthermore, since very efficient RF generators, transmission systems and wave couplers exists over most of the RF range, the need for technological development in this area is minimized. For RF heating schemes, generators, transmission and coupling systems fall in the area of technological studies, while the problem of wave absorption is an area of study in fusion physics.

In the LHRF scheme, high power *klystrons* are available [*Hawang*,(1991)] with ~50 kW per tube CW and 200 kW per tube pulsed with typical efficiency of about 50-60%. Still higher power, if required (~1 MW) in this frequency range, can be supplied by *gyrocon* which has a very high efficiency (~ 95 %) but much lower gain ($\leq$ 13 dB), so more amplifier stages will be required. Recent gyrocon developments have extended the frequency range to 100-200 MHz range which is also applicable to higher harmonics of ion cyclotron heating.

1.2.1 The Lower Hybrid Frequency Range

In connection with the problem of controlled thermonuclear reactions, RF plasma heating has been studied extensively. One frequency range which has received a great deal of attention in last two decades is the *lower hybrid frequency range of frequencies or LHRF* . The original proposal for the use of this method was by Parker. The frequency range has been particularly attractive because of following facts:

- Possibility of plasma heating in large thermonuclear devices. Since fusion reaction occurs, almost exclusively, among the highest energy ions, it is beneficial to have a scheme by which one can produce energetic ions

effectively. Ions are involved in wave motion of lower hybrid frequency range(as they are massive and lower hybrid resonance is low frequency phenomena) and therefore can be heated directly and much more effectively than would be the case if higher frequency heating scheme is used.

- Availability of efficient heating power [*Stix*(1965)]. Typical lower hybrid frequencies for fusion plasma are of the order of a few GHz, which is the highest frequency below which large amounts of power ($\geq$ 1MW) are available. On contrary, heating at electron cyclotron frequency, which is of the order of 100 GHz, limits one to presently available power of only a few kW. Since the heating power required for a tokamak type fusion reactors will be of the order of 10^9 W, this is a very important point to be taken into consideration.

- Lower hybrid waves can be made to heat deep within the plasma as the resonance is density and field dependent.

In last decade much interest has been paid, theoretically, experimentally and computationally, to the heating of plasma in d.c. magnetic field at or near the lower hybrid resonance [*Bekefi*(1966)]. It is hoped that sufficient coupling of large amounts of RF power to plasma will yield significant increase in plasma temperature. In addition, the relatively low frequency of the lower hybrid resonance permits large power levels at lower costs.

Several theoretical models have been proposed to explain the heating process at lower hybrid resonance. They are :

1. Collisional heating, [*Bekefi*(1966)]

2. Collisionless absorption [*Glagolev*(1972a)] and/or linear mode conversion [*Stix*(1965)],

3. Nonlinear interactions, especially excitation of parametric modes [*Kindel et al.(1972)*]

These theories will be discussed in brief to highlight the idea of the problem, but before we proceed, a brief discussion of the lower hybrid resonance is presented.

1.2.2 The Lower Hybrid Resonance

By definition, *a lower hybrid resonance is the resonance of the extraordinary wave in cold plasma with the ion-cyclotron frequency.* In cold plasma approximation, the dispersion relation for waves of frequencies above but near the lower hybrid frequency has the form [*Bekefi*(1966)]:

$$\beta n_x^4 - \gamma n_x^2 + \delta = 0.$$

The branch ,

$$n_x^2 = \frac{\gamma + (\gamma^2 - 4\beta\delta)^{\frac{1}{4}}}{2\beta},$$

will be of interest to us, as the choice yields $n_x^2 \approx \lambda/\beta$ as $\beta \to 0$; where

$$\beta = \epsilon_\perp,$$

and

$$\lambda = RL + \epsilon_{\|}\epsilon_\perp,$$

where $\epsilon_\perp$, ϵ_{xy} and $\epsilon_{\|}$ are the elements of the cold plasma dielectric tensor (discussed later), and are defined as

$$\begin{aligned}
\epsilon_{\perp} &\equiv \frac{1}{2}(R+L), \\
\epsilon_{xy} &\equiv \frac{1}{2}(R-L), \\
\epsilon_{\parallel} &\equiv 1-\sum_k \frac{\Pi_k^2}{\omega^2},
\end{aligned}$$

where

$$\begin{aligned}
R &\equiv 1-\sum_k \frac{\Pi_k^2}{\omega^2}\left(\frac{\omega}{\omega+\epsilon_k\Omega_k}\right), \\
L &\equiv 1-\sum_k \frac{\Pi_k^2}{\omega^2}\left(\frac{\omega}{\omega-\epsilon_k\Omega_k}\right), \\
\Pi_k^2 &\equiv \frac{4\pi n_k Z_k^2 e^2}{m_k}.
\end{aligned}$$

The solution of $\epsilon_{\perp}=0$ gives

$$\Pi_o^2 = \frac{(\omega^2-\Omega_e^2)(\omega^2-\Omega_i^2)}{\omega^2-\Omega_i^2\Omega_e^2},$$

where Π_o is the net plasma frequency $(\Pi_e^2+\Pi_i^2)^{1/2}$. The lowest value of ω that satisfies the above equation for fixed values of Ω_e, Ω_i and Π_o is the lower hybrid resonance frequency ω_{LH}. In the above case the propagation angle is nearly $\pi/2$. Fig. 1.1 shows a schematic dispersion curve n_x^2 as a function of ω (n_x is the refractive index) for cold plasma near the resonance. As the frequency approaches near the resonant frequency , the refractive index of the plasma increases sharply and, consequently, plasma can be heated near this region, since the phase velocity approaches the velocity of the particles.

As seen from Fig. 1.1, the resonance frequency decreases with increasing plasma density. As shown by Stix [*Stix*(1965)], the wave must be slowed down along

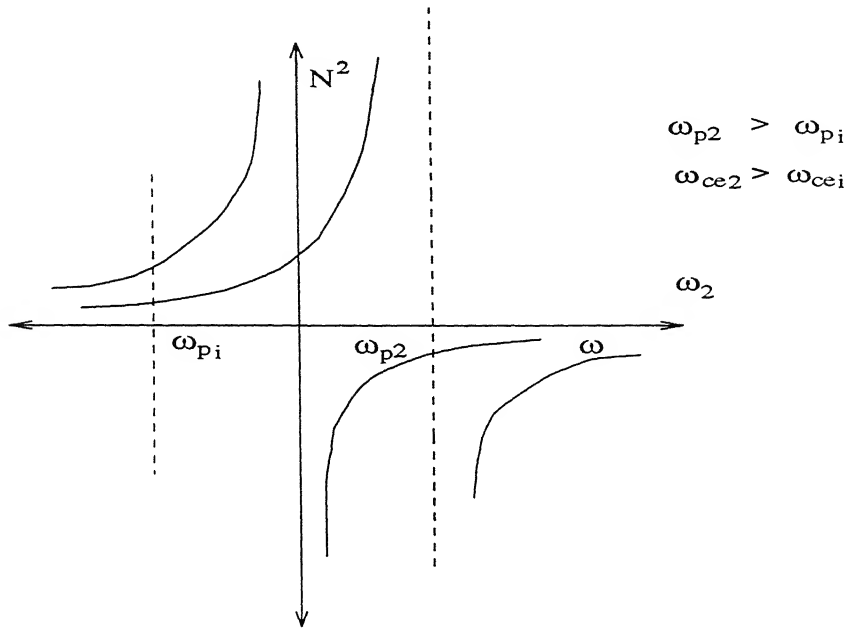

Figure 1.1: *The dispersion curves*[2] *(n_x^2 vs. ω) near the plasma resonance. ω_p and ω_{p2} are the resonance points for cold plasma.*

the magnetic field to ensure that n_x^2 increases with increase in density in a uniform magnetic field. Stix also showed that for a sufficiently strong deceleration, the electromagnetic wave in the plasma layer transforms into a plasma wave whose longitudinal electric field (with respect to the wave vector) wave vector is considerably stronger than its transverse field. Since the refractive index of the wave increases with increasing density in the plasma layer, the analysis of the wave propagation can be divided into :

1. The analysis of the 'Cold' plasma region where the refractive index is not very large, so that the influence of the thermal motion on the wave propagation can be neglected;

2. The analysis in the 'Hot' plasma region, where effects of the transformation and absorption are important.

[2]Fig. 1.1 derived from [*Glagolev*(1972a)].

In following section, various theories of lower hybrid heating are discussed in briefly in order to heighlight the idea behind this work.

1.3 Theories of Lower Hybrid Heating

1.3.1 Collisional Heating

Proposed by Bekefi [*Stix*(1965)] collisions provide the mechanisms for dissipation of the RF energy. The propagation vector obtained in the solution of the cold plasma dispersion relation will be complex. The best absorption should be at the hybrid layer, since the imaginary part of k is largest there. This provides the shortest damping length, which is inversely proportional to the collisional frequency.

1.3.2 Collisionless Absorption

This mechanism was proposed by Stix [*Stix*(1965)]. The incident electromagnetic wave may penetrate directly or excite other modes at the same frequency. The wave is then Landau or cyclotron damped, whenever its phase velocity is proportional to the particle thermal velocities, which permits the transfer of the wave energy from the wave to the particles. In order to study the collisionless absorption process, it is necessary to consider the dispersion relation for plasma waves in a 'hot' plasma in a magnetic field in the electrostatic approximation. [*Chu and Lee*(1971), *Stix*(1965)].

1.3.3 Nonlinear Processes

Nonlinear heating processes can occur if the amplitude of the electric fields inside the plasma become large enough. The dominant driving mechanism in

this interaction is the relative $\mathbf{E} \times \mathbf{B}$ drift motion of the electrons and the ions. This drift mechanism can trigger two kinds of processes which leads to growing waves in a plasma. They are :

parametric instabilities [*Bekefi*(1966)] which can occur when the driving frequency is very close to the lower hybrid resonance. In this case the ion acoustic waves with a difference between the driving frequency and the lower hybrid frequency can be excited;

streaming instabilities [*Ott and McBride*(1972)] whose frequencies are either close to upper hybrid frequency ω_{UH}, defined as

$$\omega_{UH} = \left[\Omega_e^2 + \Pi_e^2\right]^{1/2}$$

or close to lower hybrid frequency.

The parametric instability of interest here appears at the lower hybrid resonance with ion acoustic waves excited [*Hook and Bernabai*(1971)]. The threshold RF drift velocity for parametric excitation, which relates the $\mathbf{E} \times \mathbf{B}$ drift velocity, $v_d = E_{RF}/B_o$, to the thermal velocity is given by Kindel [*Kindel et.al*(1972)]. As discussed by Ott and McBride [*Ott and McBride*(1972)], plasma heating may primarily be caused by the "breaking" of the growing ion-acoustic waves until the electron temperature is raised such that the threshold condition is no longer satisfied. Ion and electron heating was observed by Kindel [*Kindel et al.*(1972)] in his computer simulation. It was found that the relative heating of ions and electron was dependent upon the magnitude of the component of the propagation vector along the d.c. magnetic field. For $k_{\|}/k > (m_e/m_i)^{1/2}$ the electrons are heated while the ions remain cold. For $k_{\|}/k \sim (m_e/m_i)^{1/2}$ the ions and electrons both interact with field and are heated simultaneously.

1.4 State of the Art

Computer simulation has proved to be a useful tool in understanding some details of the physics related to the overall plasma heating scheme, especially those aspects that are difficult to treat analytically. However, to do this economically with the present day computers one must idealize the geometry and reduce the scale lengths to manageable proportions. Since simulation of a confinement device is difficult only a basic study has been s presented so far which provided a restricted, but detailed view of the problem. The computer models presented until now far were used to calculate the self-consistent particle trajectories of electrons and ions in a magnetized or unmagnetized slab geometry to provide a complete picture of the dynamics of these plasma components over a short time scale. The purpose was to identify the various factors that may also be present in real fusion reactors, and there by suggest the problem areas which need further theoretical study. A brief historical overview of what has been accomplished with the particle simulation code in RF heating and current drive applications has been given in the published work of V. K. Decyk [*Decyk*(1986)]. Some parts of this publication which are relevant for present work are given below for the purpose of quick reference.

The very first particle simulation specifically for RF heating was by Kindel, Okuda and Dawson [*Kindel et al.*(1972)]. The geometry was one dimensional and an electrostatic algorithm was used. The purpose was to demonstrate by theory and by computer simulation that an electric field perpendicular to the d.c. magnetic field and oscillating at frequency just above the lower hybrid frequency can excite, at extremely low threshold, decay and purely growing parametric instabilities which resulted in short wavelength lower hybrid waves and ion waves leading to substantial plasma heating. The $\mathbf{E}\times\mathbf{B}$ drift was neglected and ions were unmagnetised. This work was later extended to 2D [*Chu et al.*(1976)]. Subsequent computer models for lower hybrid heating have

all been electrostatic, with $2\frac{1}{2}$ dimensions, bounded in one spatial direction and periodic in another. The magnetic field direction was chosen so that $\mathbf{E}\times\mathbf{B}$ drifts are in ignore able proportions, which means that most of the parametric decay processes cannot occur.

Later models used antennas to excite the lower hybrid waves. The early simulation with antenna was by Decyk, Morales and Dawson [*Decyk et al.*(1979)]. The main motive of the work was to understand how to excite lower hybrid waves in bounded homogeneous computer models. Vacuum boundary conditions were used with a specified external surface charge oscillating on one boundary. In the early 80's the interest was diverted to study the ion heating. Using the same model Abe and coworkers applied an external charge density, specified as an arbitrary function of the periodic coordinates, oscillating in front of one of the conducting walls. Plasma was bounded by conducting planes. The plasma density profile was inhomogeneous. The major result of the simulation was he observation of the ion-cyclotron damping [*Abe et al.*(1980)], due to the fact that ω_o/Ω_i was rather small (3 or 5), which resulted in high energy tail in the ion distribution. The same model but with inversion symmetry in one of the bounded direction was used by [*Matsuda et al.*(1980)].

Later simulations concentrated on the energy absorption mechanism by ions. Karney [*Karney*(1978), *Karney*(1979)] described that stochastic ion heating to be the mechanism of ion-absorption which was justified by the examination of test particle trajectories for $\omega_o/\Omega_i > 8$. In order to be able to launch many waves whose phase velocities along the magnetic field are large, Nakajima, Abe et. al. [*Nakajima et al.*(1982)] modified the model to use different scale lengths in parallel and perpendicular directions. In order to avoid numerical instability a finer grid spacing and a higher order interpolation scheme in the parallel direction was used specially. Inhomogeneous density and temperature profiles were used. They also concluded that stochastic absorption is the major mechanism for ino-heating.

In the mid 80's the interest in the RF simulations changed from ion-heating to current drives. A number of simulations were performed in this area in late 80's and early 90's. As our interest lies only in the heating of plasma without the current drive term we will not be going into the details of the current drive.

Until now almost all the models were based on the electrostatic/electromagnetic particle simulation algorithm in 1, $1\frac{1}{2}$, 2 or $2\frac{1}{2}$ dimensions. These algorithms are discussed in detail in a number of published works and books [*Decyk et. al.*(1979)] Almost all models used the vacuum boundary conditions (i.e. there is no charge outside the geometry). In most of the models the $\mathbf{E}\times\mathbf{B}$ drifts were neglected to isolate the propagation of the lower hybrid waves and to study plasma heating without the complications of parametric effects driven by the $\mathbf{E}\times\mathbf{B}$ drifts and scattering by the drift waves [*Decyk et al.*(1980)]. The most recent models included the $\mathbf{E}\times\mathbf{B}$ and the diamagnetic drifts by tilting the axis of magnetic field in the xz plane [*Chu et al.*(1976)]. All of these models were applied to study the parametric heating of plasma by a large amplitude pump with frequencies near the lower hybrid and to investigate the effect of the parametric instability on the cross-field transport properties of plasma.

All these models were based on the *Cold Plasma Approximation*. The effects of finite electron temperature (T_e) and ion temperature (T_i) were taken into consideration by adding the thermal correction term to the electrostatic, cold plasma dispersion relation, which was derived using the Vlasov theory(discussed in chap.2). A considerable simplification was made in the ion Vlasov analysis while deriving the dispersion relation by neglecting the magnetic field (i.e., treating ions as essentially unmagnetised, $\nabla_1 \times \mathbf{B} = 0$). This is justified in the light of the fact that $(k_\perp \rho_i)^{1/2} \gg 1$ in the core plasma region. Where $\rho_i = v_{thi}/\Omega_i$ is the ion Larmor radius. In this case the ion gyro orbits are practically straight lines as compared to the wavelength λ_i. Thus the scope of these models was limited in the sense that the region of propagation in which the 'old' plasma and hydrodynamic approximations are valid becomes smaller

as the ion and electron temperature and plasma density increases. The violation of the cold plasma and fluid approximation starts near the 'cold' plasma resonance.

By using the hydrodynamic approximation it is shown that if the magnetic field exceeds a critical value, which is given approximately by the condition $(m_e/m_i)\Omega_e^2 > \omega^2$, the electromagnetic wave should completely transform into plasma wave at some *critical density* in the plasma layer. After being reflected from the transformation point, the plasma wave exhibits a stronger deceleration as the plasma density decreases. As soon as the phase velocity of the waves approaches the ion thermal velocity, Cherenkov absorption of the waves should occur. This effect should result in heating the ion component of plasma. In this case the hydrodynamic approximation is not valid in calculating either the ion or the electron absorption. This arises from the absorption between the phase velocity of the wave along the magnetic field and the thermal velocity of the electrons. When the phase velocity of the waves is close to thermal velocity of the particles, their thermal motion should considerably affect the propagation of waves in plasma. In all the models discussed above the phase velocities were less than almost three times the electron thermal velocity ($v_{the} = \sqrt{\kappa T_e/m_e}$).

1.5 Outline of the Work

Chapter 2 The linear theory of lower hybrid waves is briefly reviewed. The dispersion relation with *cold* plasma approximation is discussed along with the warm plasma correction. Finally, plasma heating via liear mode conversion is discussed.

Chapter 3 Some of the important algorithms used in the simulaation are discussed. Various protocals are given along with a brief schematic diagram.

Chapter 4 The input parameters and the plasma model along with the bound-

ary condition are discussed. Finally, results of the simulations are discussed.

Chapter 5 Summary and conclusions of this work are presented.

Appendix A Poission's solver algorithms, for one as well as two dimensions, are given.

Chapter 2

Linear Theory of Lower Hybrid Waves in Maxwellian Plasma

2.1 Introduction

This chapter briefly reviews the theory of lower hybrid waves in electrostatic Maxwellian plasma. As outlined in Sec. 1.5 the theory of lower hybrid heating is classified as: (1) collisional, (2) collisionless, and (3) nonlinear processes. According to the nonlinear theory, plasma heating takes place because of the turbulence that is created due to enhanced level of fluctuations of the internal fields of plasma. These fields are created by the $\mathbf{E} \times \mathbf{B}$ drift motions driven by a sufficiently strong oscillating electric field, with a frequency close to one of the characteristic resonance frequencies of the plasma. Under the action of these fluctuations (or turbulence), the particle velocity distribution function changes and energy of particles increases, i.e., an anomalously fast transfer of the energy from pump field to particles occurs. This nature of the process

has attracted the attention of many researchers, resulting in a considerable amount of work in this area. On the other hand the advantages offered by the linear theory seem to be more attractive. Some of these are discussed in the following text.

Plasma heating in the nonlinear regime, as discussed earlier in Sec 1.5, requires a strong pump field. Moreover, for this case, efficient heating can tke place only above a certain threshold. In large steady state thermonuclear devices where the energy stored is of the order of 10^6-10^7 J and where the containment time is often large, it is impractical to propose to heat the plasma by nonlinear effects. One important reason is the technical problems that are associated with the devices which use high-power pulses to create the requred large amplitude fields at extremely high frequencies. More promising methods are therefore those in which the collisionless absorption can occur with small amplitude high frequency fields. Following points must be satisfied in order to achive this type of heating:

1. Penetration of high frequency fields into high density plasma;
2. Retardation of these waves to velocities such that collisionless (Cherenkov or cyclotron) absorption of the waves is possible;
3. Maintenance of plasma stability during heating.

The rest of the chapter is organized in the following manner:

Sec. 2.2 briefly reviews the theory of wave propagation in *Cold Plasma.* The section is concluded with a discussion of electrostatic and electromagnetic cold plasma dispersion relation.

Sec. 2.3 *Warm Plasma* effects are discussed. The section also summarizes the analytic approximation to electrostatic hot plasma dispersion relation for

a Maxwellian plasma in the region of lower hybrid resonance, which in particular, is associated with the inequality

$$\frac{k_\perp v_i}{\Omega_i} \gg 1 \quad \text{or} \quad \omega_0 \gg \Omega_i$$

Sec. 2.4 Plasma heating in the linear regime via mode conversion is discussed. The conditions for the propagation and absorption of electromagnetic waves in *cold* and *hot* regions are reviewed.

Sec. 2.5 This section concludes the chpater outlining the discussion by various authors as [*Stix*(1965)], [*Glagolev*(1972a), *Glagolev*(1972b)], [*Brambilla*(1976)] and [*Chu et al.*(1976)] regarding the mechanism of energy absorption in the linear regime.

2.2 Wave Propagation in Cold Plasma

2.2.1 Electrostatic Approximation [*Bonoli*,(1983)]

For the situation shown in Fig. 2.1 with ambient electron and ion plasma density $n_o(x)$ and static magnetic field $\mathbf{B_o} = \hat{z}B_o$, an electrostatic oscillation is setup with frequency ω_0 and wave number $\mathbf{k} = \hat{x}k_\perp + \hat{z}k_\parallel$. Without loss of generality $\mathbf{k}$ has been taken to have only components in x and z directions. The frequency ω_0 is assumed to satisfy $\Omega_e^2 \gg \omega_0^2 \gg \Omega_i^2$, where $\Omega_k^2 = q_k B_o/m_k$ is the gyrofrequency of the k^{th} species. The perturbed electric field $\delta\mathbf{E}$ is related to the perturbed electron density δn_e and the perturbed ion density δn_i by the linearized Poisson's equation [*Bonoli*(1983)],

$$\nabla \cdot \delta\mathbf{E} = \frac{q}{\epsilon_o}(\delta n_i - \delta n_e)\,. \tag{2.1}$$

In the electrostatic approximation, the perturbed electric fields satisfies the relations $\nabla \times \delta\mathbf{E} = 0$ and $\delta\mathbf{E} = -\nabla\phi(\mathbf{x}, t)$, where $\phi(\mathbf{x}, t)$ is the electrostatic

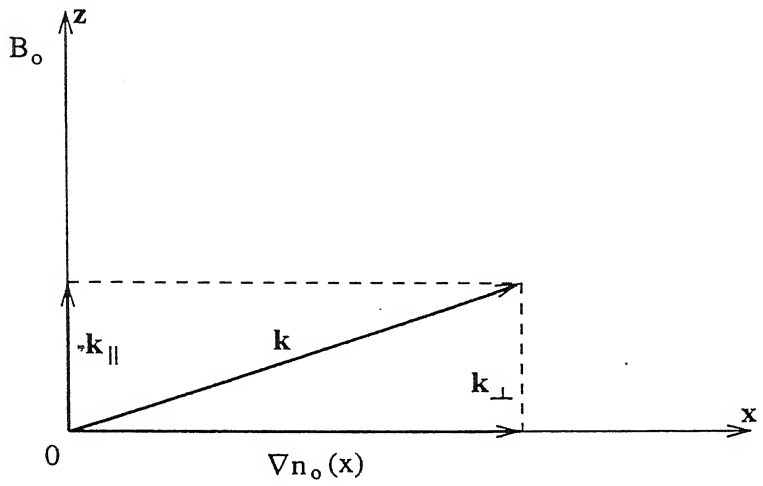

Figure 2.1: *Cartesian geometry for slab analysis of wave propagation*

potential. The perturbed densities must also satisfy the linearised continuity equations

$$\frac{\partial \delta n_e}{\partial t} + \nabla \cdot (n_o \delta \mathbf{v}_e) = 0, \tag{2.2}$$

$$\frac{\partial \delta n_i}{\partial t} + \nabla \cdot (n_o \delta \mathbf{v}_i) = 0, \tag{2.3}$$

where $\delta \mathbf{v}_e$ and $\delta \mathbf{v}_i$ are respectively the perturbed electron and ion fluid velocities and $\mathbf{v}_{eo} = \mathbf{v}_{io} = 0$ has been assumed (*'cold' plasma approximation*). The perturbed densities are assumed to have the waveforms

$$\delta n_e = \tilde{n}_e e^{i\mathbf{k}\cdot\mathbf{x} - i\omega_0 t}, \tag{2.4}$$

$$\delta n_i = \tilde{n}_i e^{i\mathbf{k}\cdot\mathbf{x} - i\omega_0 t}, \tag{2.5}$$

$$\phi = \tilde{\phi}_i e^{i\mathbf{k}\cdot\mathbf{x} - i\omega_0 t}, \tag{2.6}$$

$$\delta \mathbf{v}_e = \tilde{\mathbf{v}}_e e^{i\mathbf{k}\cdot\mathbf{x} - i\omega_0 t}, \tag{2.7}$$

$$\delta \mathbf{v}_i = \tilde{\mathbf{v}}_i e^{i\mathbf{k}\cdot\mathbf{x} - i\omega_0 t}, \tag{2.8}$$

where $\tilde{n}_e, \tilde{n}_i, \tilde{\phi}_i, \tilde{\mathbf{v}}_e, \tilde{\mathbf{v}}_e$ are constant amplitudes. Now Eqs. 2.1, 2.2 and 2.3 can be rewritten as

$$k^2\phi = \frac{q}{\epsilon_o}(\delta n_i - \delta n_e), \tag{2.9}$$

$$\delta n_e = \frac{n_o}{\omega_0}\mathbf{k}\cdot\delta\mathbf{v_e}, \tag{2.10}$$

$$\delta n_i = \frac{n_o}{\omega_0}\mathbf{k}\cdot\delta\mathbf{v_i}, \tag{2.11}$$

where $k^2 = k_\perp^2 + k_\parallel^2$. For the above equations to be valid, the WKB approximation must be satisfied, according to which

$$\mid \mathbf{k} \mid \gg \mid \frac{1}{n_o}\frac{\partial n_o}{\partial x}\, q \mid .$$

The perturbed fluid velocities are solved in terms of ϕ using the electron and ion momentum equations,

$$m_e\frac{\partial\delta\mathbf{v_e}}{\partial t} = -q(\delta\mathbf{E} + \delta\mathbf{v_e}\times\mathbf{B_o}), \tag{2.12}$$

$$m_i\frac{\partial\delta\mathbf{v_i}}{\partial t} = -q(\delta\mathbf{E} + \delta\mathbf{v_i}\times\mathbf{B_o}), \tag{2.13}$$

The results for $\delta\mathbf{v_e}$ and $\delta\mathbf{v_i}$, correct to order (ω_0/Ω_e) and to order (Ω_i/ω_0), respectively, are (in the limit $\Omega_e^2 \gg \omega_0^2 \gg \Omega_i^2$),

$$\delta v_{ex} = \frac{\omega_0}{\Omega_e}\frac{k_\perp\phi}{B_o}, \tag{2.14}$$

$$\delta v_{ey} = \frac{ik_\perp\phi}{B_o}, \tag{2.15}$$

$$\delta v_{ez} = \frac{\omega_0}{\Omega_e}\frac{k_\perp\phi}{B_o}, \tag{2.16}$$

$$\delta v_{ix} = -\frac{\Omega_i}{\omega_0}\frac{k_\perp\phi}{B_o}, \tag{2.17}$$

$$\delta v_{iy} = 0, \tag{2.18}$$

$$\delta v_{iz} = \frac{\Omega_i}{\omega_0}\frac{k_\parallel \phi}{B_o}. \tag{2.19}$$

Using Eqs. 2.14 to 2.19 in Eqs. 2.10 and 2.11, and combining the results with Eqn. 2.9 yields the electrostatic lower hybrid dispersion relation,

$$\frac{k_\parallel^2}{k_\perp^2}\epsilon_\perp + \frac{k_\parallel^2}{k_\perp^2}\epsilon_\parallel = 0, \tag{2.20}$$

where

$$\epsilon_\perp = 1 + \left(\frac{\Pi_e}{\Omega_e}\right)^2 - \left(\frac{\Pi_i}{\omega_0}\right)^2, \tag{2.21}$$

$$\epsilon_\parallel = 1 - \left(\frac{\Pi_e}{\omega_0}\right)^2 - \left(\frac{\Pi_i}{\omega_0}\right)^2, \tag{2.22}$$

are the dielectric tensor components

$$\Pi_e = \left(\frac{n_o q^2}{\epsilon_o m_e}\right)^{1/2},$$

is the electron plasma frequency and

$$\Pi_i = \left(\frac{n_o Z^2 q^2}{\epsilon_o m_i}\right)^{1/2},$$

is the ion plasma frequency.

If Eqn. 2.20 is solved for $k_\perp^2$, we get,

$$k_\perp^2 = -k_\parallel^2 \epsilon_\parallel / \epsilon_\perp, \tag{2.23}$$

so that there is a plasma resonance ($k_\perp \to \infty$) for $\epsilon_\perp = 0$ and plasma cutoff ($k_\perp \to 0$) for $\epsilon_\parallel = 0$. Using Eqn. 2.21, the condition $\epsilon_\perp = 0$ can be solved for ω_0^2 to define the lower hybrid frequency ω_{LH} as

$$\omega_{LH}^2 \equiv \omega_0^2 = \frac{\Pi_i^2}{(1 + \Pi_e/\Omega_e^2)}, \tag{2.24}$$

which can also be written in the form first given by Stix [*Stix*(1962)] as

$$\frac{1}{\omega_{LH}^2} \equiv \frac{1}{\omega_0^2} = \frac{1}{\Omega_e \Omega_i} + \frac{1}{\Pi_i^2}.$$

The frequency $\Omega \equiv (\Omega_e \Omega_i)^{1/2}$ is the same frequency referred by Stix as the "gm gyrofrequecy", which is nothing but the geometric mean of the ion cyclotron frequency and the electron cyclotron frequency. As discussed in most of the publications the solutions of Eqn. 2.23 for typical central plasma parameters yields the useful limit

$$\left(k_\perp / k_\parallel\right)^2 \sim (\Pi_e/\omega_0)^2 \sim (m_i/m_e) \gg 1,$$

for an electrostatic lower hybrid wave.

2.2.2 Electromagnetic Case [*Bonoli*,(1983)]

The electromagnetic dispersion relation is briefed here to highlight the reason for using the electrostatic simulation algorithm, and also for the purpose of quick reference in case of future development of the code.

The electrostatic approximation made in above section is not always valid for the lower hybrid wave. For example near the plasma cutoff where $k_\perp \approx 0$, the parallel wave number ($k_\parallel$) of the wave may not be large enough to satisfy$(kc/\omega_0^2) = (k_\perp^2 + k_\parallel^2)\ (c/\omega_0)^2 \gg 1$ (so that $\nabla \times \delta\mathbf{E} = 0$ may not be assumed). The $k_\parallel$ of the wave is fixed by the axial (along $\mathbf{B_o}$) dimension of the wave guide launching structure or *grill* which can, in general, launch waves which satisfy $kc/\omega_0 \approx k_\parallel c/\omega_0 \geq 1$ near the plasma cutoff.

The situation shown in Fig. 2.1 is again considered. However, the starting point for the analysis is Maxwell's equations,

$$\nabla \times \delta\mathbf{B} = \epsilon_o \frac{\partial}{\partial t}\delta\mathbf{E} + \delta\mathbf{J}, \tag{2.25}$$

$$\nabla \times \delta\mathbf{E} = -\frac{\partial}{\partial t}\delta\mathbf{B}. \tag{2.26}$$

The perturbed electric field $\delta\mathbf{E}$, perturbed current density $\delta\mathbf{J}$, and perturbed magnetic field $\delta\mathbf{B}$, are assumed to satisfy the waveforms,

$$\delta\mathbf{E} = \tilde{\mathbf{E}} e^{i\mathbf{k}\cdot\mathbf{x} - i\omega_0 t}, \tag{2.27}$$

$$\delta\mathbf{B} = \tilde{\mathbf{B}} e^{i\mathbf{k}\cdot\mathbf{x} - i\omega_0 t}, \tag{2.28}$$

$$\delta\mathbf{J} = \tilde{\mathbf{J}} e^{i\mathbf{k}\cdot\mathbf{x} - i\omega_0 t}, \tag{2.29}$$

where $\tilde{\mathbf{E}}$,$\tilde{\mathbf{B}}$ and $\tilde{\mathbf{J}}$ are constant amplitudes and $\mathbf{k} = \hat{x}k_\perp + \hat{z}k_\parallel$ without loss of generalization. Substituting in the Maxwell's equations (Eqs. 2.25, 2.26) and combining them we can get the wave equation as,

$$-\mathbf{k} \times \mathbf{k} \times \delta\mathbf{E} = \left(\frac{\omega_0}{c}\right)^2 \delta\mathbf{E} + i\omega_0 \delta\mathbf{J}. \tag{2.30}$$

The perturbed current density can be expressed in terms of the fluid velocities as

$$\delta\mathbf{J} = n_o e \left(\delta\mathbf{v_i} - \delta\mathbf{v_e}\right). \tag{2.31}$$

The $\delta\mathbf{v_i}$ and $\delta\mathbf{v_e}$ are solved in terms of $\delta\mathbf{E}$ using the momentum Eqs. 2.12 and 2.13. Substituting these results in Eqn. 2.31 we can solve $\delta\mathbf{J}$, then using Eqn. 2.30 we get the wave equation as [*Bonoli*(1983)]

$$\mathbf{k} \times \mathbf{k} \times \delta\mathbf{E} + \left(\frac{\omega_0}{c}\right)^2 \mathbf{K} \cdot \mathbf{E} = 0, \tag{2.32}$$

$$\mathbf{K} = \begin{bmatrix} \epsilon_\perp & -i\epsilon_{xy} & 0 \\ i\epsilon_{xy} & \epsilon_\perp & 0 \\ 0 & 0 & \epsilon_\parallel \end{bmatrix}, \tag{2.33}$$

where $\mathbf{K}$ is the famous dielectric tensor of Stix [*Stix*(1962)], evaluated in the limit $\Omega_e^2 \gg \omega_0^2 \gg \Omega_i^2$ and the components are defined as follows:

$$\epsilon_\perp \equiv \frac{1}{2}(R+L), \qquad \epsilon_{xy} \equiv \frac{1}{2}(R-L), \tag{2.34}$$

$$R \equiv 1 - \sum_k \frac{\Pi_k^2}{\omega_0^2}\left(\frac{\omega_0}{\omega_0 + \epsilon_k \Omega_k}\right), \tag{2.35}$$

$$L \equiv 1 - \sum_k \frac{\Pi_k^2}{\omega_0^2}\left(\frac{\omega_0}{\omega_0 - \epsilon_k \Omega_k}\right), \tag{2.36}$$

$$P \equiv 1 - \sum_k \frac{\Pi_k^2}{\omega_0^2}, \tag{2.37}$$

$$\Pi_k^2 \equiv \frac{4\pi n_k Z_k^2 e^2}{m_k}. \tag{2.38}$$

Using the dielectric tensor equation Eqn. 2.33 the wave equation 2.32 can be written in a more compact form by defining

$$\mathbf{D} = \mathbf{k} \times \mathbf{k} \times 1 + \left(\frac{\omega_0}{c^2}\right)\mathbf{K}. \tag{2.39}$$

Then the equations of the wave becomes

$$\mathbf{D} \cdot \delta\mathbf{E} = 0. \tag{2.40}$$

If θ is to be the angle between $\mathbf{B}_0 = \hat{\mathbf{z}}B_0$ and n, and if we assume $\mathbf{n}$ to be increasing in the positive x direction, then Eqn. 2.40 becomes

$$\begin{bmatrix} \epsilon_\perp - n^2\cos^2\theta & -i\epsilon_{xy} & n^2\cos\theta\sin\theta \\ i\epsilon_{xy} & \epsilon_\perp - n^2 & 0 \\ n^2\cos\theta\sin\theta & 0 & \epsilon_\parallel - n^2\sin^2\theta \end{bmatrix} \begin{bmatrix} E_x \\ E_y \\ E_z \end{bmatrix} = 0. \tag{2.41}$$

The condition for a nontrivial solution is that the determinant of the square matrix be zero, thus

$$\begin{vmatrix} \epsilon_\perp - n^2\cos^2\theta & -i\epsilon_{xy} & n^2\cos\theta\sin\theta \\ i\epsilon_{xy} & \epsilon_\perp - n^2 & 0 \\ n^2\cos\theta\sin\theta & 0 & \epsilon_\parallel - n^2\sin^2\theta \end{vmatrix} = 0. \tag{2.42}$$

This condition gives the famous dispersion relation, or the equation for the wave normal surface as [*Stix*(1962)]:

$$\beta n_x^4 - \gamma n_x^2 + \delta = 0, \tag{2.43}$$

where β, γ and *delta* are the coefficients given by:

$$\beta = \epsilon_\perp \sin^2\theta + \epsilon_\parallel \cos^2\theta, \tag{2.44}$$

$$\gamma = RL\sin^2\theta + \epsilon_\parallel\epsilon_\perp(1+\cos^2\theta), \tag{2.45}$$

$$\delta = \epsilon_\parallel RL, \tag{2.46}$$

and R, L and P are as given in Eqs. 2.35, 2.36 and 2.37, respectively.

2.3 Thermal Corrrection to 'Cold' Plasma Dispersion Relation

The thermal corrections to the cold plasma dispersion relations (Eqn. 2.20) are derived using the Vlasov theory ([*Karney*(1986)] and [*Krall et.al. (1973)*]). The electrostatic equations are used as plasma effects should only be important in the high temperature regions of the plasma where the electron and ion densities are high enough to satisfy $(kc/\omega_0)^2 \gg 1$. As electrostatic oscillations are considered Poisson's equation is used. Assuming wave forms for ϕ, δn_e and δn_i similar to those in the previous section, Eqn. 2.9 can be rewritten as ([*Stix*(1965)] and [*Bonoli*(1983)]):

$$1 + \chi_e + \chi_i = 0, \tag{2.47}$$

$$\chi_k = \frac{q\delta n_k}{k^2 \phi \epsilon_o}, \tag{2.48}$$

where χ_k is the susceptibility function for the k^{th} species. The perturbed electron and ion densities are calculated from the kinetic theory [*Krall et.al (1973)*],

$$\delta n_e = n_o \int \delta f_e(\mathbf{v})\, d\mathbf{v}, \tag{2.49}$$

$$\delta n_i = n_o \int \delta f_i(\mathbf{v})\, d\mathbf{v}, \tag{2.50}$$

where δf_e and δf_i are respectively the perturbed electron and ion distribution functions.

2.3.1 Electron Vlasov Analysis [*Bonoli*,(1983)]

The perturbed electron distribution is calculated from the electron Vlasov equation

$$\frac{\partial F_e}{\partial t} + \mathbf{v} \cdot \frac{\partial F_e}{\partial \mathbf{x}} - \frac{q}{m_e}(\mathbf{E} + \mathbf{v} \times \mathbf{B_o}) \cdot \frac{\partial F_e}{\partial \mathbf{v}} = 0. \tag{2.51}$$

F_e is expanded as

$$F_e(\mathbf{x}, \mathbf{v}, t) = f_{eo}(\mathbf{v}) + \delta f_e(\mathbf{x}, \mathbf{v}, t), \tag{2.52}$$

$$f_{eo} = \left(\frac{1}{2\pi}\right)^{3/2} \frac{1}{v_{the}^3} \exp\left(-\frac{v^2}{2v_{the}^2}\right), \tag{2.53}$$

where f_{eo} is the unperturbed distribution, $v_{the} = (T_e/m_e)^{1/2}$ is the electron thermal speed, and $\delta f_e \ll f_{eo}$. The equilibrium and the linearized electron Vlasov equations are

$$\frac{\partial f_{eo}}{\partial t} + \mathbf{v} \cdot \frac{\partial f_{eo}}{\partial \mathbf{x}} - \frac{q}{m_e} (\mathbf{v} \times \mathbf{B_o}) \cdot \frac{\partial f_{eo}}{\partial \mathbf{v}} = 0, \tag{2.54}$$

$$\frac{\partial f_e}{\partial t} + \mathbf{v} \cdot \frac{\partial f_e}{\partial \mathbf{x}} - \frac{q}{m_e} \delta\mathbf{E} \cdot \frac{\partial}{\partial \mathbf{v}} - \frac{q}{m_e} (\mathbf{v} \times \mathbf{B_o}) \cdot \frac{\partial f_e}{\partial \mathbf{v}} = 0, \tag{2.55}$$

where $\mathbf{E_o} = 0$ has again been used. As the electrons are strongly magnetized, the ambient magnetic field is retained. This fact is justified in the light of the fact that electron gyro orbit is very small as compared to the perpendicular wavelength, $(k_\perp \rho_e)^2 \ll 1$. Here $\rho_e = v_e/\Omega_e$ is the electron gyro-radius. The inequality $(k_\perp \rho_e)^2 \ll 1$ is easily justified using $k_\perp^2 \approx k_\parallel^2 (\Pi_e/\omega_0)^2$.

The linearized equation (Eqn. 2.55) is solved by first transforming $\mathbf{v} = (v_x, v_y, v_z)$ to a cylindrical coordinate system [*Bonoli*(1983)] $(v_\perp, v_\parallel, v_z)$ where

$$v_x = v_\perp \cos\theta, \tag{2.56}$$

$$v_y = v_\perp \sin\theta, \tag{2.57}$$

$$v_\perp^2 = v_x^2 + v_y^2. \tag{2.58}$$

$$\tag{2.59}$$

With these transformations the velocity gradient transforms as

$$\frac{\partial}{\partial v_x} = \cos\theta \frac{\partial}{\partial v_\perp} \frac{\sin\theta}{v_\perp} \frac{\partial}{\partial \theta}, \tag{2.60}$$

$$\frac{\partial}{\partial v_y} = \sin\theta \frac{\partial}{\partial v_\perp} + \cos\theta \frac{\partial}{\partial \theta}, \tag{2.61}$$

$$\frac{\partial}{\partial v_z} = \frac{\partial}{\partial v_\parallel}. \tag{2.62}$$

This transforms the unperturbed distribution function $f_{eo}(v^2)$ to a function of $(v_\perp, v_\parallel)$ because $v^2 = v_\perp^2 + v_\parallel^2$. $f_{eo}(v_\perp, v_\parallel)$ can also be obtained from equilibrium Vlasov equation Eqn. 2.54. Recalling that f_{eo} now is independent of $\mathbf{x}$ and t,

and transforming the velocity gradient, Eqn. 2.54 yields

$$\Omega_e \frac{\partial f_{eo}}{\partial \theta} = 0.$$

Thus, $f_{eo}(v_\perp, v_\parallel)$ is independent of θ. The electron orbits are governed by the equations of motion

$$\frac{d\mathbf{x}(t')}{dt'} = \mathbf{v}(t'), \tag{2.63}$$

$$\frac{d\mathbf{v}(t')}{dt'} = \frac{q}{m_e}\mathbf{v}(t') \times \mathbf{B}_0. \tag{2.64}$$

Scalar multiplication of Eqn. 2.64 with unit vector $\hat{\mathbf{b}}$ in the direction of the magnetic field gives $dv_\parallel/dt' = 0$, where, $v_\parallel = \hat{\mathbf{b}} \cdot \mathbf{v}(t^t)$. Thus, $v_\parallel$ is constant of particle orbit motion. Let W_k stands for total electron kinetic energy

$$W_k = W_\parallel + W_\perp, \tag{2.65}$$

where $W_\parallel = \frac{1}{2}m_e v_\parallel^2$ and $W_\perp = \frac{1}{2}m_e v_\perp^2$. Since W_k must be conserved,

$$\frac{dW_k}{dt} = m_e\left(v_\parallel \frac{dv_\parallel}{dt} + v_\perp \frac{dv_\perp}{dt}\right) = 0. \tag{2.66}$$

The linearized Vlasov equation (Eqn. 2.55) is now solved by integrating along the orbits of the electrons (Eqn 2.63) in the unperturbed fields. Eqn. 2.55 can now be written as

$$\frac{d\delta f_e}{dt'}[\mathbf{x}(t'), \mathbf{v}(t'), t'] = \frac{q}{m_e}\delta\mathbf{E}[\mathbf{x}(t'), t'] \cdot \frac{\partial f_{e0}}{\partial \mathbf{v}} f_{e0}[\mathbf{v}(t')], \tag{2.67}$$

where the left hand side is now the exact differential. Being constructed from the constants of motion, f_{e0} is constant along the orbits. Integrating Eqn. 2.67 in the limits $t' = -\infty$ to $t' = t$, assuming $\delta f_{e0} = 0$ as $t' \to -\infty$ yields

$$\delta f_e[\mathbf{x}(t),\mathbf{v}(t),t] = -i\frac{q}{m_e}\int_{-\infty}^{t} dt' \int_{-\infty}^{0} d\tau[k_\perp \cos\theta(\tau)\frac{\partial f_{e0}}{\partial v_\perp} + k_{||}\frac{\partial f_{e0}}{\partial v_{||}}, \quad (2.68)$$

where τ is defined as $\tau = t' - t$. Using Eqs. 2.60 to 2.62 to transform $\mathbf{k}\cdot(\partial/\partial\mathbf{v})$ and performing a change of variable in the integral to $\tau = t' - t$ we have

$$\begin{aligned}\delta f_e[\mathbf{x}(t),\mathbf{v}(t),t] &= -i\frac{q}{m_e}\phi[\mathbf{x}(t),t]\int_{-\infty}^{0} d\tau \\ &\quad [k_\perp \cos\theta(\tau)\frac{\partial f_{e0}}{\partial v_\perp} + k_{||}\frac{\partial f_{e0}}{\partial v_{||}}]\cdot \\ &\quad \exp\left(i\frac{k_\perp v_\perp}{\Omega_e}[\sin(\Omega_e\tau - \theta(t))\sin\theta(t)] + i(k_{||}v_{||} - \omega_0)\tau\right).\end{aligned} \quad (2.69)$$

Using Eqn. 2.69 in Eqs. 2.49 and 2.49 expression for χ_e is obtained as

$$\begin{aligned}\chi_e &= -i\frac{\Pi_e^2}{k^2}\int_0^{2\pi} d\theta \int_0^{\infty} v_\perp dv_\perp \int_{-\infty}^{\infty} dv_{||} \int_{-\infty}^{0} d\tau \\ &\quad [k_\perp \cos\theta(\tau)\frac{\partial f_{e0}}{\partial v_\perp} + k_{||}\frac{\partial f_{e0}}{\partial v_{||}}]\cdot \\ &\quad \exp\left(i\frac{k_\perp v_\perp}{\Omega_e}[\sin(\Omega_e\tau - \theta(t))\sin\theta(t)] + i(k_{||}v_{||} - \omega_0)\tau\right),\end{aligned} \quad (2.70)$$

where $dv_x dv_y dv_z = d\theta v_\perp dv_\perp dv_{||}$ is used. Eqn. 2.70 can be written in the approximate form, as given by Glagolev [*Glagolev*(1972b)]

$$\chi_e = -\frac{2\Pi^2}{k^2 v_{the}^2}\left(Z\left(\frac{\omega_0}{k_{||}v_{the}}\right)q(\mathrm{e}^{-z_e})I_o - 1\right), \quad (2.71)$$

where,

$$Z = X - iY, \quad (2.72)$$

$$X = 2x\mathrm{e}^{-x^2}\int_0^x \mathrm{e}^{t^2}dt, \quad (2.73)$$

$$Y = x\sqrt{\pi}\mathrm{e}^{-x^2}, \quad (2.74)$$

$x = \omega_0/k_\parallel v_{the}$, $I_o = I_o(Z_e)$, $Z_e = k_\perp^2 T_e/m_e\Omega_e^2$ I_o is the Bessel function of zeroth order. For $\omega_0/k_\parallel v_{the} \gg 1$, χ_e is approximately

$$\begin{aligned}\chi_e &= \frac{\Pi_e^2}{\Omega_e^2}\frac{(1-I_o e^{-Z_e})}{Z_e} - \frac{\Pi_e^2}{\omega_0^2}\frac{k_\parallel^2}{k^2} I_o e^{-Z_e} \\ &\quad +2i\sqrt{\pi}\frac{\Pi_e^2}{\omega_0^2}\frac{k_\parallel}{k^2} I_o e^{-Z_e}\xi_e^{3/2} e^{\xi_e},\end{aligned} \tag{2.75}$$

where $\xi_e = \omega_0^2 k_\parallel^2 v_{the}^2$

2.3.2 Ion Vlasov Analysis [*Bonoli*,(1983)]

The ion Vlasov equation is

$$\frac{\partial F_i}{\partial t} + \mathbf{v}\cdot\frac{\partial F_i}{\partial \mathbf{x}} - \frac{q}{m_i}(\mathbf{E}+\mathbf{v}\times\mathbf{B_o})\cdot\frac{\partial F_i}{\partial \mathbf{v}} = 0. \tag{2.76}$$

The perturbed ion distribution is calculated using the above equation. The total ion distribution function is expanded as

$$F_i(\mathbf{x},\mathbf{v},t) = f_{i0}(\mathbf{v}) + \delta f_i(\mathbf{x},\mathbf{v},t), \tag{2.77}$$

$$f_{i0} = \left(\frac{1}{2\pi}\right)^{3/2}\frac{1}{v_{thi}^3}\exp\left(-\frac{v^2}{2v_{thi}^2}\right), \tag{2.78}$$

with f_{i0} as the unperturbed ion distribution, $v_{thi} = (\kappa T_i/m_i)^{1/2}$, the ion thermal speed, $\delta f_i \ll f_{i0}$, and $v^2 = v_x^2 + v_y^2 + v_z^2$. The linearized Vlasov equation is then

$$\frac{\partial \delta f_i}{\partial t} + \mathbf{v}\cdot\frac{\partial \delta f_i}{\partial \mathbf{x}} + \frac{q}{m_i}\delta\mathbf{E}\cdot\frac{\partial f_{i0}}{\partial \mathbf{v}} = 0, \tag{2.79}$$

where the unperturbed electric field $\mathbf{E}_0 = 0$. In writing Eqn. 2.79 a considerable simplification is done by neglecting the magnetic field (i.e., treating ions as essentially unmagnetized). This is justified in the light of the fact that the lower hybrid resonance region is particularly having very long ion gyro orbits as compared to the perpendicular wavelength $\lambda_\perp$ (i.e., $(k_\perp \rho_i)^2 \gg 1$).

Assuming that δf_i can be represented by a waveform

$$\delta f_i(x, v, t) = \tilde{f}_i(v) e^{i\mathbf{k}\cdot\mathbf{x} - \omega_0 t}, \tag{2.80}$$

and

$$\delta \mathbf{E} = -\nabla\phi(\mathbf{x}, t) = i\mathbf{k}\phi(\mathbf{x}, t), \tag{2.81}$$

Eqn. 2.79 can be solved for δf_i,

$$\delta f_i = -\frac{q}{m_i} \frac{\mathbf{k} \cdot \left(\frac{\partial f_{i0}}{\partial \mathbf{v}}\right)}{\omega_0 - \mathbf{k} \cdot \mathbf{v}} \phi. \tag{2.82}$$

Using this results in Eqs. 2.48 and 2.50 yields

$$\chi_i = \frac{\Pi_i^2}{k^2} \int \frac{\mathbf{k} \cdot \left(\frac{\partial f_{i0}}{\partial \mathbf{v}}\right)}{\omega_0 - \mathbf{k} \cdot \mathbf{v}} d\mathbf{v}. \tag{2.83}$$

The approximate equation given by Glagolev [*Glagolev*(1972b)] is

$$\chi_i = -2 \frac{\Pi_i^2}{k^2 v_i^2} \left[Z\left(\frac{\omega_0}{k v_i}\right) - 1 \right], \tag{2.84}$$

where Z is as defined in Eqn. 2.72.

In this case χ_i does not include the absorption at high harmonics of the ion-cyclotron frequency which can occur when $\omega_0 \gg \Omega_i$, for which the Larmor radius is large as compared to the wavelength.

The imaginary part of the function Z in Eqs. 2.71 and 2.84 represent the Cherenkov absorption of the waves by the electrons and ions, respectively.

2.4 Plasma Heating Via Mode Conversion

When the phase velocities of the particles are larger than their respective thermal velocities, the wave propagation equations for infinite plasma are given by [*Glagolev*(1972a)]

$$\delta E_{\|} + \frac{\epsilon_{\|}}{\epsilon_{\perp}}(\epsilon_{\perp}k^2 - k_{\|}^2)E_{\|} = -\frac{\epsilon_{xy}}{\epsilon_{\perp}} \cdot k\frac{\partial H_{\|}}{\partial z} \tag{2.85}$$

$$\delta H_{\|} + \left[\left(\epsilon_{\perp} - \frac{\epsilon_{xy}^2}{\epsilon_{\perp}}\right)k^2 - k_{\|}^2\right] H_{\|} = \frac{\epsilon_{xy}}{\epsilon_{\perp}}\epsilon_{\|}k\frac{\partial E_{\|}}{\partial z} \tag{2.86}$$

Eqs. 2.85 and 2.86 characterize the 'E' and 'H' waves. For $k_{\|} = 0$, Eqs. 2.85 and 2.86 represent the *ordinary 'E'* and *extraordinary 'H'* waves, propagating in the direction perpendicular to the magnetic field, i.e., in the x direction. In case of finite $k_{\|}$, coupling occurs between the 'E' and 'H' waves. Assuming $k_{\|} = kn_{\|}$ and $k_{\perp} = kn_{\perp}$, and solving the dispersion relation (Eqn. 2.41), we get

$$n_{x_{1,2}}^2 = p \pm \sqrt{p^2 - q} \tag{2.87}$$

where $p = \gamma/2\beta$ and $q = \delta/\beta$. The (+) and (-) sign correspond to the 'E' and 'H' waves, respectively. Thus the 'H' wave, also called the *quasi extraordinary* wave, is a backward traveling wave; therefore the waves propagating from the external antenna towards the lower hybrid resonance will have a negative phase velocity. As seen from the above equation, the 'E' wave has a larger refractive index than the 'H' wave, and it is the 'E' wave that must transform into the plasma wave. Figs. 2.2 and 2.3 show the characteristic variation of n^2 with the x coordinate (representing the direction of increasing density) for the wave of 'E' type in the *cold* and *hot* plasma regions. The waves can propagate in two different ways as seen from the plots, as

1. When the electromagnetic wave ('E') converts smoothly into a plasma

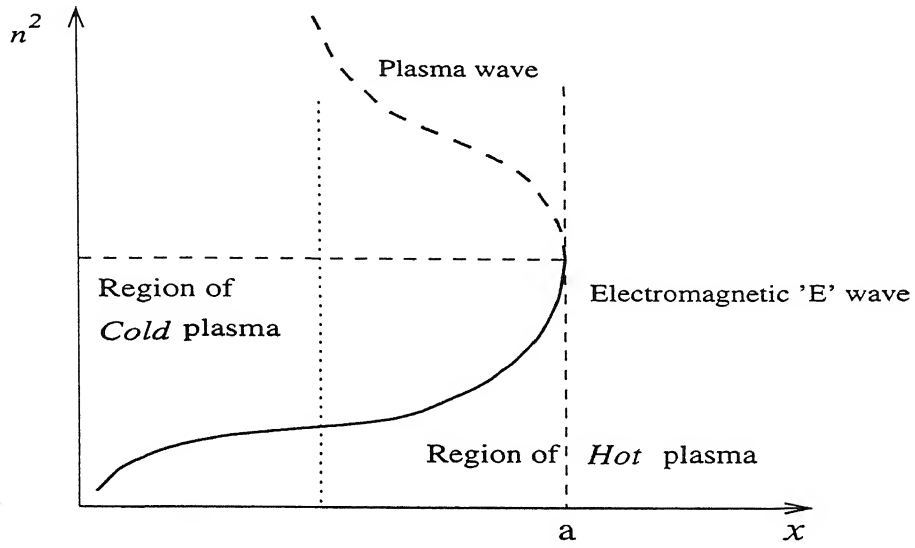

Figure 2.2: *Dependence of n^2 on x-coordinate in case of transformation of the wave into a plasma wave*

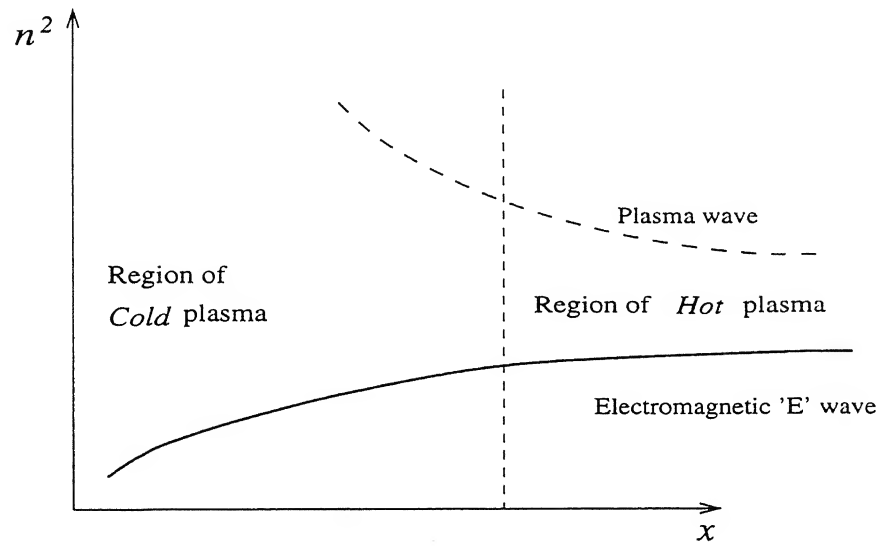

Figure 2.3: *Dependence of n^2 on x-coordinate in absence of transformation of the wave into a plasma wave*

wave (transformation point being $x = a$, Fig. 2.2);

2. When there is no smooth transformation of 'E' wave into a plasma wave.

The condition for the efficient transformation of electromagnetic 'E' wave into a plasma wave is derived by Glagolev in his work [*Glagolev*(1972a)] as

$$\sqrt{\epsilon_\perp + \frac{\Pi_e^2}{\omega_0 \Omega_e}} > n_\parallel > n_{z_1} = \sqrt{\epsilon_\perp} + \frac{\Pi_e}{\Omega_e} \tag{2.88}$$

The inequality 2.88 is also a sufficient condition for the propagation for both types of waves. The separation of the waves is observed to increases sharply with increase in $n_\parallel$ above the value given by the equation

$$n_\parallel \simeq n_z = \sqrt{\epsilon_\perp} + \frac{\Pi_e}{\Omega_e} \tag{2.89}$$

The wave damping can thus disappear in the region between *cold* and *hot* regions if a sufficiently high density is present at this layer. In this case, for small densities, the longitudinal deceleration will considerably higher as a result of which the 'E' and 'H' waves will likewise separate at the plasma boundary. Since the 'E' waves has a higher deceleration along the x axis inside the plasma layer, only that wave will be transformed into the plasma wave. Therefore, it is important to generate the 'E' wave on the plasma surface if they are to be excited inside the plasma. Nevertheless, the excitation of 'H' waves on the plasma surface can be useful for providing the hydrodynamic stability to the plasma layer. Since, 'H' waves exist only on the surface skin layer it exerts a high frequency pressure on the plasma. According to Glagolev [*Glagolev*(1972a)] this high frequency pressure leads to the hydrodynamic plasma stability.

2.5 Summary

From the discussions in Sec. 2.4, it is clear that the transformation of the waves is of great importance for the absorption of waves and therefore the heating of plasma. According to Stix [*Stix*(1965)] the 'E' and 'H' waves must sufficiently be decelerated along the magnetic field in order to penetrate into the plasma with direction of the density gradient perpendicular to the direction of magnetic field. Also the square of the propagation vector reduces as density increases, and thus the hybrid resonance layer is not accessible from the lower density side of the plasma. In order to avoid this difficulty, a component of the propagation vector parallel to the magnetic field is required (i.e., $k_{\|} > 0$).

If the magnetic field approaches the value given by

$$\frac{\omega_g^2}{\omega_0^2} > \frac{1}{\left(\frac{1}{4} + 2\frac{k_{\|}}{k}\sqrt{\left(\gamma^e T_e \frac{\omega_0^4}{\omega_g^4} + \gamma^i T_i\right)\frac{1}{m_e c^2}}\right)}, \tag{2.90}$$

where $\omega_g = \Omega_e\sqrt{m_e/m_i}$ and γ^k is the damping coefficient for the k^{th} species. as given by Glagolev [*Glagolev*(1972a)], the density corresponding to the wave transformation conditions increases without limit. Also, if the magnetic field is less than the value specified by Eqn. 2.90, transformation of the 'E' wave into plasma wave is impossible. In other words it can be stated that, if the magnetic field exceeds the critical value corresponding approximately to the condition $\sqrt{\Omega_e\Omega_i} > \omega_0$, the electromagnetic '$E$' wave will, at some definite value of density in the plasma wave, completely transform into the plasma wave. After reflection from the point of transformation, the deceleration of the ion hybrid waves increases with the plasma density. As soon as the phase velocity of the waves approaches the ion velocity, Cherenkov absorption of the waves by ions occurs. This effect leads to the absorption of the waves and heating of the ion component of the plasma.

When the phase velocity is close to the ion thermal velocity , their thermal

motion should considerably affect the propagation of the waves. The components of the dielectric tensor then depend on the plasma temperature and phase velocity and are found by means of the kinetic equation. Glagolev [*Glagolev*(1972b)], has solved Eqn. 2.47 using Eqs. 2.75 and 2.84 and obtained the approximate equations

$$\frac{\Pi_i^2}{\omega_0^2} = \frac{1}{\left[1 + 3\frac{\omega_g^2}{\omega_0^2}\frac{T_i}{T_e}Z_e + \frac{k_\parallel^2 v_{the}^2}{2\omega_0^2}\frac{I_0 e^{-Z_e}}{Z_e} - \frac{\omega_0^2}{\omega_g^2}\frac{(1-I_0 e^{-Z_e})}{Z_e}\right]},$$

and

$$\frac{\omega_{2i}}{\omega_0} = \frac{\sqrt{\pi}\zeta_i^{3/2} e^{-\zeta_i}}{\left(1 + 3\frac{k^2 v_{thi}^2}{\omega_0^2} + I_0 e^{-Z_e}\frac{k_\parallel^2}{k^2}\frac{m_i}{m_e}\right)},$$

$$\frac{\omega_{2e}}{\omega_0} = \frac{\sqrt{\pi}\frac{k_\parallel^2}{k^2}\frac{m_i}{m_e}\zeta_e^{3/2} e^{-\zeta_e} e^{-Z_e} I_0}{\left(1 + 3\frac{k^2 v_{thi}^2}{\omega_0^2} + I_0 e^{-Z_e}\frac{k_\parallel^2}{k^2}\frac{m_i}{m_e}\right)},$$

where $\omega_2 = \omega_{2i} + \omega_{2e}$ and $\zeta_k = \omega_0^2 k_\parallel^2 v_{thk}^2$ for k^{th} species. In this expression ω_{2i} and ω_{2e} represent respectively the Cherenkov ion and electron absorptions. The numerical solutions of this equations (refer, [*Glagolev*(1972b)]) yields the following conclusions:

1. The critical density increases as the magnetic field decreases;

2. As ion temperature increases the transformation region shifts to the lower density side. This implies that increase in ion temperature improves the wave transformation;

3. The plasma density corresponding to the maximum absorption increases slightly with decrease in the magnetic field;

4. The electron absorption increases with the phase velocity of the wave. Therefore, the electron absorption is maximum for small plasma densities.

5. As electron temperature increases the electron absorption decreases.

6. Electron absorption decreases as Z_e increases; i.e., if the electron Larmor radius increases when the wavelength becomes smaller compared to the Larmor radius ($Z_e \gg 1$), the electron absorption decreases considerably.

7. Electron absorption increases with decrease in the phase velocity along the magnetic field.

This process of mode conversion is also explained by Stix [*Stix*(1965)], Brambilla [*Brambilla*(1976)] and Wong [*Wong and Tang*(1976)]. The validity of this approach is evident from the form of Eqn. 2.43 in which the magnetic field has completely disappeared from the ion term. Indeed for $k_\perp^2 v_{thi}^2/\Omega_i^2 \gg 1$, $\omega_0 \gg \Omega_i$, which is a characteristic of lower hybrid frequency range, one expects the magnetic field to play little role on the dielectric properties of the ion fluid. When this condition is satisfied the damping length perpendicular to the static magnetic field can be estimated from Eqn. 2.43 by substituating $\gamma = \delta_e - i\delta_i$. δ_e includes finite temperature corrections for electrons, in particular electron Landau damping along the static magnetic field. On the other hand for purely perpendicular propagation the hot plasma dispersion relation admits only real roots for $n_\perp^2$, and no damping for ions is possible. While, as discussed by [*Glagolev*(1972b)], if the effects of the static magnetic field on the ions are negligible, an ion Landau damping is expected by free-streaming of ions. It is important to note this conflicting point. This contradiction is explained to some extent by the concept of phase mixing, such that, for $\omega_0 \gg \Omega_i$ phase mixing appeares for times $\omega_0^{-1} \ll \Delta t \ll \Omega_i^{-1}$, but after a whole cyclotron period the exact phase correlation is restored, and no damping is left over.

Chapter 3

Overview of the Algorithm and Structure of the Program

3.1 Introduction

The idea of obtaining more or less a valid plasma physics using a computer to trace the charged particles till their fusion was proposed by many people as early as 1950's . The development of computers and considerable research on the the numerical techniques has led to the refinement these algorithms . The simulation tools are now capable of producing almost all the electric and magnetic interactions as they occur in real plasmas.

A simulation of real laboratory plasma using a particle approach will lead to the obvious difficulty of storing the position and velocity vectors for all the particles in the computer's volatile memory for processing . To avoid this the simulation algorithm uses a reduced number of particls each with large charge and mass keeping the charge to mass rato neraly same for electrons . This

results in increasing fluctuations about the mean (say, of density, $\approx 1/\sqrt{n}$) called as the *shot noise*. Another difficulty is the non-physical interaction of the particles with the spatial and temporal grid used for computing the quantities such as the charge densities, plasma potential, electric field and forces, which also results in increased noise, called the, *grid noise*. If the noise level rises above a limit it can mask out the desired simulation.

With the present day fast processors and volatile memory (or RAM) available in the range of few Mbytes to something around Gbytes one can attempt to reduce these noise levels by increasing the number of particles and using a finer grid. This can be easily applied in one dimension, can be pushed to two and two and ane-half Dimensions, but presently seems impossible in three dimensional simulations.

3.2 Validity of The Algorithm

An obvious question that may be asked is how a valid physics can be obtained by simulating a real plasma with a density of about 10^{22} $\#m^{-3}$ using a model which uses a few hundred particles? Before answering this question the definition of plasma has to be considered .

Definition of Plasma

A plasma is a conglomeration of positively and negatively charged particles. It is on an average neutral, as the total negative and positive densities are same. The plasma is said to be *fully ionized* if it does not contain any neutral species. A fully ionized plasma has two kinds of charge carriers : free electrons and positive ions. Sometimes it also contains negative ions and more than one kind of positive ions. Ions may be singly charged or multiply charged; they

may also be atomic or molecular.

Any ionized gas can't be called a plasma, as there is always some small degree of ionization in any gas. So a complete definition of plasma can be constructed as follows :

A plasma is a quasineutral gas of charged and neutral particles which exhibits collective behavior.

By *quasineutrality* we refer to the fundamental characteristic of the behavior of plasma to shield out electric potentials that are applied to it. For the purpose of definition it can be stated that if L a characteristic dimension the system, is much longer than Debey length λ_D , then whenever a local concentration of charge arises or external potentials are introduced into the system these are shielded out at a distance short compared with L leaving the bulk of the system free of electric potentials.

The term collective behavior comes into picture as a small density perturbation or local concentration of charge produces electric and magnetic fields within the system and affects the motion of other particles.

Physically, electrons and ions are point particles for most of plasma physics. Some interparticle interactions occur at short range in short times, producing effects at short wavelengths and high frequencies. Fortunately the details of such interactions are of little interest for many purposes. The more important effects are the *collective, long range* interactions which produce wavelengths much larger than interparticle spacing and frequencies with periods much larger than the time taken by the particles in crossing the grids. As we are more interested in the collective behavior of the plasma,at wavelengths larger than the Debey length $\lambda \geq \lambda_D$. And secondly the models used are intended to produce the *essence of the plasma* without all of its details. Since we simulate over limited time and space , small errors are tolerated and use of

ion-to-electron mass ratios (m_i/m_e) like 10 or 100 is used.

3.3 Overview of the Program

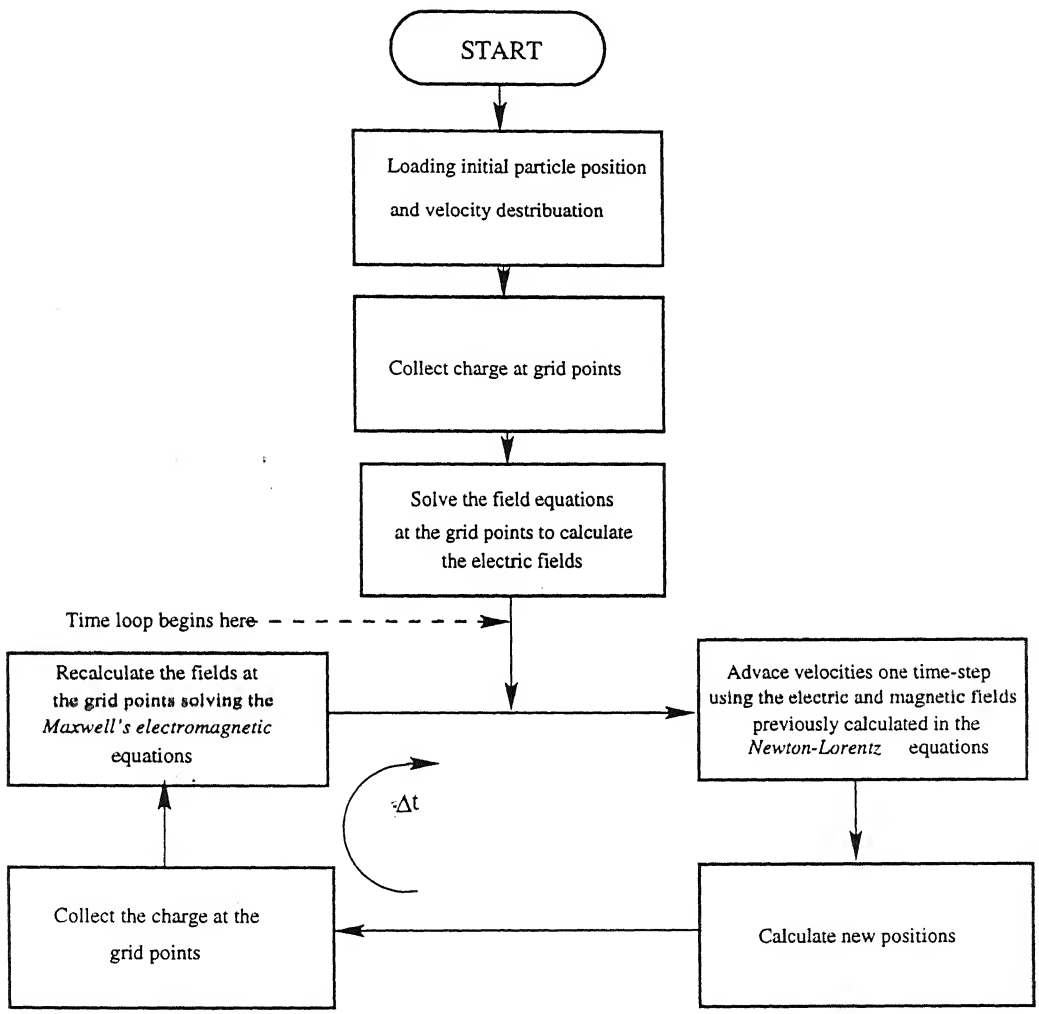

Figure 3.1: *A typical time cycle in the program. The time loop is repeated for each desecrate time step till a specified time is reached.*

The program discretizes time and proceeds discontinuously with finite time steps, thus using digital rather than an analog computation. In each time

cycle the fields are calculated about spatial the grid points solving *Maxwell's electromagnetic equations*, knowing the positions and velocities of the particles. These calculated electric and magnetic fields are substituted in the *Newton-Lorentz* equations of motion to calculate the forces on the particles. The forces are then used to calculate the velocities in next time step and hence the positions. This procedure is repeated at every time step (see Fig: 3.1). The time cycle starts at $t = 0$, with specified initial conditions for positions and velocities . The program runs for a specified number of time steps.

3.4 Particle Weighting

At any time step the program calculates the fields at the grid points by collecting the charges around the grid. This procedure of collecting the charges from the particle position coordinates is called *weighting*. The weighting may be of *first-order*, *second-order* or *higher-order* depending upon the order of the equation used in the interpolation. A number of weighting schemes are available for any order. PIC or *Particle-In-Cell* being the most widely used first-order scheme is followed in this program.

3.4.1 The Particle-In-Cell Method

Originally developed by Frank Harlow [*Harlow*(1964)] and collaborators at Los Alamos in 1955 for doing multidimensional compressible fluid computations, this scheme gained a wide popularity in the particle simulation area. The basic ides of PIC is to combine the best of the Eulerian and Lagrangian features. The numerical instability and mass diffusion of the Eulerian methods and the cell distortion difficulties of the Lagrangian methods are overcome. The region of interest is divided into Eulerian cells for purpose of computing the field variables and the material is transported from cell to cell, as in the Lagrangian

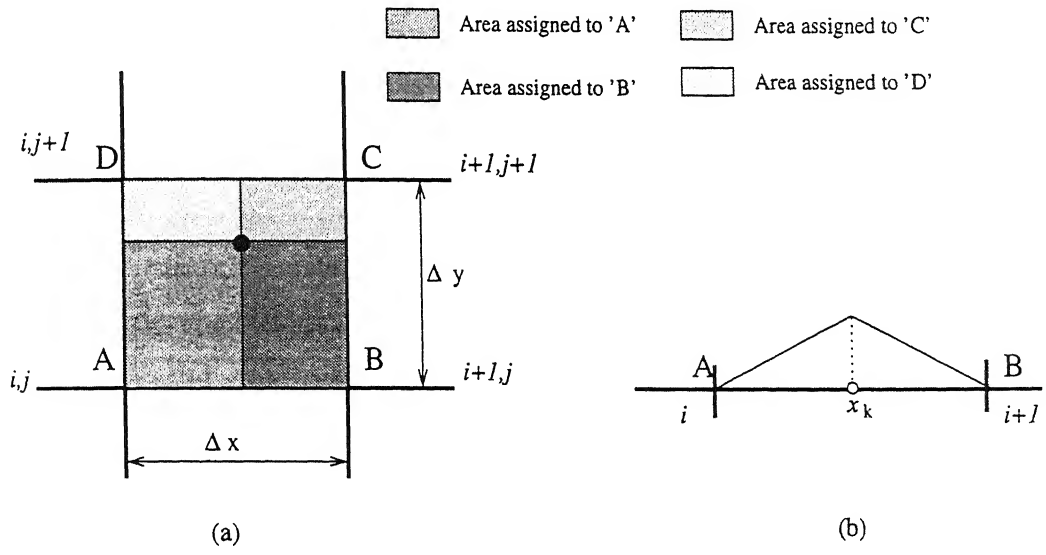

Figure 3.2: *PIC weighting used in charge assignment showing the (a) area assigned to the various grid points in 2D, and (b) effective particle shape $S(x)$ in 1D.*

approach, in the form of disecrate simulation particles. In the compressible fluid computations, where this scheme was applied first, the velocity is a single valued function of position and therefore is a grid quantity. On the contrary, in collisionless plasma computations their is a distribution of particles at every point in space, and it become important to treat the microstructure in detail in order to obtain important physics. Accordingly, velocity becomes particle quantity, and a simulation particle represents a number of real particles with the same electric charge, mass, position and velocity. The grid quantities then are the summed up charges and electric fields calculated using the above procedure .

The PIC scheme is also called the *area weighting* or *bi-linear weighting* due to its geometric interpretation. As shown in (Fig: 3.2(a)), the weights are given as :

$$\rho_{j,k} = \rho_c \frac{(\Delta x - x_k)(\Delta y - y_k)}{\Delta x \Delta y}$$

$$\rho_{j+1,k} = \rho_c \frac{x_k(\Delta y - y_k)}{\Delta x \Delta y}$$

$$\rho_{j,k+1} = \rho_c \frac{(\Delta x - x_k)y_k}{\Delta x \Delta y}$$
$$\rho_{j+1,k+1} = \rho_c \frac{x_k y_k}{\Delta x \Delta y}$$

where, $x_k$andy_k are particle positions relative to the grid point (i, j), ρ_c is the uniform charge density filling the cell ($\sum_j q_j/A$, where $j = 1, \cdots$, total no. of particles in the cell and A = cell area). In order to resolve the details deemed necessary and avoid non-physical instabilities the grid size must be kept as small as possible, whereas, in order to make the program computationally possible or inexpensive the grid size must be large. Thus an optimization is required to cater to both the needs.

In one-dimension the PIC is just a linear interpolation between two adjacent grid points and hence the *shape factor* ($S(x)$) (see Fig: 3.2(b), produced is triangular in shape.

The forces are calculated in a manner similer to the one used in the assignment of charges. Considering the fields on the grid points, a reverse interpolation is made and forces are assigned to the particles.

Various other schemes are also available for calculating shape factors. The most commonly used schemes in the particle simulation are :

- **NGP** or Nearest Grid Point (*Zeroth-order*) [*Birdsall and Langdon*(1986)],
- **CIC** or Cloud-in-Cell (*First-order*) [*Birdsall and Fuss*(1969)],
- **Multipole Expansion** (*First-order*) [*Dawson et al.*(1973)],
- **Energy Conserving** (*First-order*) [*Lewis*(1970)], etc.

each having its own advantages and disadvantages. Our program is designed to use the NGP, PIC, CIC and Energy Conserving schemes and prompts the user for his choice.

3.5 Integration of Field Equations

After the charges are collected at the grid points the electric and magnetic fields are calculated using the Maxwell's equations. Due to the density perturbation of electrons and ions the electric field generated is given by Eqn. 2.1:

$$\begin{aligned} \nabla \cdot \mathbf{E} &= \frac{q4\pi}{\epsilon_0}(n_i - n_e), \\ &= \frac{\rho}{\epsilon_0} \end{aligned} \tag{3.1}$$

where, ρ is the charge density. Solving Maxwell's equations for an electrostatic approximation discussed in Sec. 2.2.1 we have:

$$\begin{aligned} \nabla \times \mathbf{E} &= \frac{\partial \mathbf{B}_0}{\partial t} \approx 0, \quad \text{so that,} \\ \mathbf{E} &= -\nabla\phi \end{aligned} \tag{3.2}$$

Using Eqs. 3.1 and 3.2 we obtain the *Poisson's Equation*,

$$\nabla^2\phi = -\frac{\rho}{\epsilon_0} \tag{3.3}$$

$$\Rightarrow \frac{\partial^2 E_x}{\partial x^2} = -\frac{\rho}{\epsilon_0} \quad \text{(in 1D)} \tag{3.4}$$

$$\Rightarrow \frac{\partial^2 E_x}{\partial x^2} + \frac{\partial^2 E_y}{\partial y^2} = -\frac{\rho}{\epsilon_0} \quad \text{(in 2D)} \tag{3.5}$$

Once the charge densities at all the grid points are known, they become the right hand side of the *Poisson's equation*,

$$\nabla^2\phi(x,y) = -\rho(x,y) \tag{3.6}$$

with the following finite deference form :

$$\frac{(\Delta\phi_{i+1,j} + \Delta\phi_{i-1,j} - 2\Delta\phi_{i,j})}{\Delta x^2} + \frac{(\Delta\phi_{i,j+1} + \Delta\phi_{i,j-1} - 2\Delta\phi_{i,j})}{\Delta y^2} = -\rho_{i,j} \tag{3.7}$$

The above set of equations is solved for all $\phi_{i,j}$ using appropriate boundary conditions (open, bounded, periodic, etc.). The GS-SOR iterative technique is used in 2D case; for 1D case the equation is simply of the form :

$$\frac{(\Delta\phi_{i+1} - \Delta\phi_{i-1})}{2\Delta x} = -\rho_i, \tag{3.8}$$

and is solved by Gauss elimination using Thomas algorithm.

Once the plasma potential ϕ is known at all the grid points the $\mathbf{E}$'s are obtained using Maxwell's equation,

$$\mathbf{E}(\mathbf{x}) = -\nabla\phi(\mathbf{x}), \tag{3.9}$$

with the two point, Center Space finite difference form being:

$$(E_x)_{i,j} = -\frac{(\phi_{i+1,j} - \phi_{i-1,j})}{2\Delta x}, \tag{3.10}$$

$$(E_y)_{i,j} = -\frac{(\phi_{i,j+1} - \phi_{i,j-1})}{2\Delta y}. \tag{3.11}$$

This completes the integration of the field equations. The model being electrostatic ($\partial\mathbf{B}_0/\partial t \approx 0$), only static magnetic ($\mathbf{B_0}$) fields are to be used in the Newton-Lorentz equations of motion.

3.6 Integration of Equations of Motion

The charge density at the laboratory coordinate $\mathbf{x}'$ of a cloud whose center is at $\mathbf{x}$ is changed from $q\delta(\mathbf{x}' - \mathbf{x})$ for a point particle, to $qS(\mathbf{x}' - \mathbf{x})$ for a cloud,where q is the total charge given by $q\int d\mathbf{x}' S(\mathbf{x}' - \mathbf{x})$. If $\mathbf{J_p}$ and ρ_p are the current and charge densities of a system of point charges located at the $(\mathbf{x}')$, then the densities $\mathbf{J}_c$ and ρ_c for a system of clouds, whose centers coincide with the point particles are [*Birdsall and Langdon*(1986)]:

$$\begin{bmatrix} \rho_c(\mathbf{x},t) \\ \mathbf{J}_c(\mathbf{x},t) \end{bmatrix} = \int d\mathbf{x}' S(\mathbf{x}' - \mathbf{x}) \begin{bmatrix} \rho_p(\mathbf{x}',t) \\ \mathbf{J}_p(\mathbf{x}',t) \end{bmatrix}. \tag{3.12}$$

These clouds, when used in Maxwell's equation, give the electric ($\mathbf{E}$) and magnetic ($\mathbf{B}_0$) fields. The Newton-Lorentz force on one cloud of total change q, with (center) position $\mathbf{x}$ and velocity $\mathbf{v}$ is then [*Birdsall and Langdon*(1986)]

$$\mathbf{F}(\mathbf{x},\mathbf{v},t) = q\int d\mathbf{x}' S(\mathbf{x}'-\mathbf{x})\cdot\left[\mathbf{E}(\mathbf{x}',t)+\mathbf{v}\times\mathbf{B}_0(\mathbf{x}',t)\right]. \tag{3.13}$$

In simple form this equation can be written as (which essentially the form given by Eqn. 2.13

$$m\frac{d\mathbf{v}}{dt} = \mathbf{F}, \tag{3.14}$$

$$\frac{d\mathbf{x}}{dt} = \mathbf{v}, \tag{3.15}$$

where,

$$\begin{aligned}\mathbf{F} &= \mathbf{F}_{electric}+\mathbf{F}_{magnetic}\\ &= q(\mathbf{E}+\mathbf{v}\times\mathbf{B}_0)\end{aligned}$$

In our $2\frac{1}{2}$D case (see Fig: 3.3), the position is resolved in x and y directions and velocity is resolved in v_x, v_y and v_z components. In order to include the $\mathbf{E}\times\mathbf{B}_0$ drift in the model, so as to study the dynamics of ion component of the plasma, the magnetic field is tilted with respect to the z axis in the xz-plane. In this case the static magnetic field $\mathbf{B}_0$ is making an angle θ with the z direction. The self-consistent electric field $\mathbf{E}$ and wave vector $\mathbf{k}$ are along x-axis. Then $v_{\|}$ is the parallel velocity of the particles (along $\mathbf{B}_0$) and $v_{\perp}$ is the perpendicular velocity (along x direction). At this point it is convenient to solve the motion in the parallel and perpendicular directions with respect to $\mathbf{B}_0$ which leads to the invention of a new coordinate axis x' perpendicular to $\mathbf{B}_0$ and making an angle θ with x-axis. Due to this third axis this model is sometimes called a *two and one-half dimensional* model.

In this new coordinate system the Eqs. 3.14 and 3.15 are solved using commonly used integration called *leap-frog method.* In the leap-frog scheme the

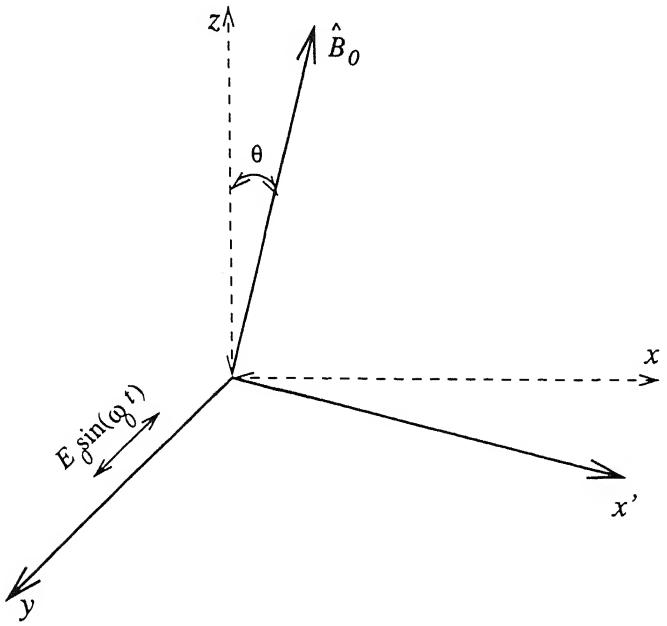

Figure 3.3: *The two and one-half dimensional simulation model for the lower hybrid heating in linear regime. External E_0 is along y direction, B_0 in the xz plane. Self consistent field in the xy plane.*

finite-difference form of the equations is [*Birdsall and Langdon*(1986)]:

$$\frac{\mathbf{v}_{t+\Delta t} - \mathbf{v}_t}{\Delta t} = \frac{1}{m}\mathbf{F}_t, \tag{3.16}$$

$$\frac{\mathbf{x}_{t+\Delta t} - \mathbf{x}_t}{\Delta t} = \mathbf{v}_t, \tag{3.17}$$

where $\mathbf{v}_{t+\Delta t}$ and $\mathbf{x}_{t+\Delta t}$ are new values of velocities and position respectively in time, as against $\mathbf{v}_t$ and $\mathbf{x}_t$ which are old and therefore known values.

In the leap-frog integration there is a phase difference of half a time step in position and velocity. Thus the velocity is lagging by half a time step with respect to the position. Thus in order to adjust the kinetic energy (due to v) and the potential energy (due to x) at same time an additional work is to be done in shifting the velocities by half a time-step forward using the force F calculated at $t = 0$.

With only a static magnetic field B_0 (as our model is electrostatic) the term $q(\mathbf{v} \times \mathbf{B}_0)$ in the Newton-Lorentz equation is just a rotation of $\mathbf{v}$, i.e., $\mathbf{v}$ does not change in magnitude. However, $q\mathbf{E} = \hat{x}qE_x + \hat{y}qE_y$ does affect the v_x and v_y components of $\mathbf{v}$. Hence a physically reasonable scheme, proposed by Boris [*Boris*(1970)] is used. It is centered in time as follows :

The equation of motion for the particles to be integrated is

$$\frac{d\mathbf{v}}{dt} = \frac{q}{m}(\mathbf{E} + \mathbf{v} \times \mathbf{B}_0). \tag{3.18}$$

The finite-difference form of Eqn. 3.18 using *Center-Time* scheme is

$$\frac{\mathbf{v}_{t+\Delta t/2} - \mathbf{v}_{t-\Delta t/2}}{\Delta t} = \frac{q}{m}\left(\mathbf{E} + \frac{\mathbf{v}_{t+\Delta t/2} + \mathbf{v}_{t-\Delta t/2}}{\Delta t} \times \mathbf{B}_0\right). \tag{3.19}$$

The vector equation for $\mathbf{v}_{t+\Delta t/2}$ can be solved for three simultaneous scalar equations, one for each component. Other than this the the method suggested by Boris, which separates the electric and magnetic forces completely is used. Accordingly,

$$\mathbf{V}_{t-\Delta t/2} = \mathbf{v}^- - \frac{q\mathbf{E}}{m}\frac{\Delta t}{2}, \tag{3.20}$$

$$\mathbf{V}_{t+\Delta t/2} = \mathbf{v}^+ + \frac{q\mathbf{E}}{m}\frac{\Delta t}{2}. \tag{3.21}$$

Substituting these equations in Eqn. 3.18

$$\frac{\mathbf{v}^+ - \mathbf{v}^-}{\Delta t} = \frac{q}{m}\left(\mathbf{v}^+ + \mathbf{v}^-\right) \times \mathbf{B}_0 \tag{3.22}$$

This leaves only the rotation of $\mathbf{v}$. The equations of motion in the (x', y, B_0) coordinates are then integrated in three steps:

1. add half acceleration to $\mathbf{v}_{t-\Delta t}$ to calculate $\mathbf{v}^-$,
2. rotation of velocity as per Eqn. 3.22 to calculate $\mathbf{v}^+$,
3. again adding an half acceleration to calculate $\mathbf{v}_{t+\Delta t}$.

This is commonly called as *accel-rot-accel* scheme.

Consider the case where $\mathbf{B}_0$ is parallel to z axis. In the $x-y$ plane the rotation is through an angle θ where,

$$\tan\frac{\theta}{2} = -\frac{qB_0}{m}\frac{\Delta t}{2}.$$

In the electrostatic case B_0 is fixed, thus,

$$\tan\frac{\theta}{2} = -\tan\left(\frac{qB_0}{m}\frac{\Delta t}{2}\right) = \tan\left(\Omega_k\frac{\Delta t}{2}\right).$$

Let

$$t = -\tan\frac{\theta}{2}$$

then using the half angle formulas, we have

$$s \equiv -\sin\theta = \frac{2t}{1+t^2},$$

$$c \equiv \cos\theta = \frac{1-t^2}{1+t^2}.$$

Then as per the Boris scheme the rotation becomes

$$\begin{bmatrix} c & s \\ -s & c \end{bmatrix}\begin{bmatrix} v_x^- \\ v_y^- \end{bmatrix} = \begin{bmatrix} v_x^+ \\ v_y^+ \end{bmatrix}.$$

In our case when the directions of $\mathbf{B}_0$ and $\mathbf{v}$ are arbitrary, the method proposed by Boris is used. First $\mathbf{v}^-$ is incremented to produce $\mathbf{v}'$ which is perpendicular to $(\mathbf{v}^+ + \mathbf{v}^-)$ and $\mathbf{B}_0$. Then

$$\mathbf{v}' = \mathbf{v}^- + \mathbf{v}^- \times \mathbf{t}.$$

Since the angle between $\mathbf{v}^-$ and $\mathbf{v}'$ is $\theta/2$, we have

$$\mathbf{t} \equiv -\hat{\mathbf{b}}\tan\frac{\theta}{2} = \frac{q\mathbf{B}_0}{m}\frac{\Delta t}{2}.$$

Finally, $(\mathbf{v}^+ + \mathbf{v}^-)$ is perpendicular to $\mathbf{v}' \times \mathbf{B}_0$, so

$$\mathbf{v}^+ = \mathbf{v}^- + \mathbf{v}' \times \mathbf{s},$$

where s is parallel to $\mathbf{B}_0$ and its magnitude is determined by the requirement $|\mathbf{v}^-|^2 = |\mathbf{v}^+|^2$:

$$\mathrm{s} \equiv \frac{2\mathrm{t}}{1+t^2}.$$

The scalar equations of this vector form in (x', y, B_0) can be written as:

$$\begin{aligned} v_{x_1'} &= v_x(t-\Delta t/2) + \frac{q}{m}\frac{\Delta t}{2}E_x\cos\theta \\ v_{y_1} &= v_y(t-\Delta t/2) + \frac{q}{m}\frac{\Delta t}{2}E_y + \frac{q}{m}\frac{\Delta t}{2}E_{ext} \end{aligned}$$

$$\begin{aligned} v_{x'}(t+\Delta t/2) &= cv_{x_1'} + sv_{y_1} + \frac{q}{m}\frac{\Delta t}{2}E_x\cos\theta \\ v_y(t+\Delta t/2) &= -sv_{x_1'} + cv_{y_1} + \frac{q}{m}\frac{\Delta t}{2}E_y + \frac{\Delta t}{2}E_{ext} \\ v_{\hat{B}_0}(t+\Delta t/2) &= v_{\hat{B}_0}(t-\Delta t/2) + \frac{q}{m}\frac{\Delta t}{2}E_x\sin\theta. \end{aligned}$$

As discussed above the complications arising due to the initial conditions for x and v being specified at the same time, i.e. at $t = 0$, and the main loop running with v leading x by half the time step, i.e. by $\Delta t/2$, are resolved by first rotating $\mathbf{v}(0)$ by an angle $\Delta\theta = +\Omega\Delta t/2$ and applying half acceleration using $-\Delta t/2$ based on $\mathbf{E}(0)$ obtained from $\mathbf{x}(0)$. This point is discussed in detail in [*Birdsall and Langdon*(1986)].

3.7 Initial Particle Loading

Starting with prescribed density profiles for position n_0(x,y) and velocity $f_0(\mathbf{v})$, i.e. the velocity distribuation function, and assigning initial particle position $(\mathbf{x},\mathbf{v})_i$, is termed as *initial particle loading* in particle simulation language. The formal process is called *inversion of the cumulative density.*

3.7.1 Position Loading

Assigning particle position $(x, y)_i$ from the known density is called *Position loading*. As a *weakly homogeneous* plasma is considered in this model, the density distribution is a linear function of x while it is constant in rest of the coordinate directions. The linear function must be such that a variation of 2:1 is achieved in the positive x direction. This function is generated by the program using equation

$$n_0(x) = a(1.0 + x/L_x),$$

where a is calculated such that if n_{x0}, n_{y0} are total number of particles in respective coordinate directions,

$$\sum_{x=0}^{L_x} (n_0(x))_x = n_{x0}.$$

Thus, a general form of equation can be written as

$$\begin{aligned} \mathrm{y}_i &= L_y/n_{y0}, \\ \mathrm{x}_i &= L_x/n_0(\mathrm{x}). \end{aligned}$$

3.7.2 Velocity Loading

The model considers only the Maxwellian or Gaussian particles where the velocity distribution in v is Maxwellian (or Gaussian) of the form $\exp(-v^2/2v_{th}^2)$. Then using the method of *inverting Gaussian* the velocities are assigned to the particles. A thermodynamic equilibrium distribution, which is Maxwellian, is of the form given in Fig: 3.4. Around 99% of the particles are in region $v/v_{th} = 3$ and thus we place all the particles in the region $v = v_{th}$.

Let R_s be a set of uniformly distributed random numbers varying from 0 to 1. Then the cumulative distribution function for $v =\mid \mathrm{v} \mid$ is

$$v_y = R_{12} v_{th}$$
$$v_z = R_{12} v_{th}$$

where, $R_{12} = (\sum_{i=1}^{12} R_i - 6.0)$, and R_i is a random number between 0 and 1.

3.8 Organization of the Program

The program is divided into different modules as per their functions; each source module is therefore dedicated for one particular operation. The details of various modules and a brief schematic flow-diagram is as follows.

Input The required data is read either from the input file or from the screen as specified. The input file is created using a special program module *input* which is run separately.

Init After the data is read the module *init* is invoked which does the initial position and velocity loading.

ranf Assigns a Maxellian's distribution to the particle velocity profile.

norm_vx Here the velocities are shifted half a time step back on time scale. This module invokes module *advance* for the purpose. *Advance* is thus shared by *norm_vx* and *accel.* Thus the input values assigned to *advance* are important, and accordingly *advance* shifts velocity either forward in time or backward.

bnd_condn Boundary conditions are applied using this module. This module is designed to apply either singly periodic, doubly periodic or open circuit boundary conditions.

set_rho Set_rho is used to collect charges as per the weighting specified.

fields The grid quantities are calculated using *fields*. *Fields* invokes module *Poisson_solver* to solve the field equations.

Poisson_solver The Poisson's equations are solved using this module. For 2D case it uses a GS-SOR iterative method and for 1D Thomas algorithm based on the Gauss-elimination is used.

advance As per the weighting specified this module calculates the force on each particles. Then substituting the electric and magnetic fields calculated earlier in other modules it solves the Newton-Lorentz force equations to calculate the velocities in next time step.

accel Calculates velocities in next time step by invoking *advance*.

move Advances the position using the new velocity calculated in module *accel*.

The program starts by reading the input either from a keyboard or from the input file created by module *input* (see Fig: 3.5). At $t = 0$ modules *init, norm_vx and bnd_condn* are executed for each species. Modules *set_rho* and *fields* are then invoked to calculate initial fields.

After completing the initial processing at $t = 0$ the program steps into the time loop. At the start of the time loop module *accel* is executed followed by *move*. Module *plots* does the job of making a copy of specified variables at specified time steps on a magnetic tape. Finally the charges are recollected knowing the new positions and velocities. The time iteration ends with calculating fields at grid points; the program then starts the next time iteration beginning with *accel*. This process is repeated for a specified number of time cycles. After coming out of the time loop, the program ends making history plots for kinetic energy.

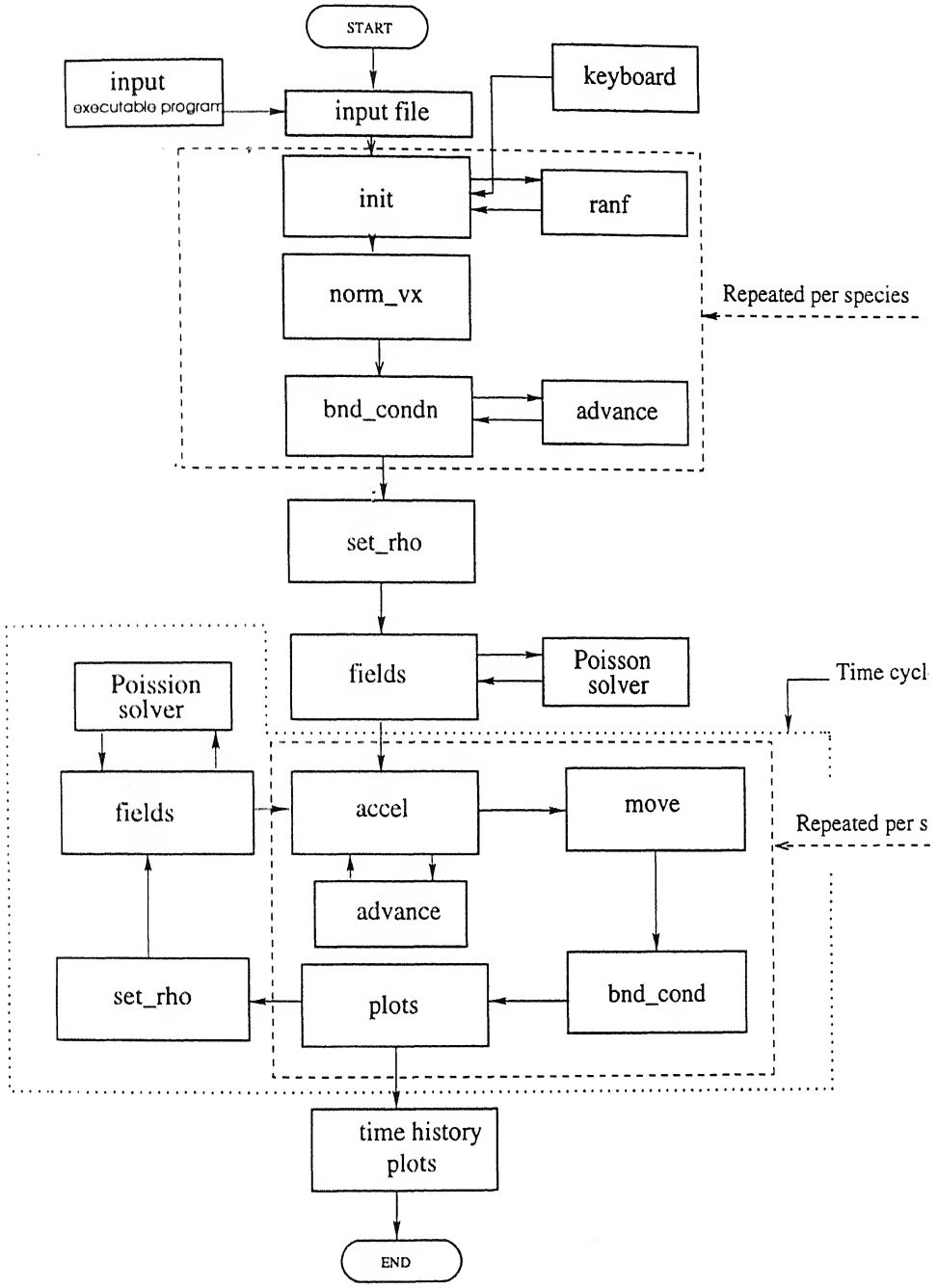

Figure 3.5: *A schematic diagram showing a typical run. The names in the boxes represents the actual filenames of various modules used in the program.*

3.9 About the Program

The program is developed in C++ to take the advantage of the *Object Oriented Programming* or OOP's facilities provided by it. The compilation was done using GNU C++ compiler *g++*. Error handling was done with *LINT* package on *Digital Unix version V3.2C (rev. 148)*. For the purpose of fast compiling the use of *archives* was made. The program modules are listed in the archive file named *mainlib.a*. The code processing was done via SCCS (Source Code Control System) to keep the record of major changes in the source files. Debugging was done in GNU debugger *gdb*. Finally the platform used was Digital Unix version V3.2C on DEC-Alpha dual processor machine.

At various points in the code the concept of dynamic memory allocation is used so as to save the floating memory (RAM) consumption. This increases the speed considerably and also improves the memory mapping performance of the processor thereby increasing the floating point accuracy. The output files generated for various variables are according to the specification of various graphic packages, so that they can be directly loaded on any of them. The program offers the facility of producing directly the input file for *Gnuplot*, a generally used graphic package on UNIX operating systems, for plotting the phase-space plots in one or two dimensions in space and any one dimension in phase.

Chapter 4

Discussion of Results

4.1 Computer Model

An two and one-half dimensional (v_x, v_y, v_z, x, y) electrostatic particle simulation code has been used. The field quantities and the particle positions are two dimensional, while all the three velocity components are retained in the particle orbits. Doubly periodic boundary conditions were used. The fields are periodic in the direction of the external applied (static) magnetic field($\hat{z}$) and bounded in the perpendicular ($\hat{x}$) direction. For the purpose of this simulation, finite-sized (Maxwellian) particles are used.

For the simulation results presented here, vacuum boundary conditions are imposed in the $\hat{x}$ direction at $x = 0$, i.e., no charge exists outside the boundary. The model is made periodic in rest of the boundaries. The physical consequence of these boundary conditions is that, the charges which cross one boundary (say, at $y = L_y$) are represented at the previous boundary (i.e., at

$y = 0$) as image charges with same parameters as velocity, etc. Thus, the plasma model in this case represents a slice of an infinite plasma. Also with such boundary conditions we can avoid the effects of surface waves and sheaths, and therefore can isolate the lower hybrid waves.

The external electric fields are applied as oscillating charges at one of the boundary. In this model we have specified these sources at $x = 0$ and due to the periodicity they appear as image sources at $x = L_x$. The static external magnetic field is specified at an arbitrary angle θ with respect to the $\hat{z}$ as shown in Fig. 3.3. The full dynamics of the particles are used and there is no guiding centre approximation made in this code. Finite-sized particles are followed with their self consistent fields plus the externally applied driving fields.

The initial plasma density is taken uniform in y and weakly inhomogeneous (with a density variation of 2:1) in x direction having the maximum density at $x = L_x$. Different initial temparature profiles are used for both the species and are uniform in space. These are specified as temperature ratios. The initial electron thermal velocity was choosen to be $v_{the} = 0.75\delta\tilde{\Pi}_e$, where δ is the finite grid spacing used in the simulation, and $\tilde{\Pi}_e$ is the average plasma frequency. The dimensionless, average Debye length $\tilde{\lambda}_{D_e}$ is then 0.75, where $\tilde{\lambda}_{D_e}$ is defined as $\tilde{\lambda}_{D_e} = v_{the}/\delta\Pi_e$. The ratio of electron cyclotron frequency to average plasma frequency (Ω_e/Π_e) of 1.5 is used. Except when otherwise specified, ion to electron mass ratio (m_i/m_e) of 100.0 is used throughout. A time step of $0.25\Pi_e^{-1}$ is used to filter out the high frequency phenomena and isolate the low frequency, lower hybrid, physics. The reflection of the particles implies that there is no mechanism for net energy loss in the system. Number of grid points used is $L_x/\delta = L_y/\delta = 64$.

The external source in this simulation is determined by specifying an external surface charge density oscillating with a specified frequency ω_0 on one of the boundary. Because the magnitude of the charge density is fixed externally, such

a source corresponds to a constant current driver. The phase of oscillation is such that the fields generated by these charges are zero initially. This is also called as a *quasi-adiabatic turn on.*

4.2 Organization of the Results

The results are organized in the form of different sets, each set containing the results collected for different parameter values as given below :

Set I Keeping the temperature profile same results are presented varying the ion to electron mass ratio to see the effect of using different mass ratio on the nature of the curve.

Set II Results are presented for different exciter frequencies keeping the ion to electron mass ratio and electron to ion temperature ratio constant.

Set III To see the effect of temperature on heating of various species, the mass ratio is kept constant while the temperature ratio is varied.

Set IV Results are collected for various values of magnetic fields.

Set V Results are presented regarding the spatial variation of kinetic energy for both the plasma components.

4.3 Simulation Results

As the aim of this work is to study the mechanism of the heating phenomena in plasmas, the results are discussed on the basis of the time evolution of kinetic energies of the species. Instead of considering the total kinetic energy, the kinetic energy calculated using the most significant velocity component

(i.e., $v_{\|}$ or $v_{\perp}$) of the species is considered. Thus, for the ion case the perpendicular kinetic energy ($W_{\perp} = \frac{1}{2}(mv_{\perp}^2)_i$) is considered, while for the electron case the parallel kinetic energy ($W_{\|} = \frac{1}{2}(mv_{\|}^2)_e$) is considered. Energies in the simulation are normalized to initial total electron thermal energy. Thus [*Decyk et al.*(1980)]

$$W_{\|}^e = \frac{1}{3N_p\kappa T_e} m_e \sum_j (v_{\|}^2)_j$$

$$W_{\perp}^i = \frac{1}{3N_p\kappa T_e} m_i \sum_j (v_{\perp}^2)_j$$

If τ is the nondimensional time then $\tau = t\Pi_e$. Thus, the abscissae physically represent the number of plasma cycles at electron plasma frequency, while the ordinates represent the kinetic energy calculated using the msot significant veocity component for the respective species, as a percentage of the total initial kinetic energy.

4.3.1 Set I

As we simulate over a limited time and space small errors are tolerated and ion-to-electron mass ratios (m_i/m_e) like 10.0 or 100.0 are used. Even though, to see the variation of different mass ratios on the nature of heating curve, following results were collected. Keeping the temperature ratio same, $T_e/T_i = 16.0$, mass ratios of $m_i/m_e = 10.0$ and $m_i/m_e = 100.0$ were used. Other parameters were, $k_{\|}/k = 2.5(m_e/m_i)^{1/2}$, $\omega_0/\Pi_e = 0.15$, $\omega_0^2/\omega_g^2 = 1.0$. $\Pi_e = \Omega_e$, $\lambda_{D_e} = 2.0$, $E_0^2/4\pi nT_e = 1/200.0$. Number of particles per species used in the simulation were $2 \times 128 \times 128$ on a 64-cell grid.

Fig. 4.1 to Fig. 4.4 show the results of simulation using a weak pump where the pump energy is small as compared with the initial electron thermal energy ($\alpha = 150$, where alpha is the ratio of initial electron thermal energy to pump field amplitude, both measured in energy units). For the electron case (Fig. 4.1 and

Fig. 4.3), no significant variation in energy is observed for the different mass ratios used. For ions (Fig. 4.2 and Fig. 4.4), even though, $W_{\perp}^{e}$ is observed to be lower than the previous case, the nature of variation of the ion perpendicular kinetic energy is similar for the two mass ratios. The difference is because of the different mass ratios used.

4.3.2 Set II

This set contains results obtained using different exciter frequencies. Keeping the mass and temperature ratios constant results are obtained for different exciter frequencies. The parameter set is as in set I with $E_0^2/4\pi nT_e = 150.0$, $\lambda_{D_e} = 2.0$, $m_i/m_e = 100.0$ and $T_e/T_i = 16.0$.

It is observed that when $\omega_0 > \omega_g$, the ion absorption is hampered (Fig. 4.6 and Fig. 4.8), while the electron absorption increases (Fig. 4.5 and Fig. 4.7).

4.3.3 Set III

The initial temperature profile does have an impact on the absorption of the electromagnetic energy by a species. For higher temperature ratios it is observed that the electron absorption is weakened (Fig. 4.11). On the other hand, no significant difference is observed for the absorption by the ion component of the plasma (Fig. 4.12).

The parameter set used was, $k_{\parallel}/k = 2.5(m_e/m_i)^{1/2}$, $\omega_0/\Pi_e = 0.15$, $\Pi_e = \Omega_e$, $\omega_0^2/\omega_g^2 = 1.0$, $\lambda_{D_e} = 2.0$, $E_0^2/4\pi nT_e = 1/150$. Number of particles per species used in the simulation were $2 \times 128 \times 128$ on a 64-cell grid.

4.3.4 Set IV

As discussed in Sec. 2.4, an electromagnetic wave can propagate in two different ways inside the plasma: (1) when there is a smooth transformation of the electromagnetic waves into the plsama waves, and (2) when the waves do not transform. This mode conversion process is of great importance in the absorption, and therefore, heating of the plasma. Glagolev, in his work [*Glagolev*(1972a)] has derived the condition for the efficient transformation of the electromagnetic wave into the plasma wave depending upon the external static magnetic field. This is given by Eqn. 2.90. Thus, in this set of results we have tried to verify this inequality. The aim was not to find the critical magnetic field, neither to verify the validity of Eqn. 2.90, but to see the nature of the heating curve in case when the magnetic field is very small (or, in fact, negligible for the simulation purpose).

Fig. 4.14 and Fig. 4.13 shows the variation of total electron and ion kinetic energies with time. Major observation here is the absence of the resonance heating of either species. The total heating observed can be explained to be the heating which takes place under the action of pump fields and in accordance with the collisional Joule heating. Thus, these observations state that the transformation of the electromagnetic waves into the plasma has not taken place for this case when the external static magnetic field $\mathbf{B}_0$ is very small.

The parameter set used was, $k_\parallel/k = 2.5(m_e/m_i)^{1/2}$, $\omega_0/\Pi_e = 0.15$, $\Pi_e = \Omega_e$, $\omega_0^2/\omega_g^2 = 1.0$, $\lambda_{D_e} = 2.0$, $E_0^2/4\pi nT_e = 1/150$. Number of particles per species used in the simulation were $2 \times 128 \times 128$ on a 64-cell grid.

4.3.5 Set V

In this set of results we discuss the spatial dependence of the ion perpendicular kinetic energy and electron parallel kinetic energy. As discussed in

Sec. 2.4, the irradiated electromagnetic radiation propagates inside the plasma by first splitting into two waves; the ordinary 'E' and quasi-extraordinary 'H' waves. The 'E' wave having a larger refractive index than the 'H' waves penetrates the plasma and transform into plasma waves. As discussed by Glagolev [*Glagolev*(1972a)], this separation occurs near the plasma boundary. The presence of 'H' waves on the plasma surface skin-layer leads to considerable heating of electrons at this point.

As seen from Fig. 4.18, the energy gain for electrons is inhomogeneous and localized in space within a few electren Larmor diameters from the source. Fig. 4.19 and Fig. 4.20 show the variation in the energy gain with time. It can therefore be concluded that the electron absorption increases with increase in the phase velocity of the waves; and the electron absorption is maximum for small plasma densities.

Like the electron case, the ion spatial kinetic energy distribution is inhomogeneous in space. But as discussed by many authors [*Decyk et al.*(1979)], surface ion heating is not observed; instead, the ion heating was localized almost at the centre of the plasma. This distribution is observed to be varying with time. After almost six plasma cycles the distribution profile is uniform in space.

At the end the phase-space plots for parallel and perpendicular velocity components of electrons and ions respectively are presented (Fig. 4.21 to Fig. 4.29). The the cones observed for both the species are most propbably the resonance cones as predected by the cold plasma theory. Fig. 4.21 and Fig. 4.23 show the sheath region arround the source.

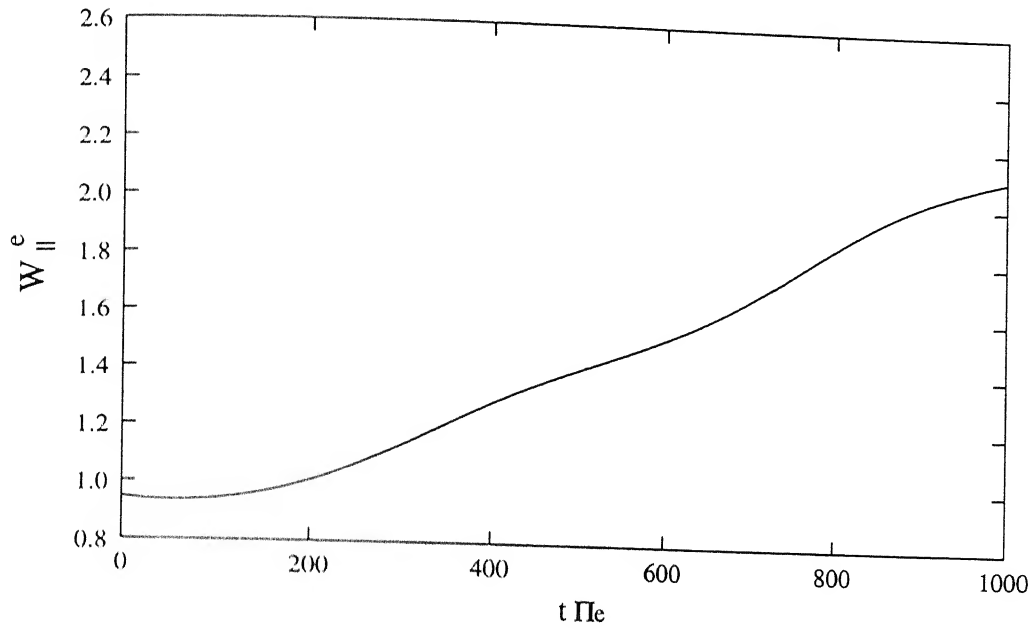

Figure 4.1: *(set I) Time evolution of the electron parallel kinetic energy ($W^e_{\|}$) for m_i/m_e = 10.0*

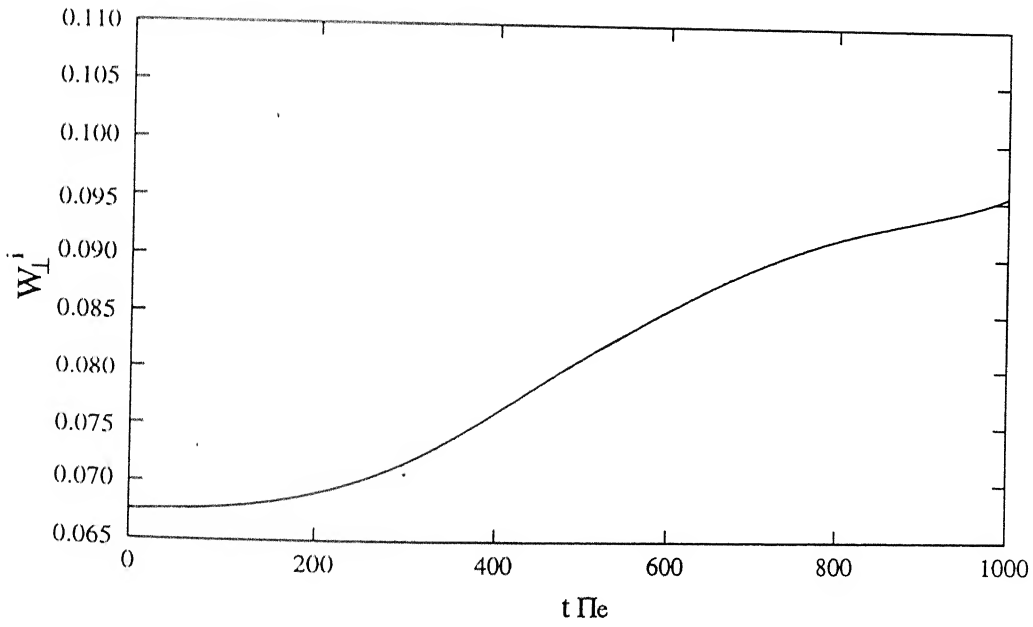

Figure 4.2: *(set I) Time evolution of the ion perpendicular kinetic energy ($W^i_{\perp}$) for m_i/m_e = 10.0.*

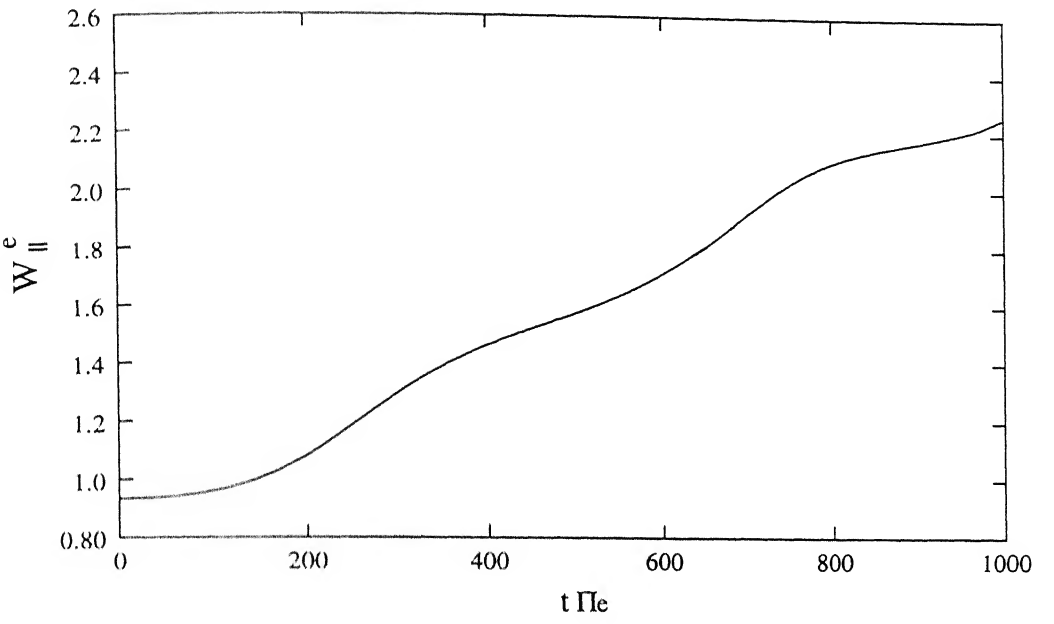

Figure 4.3: *(set I) Time evolution of the electron parallel kinetic energy* ($W^e_{\|}$) *for* $m_i/m_e = 100.0$

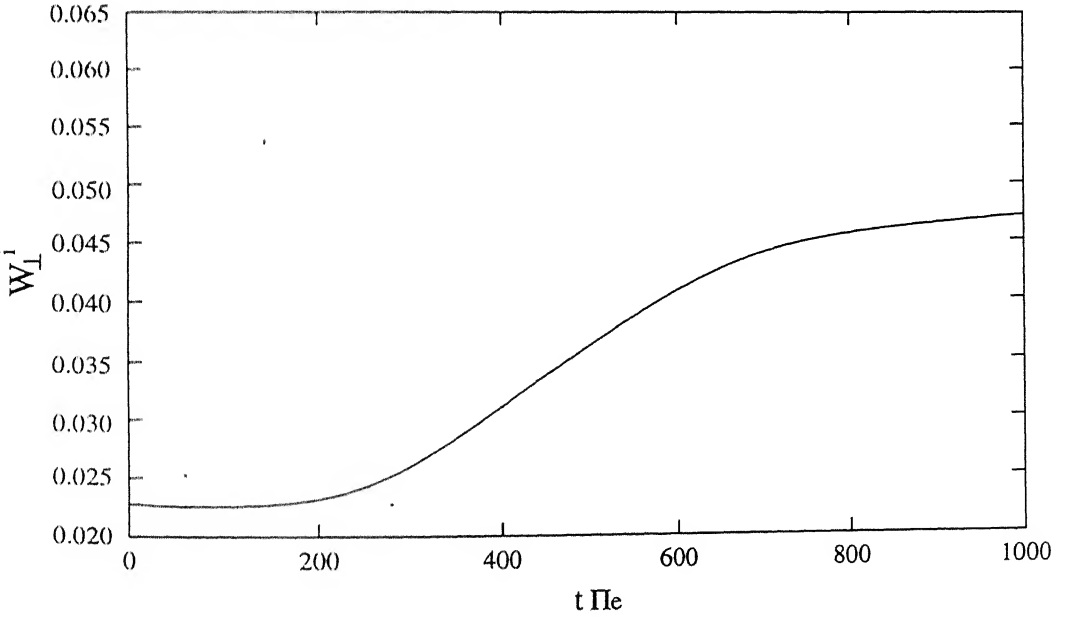

Figure 4.4: *(set I) Time evolution of the ion perpendicular kinetic energy* ($W^i_{\perp}$) *for* $m_i/m_e = 100.0$.

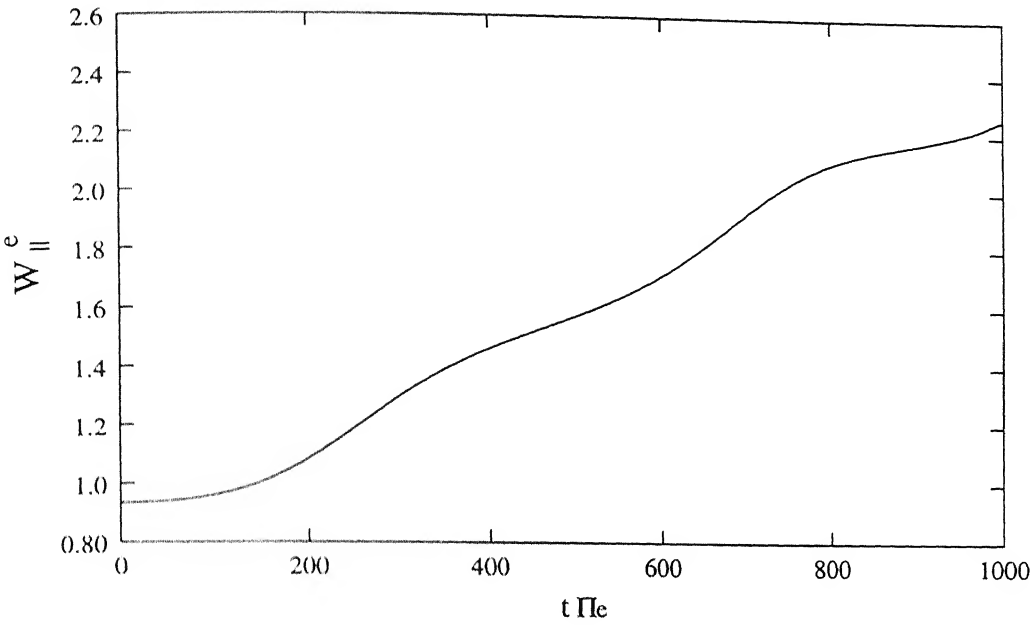

Figure 4.5: *(set II) Time evolution of the electron parallel kinetic energy ($W_{\parallel}^{e}$) for m_i/m_e = 100.0, T_e/T_i = 16.0 and ω_0/ω_g = 1.0.*

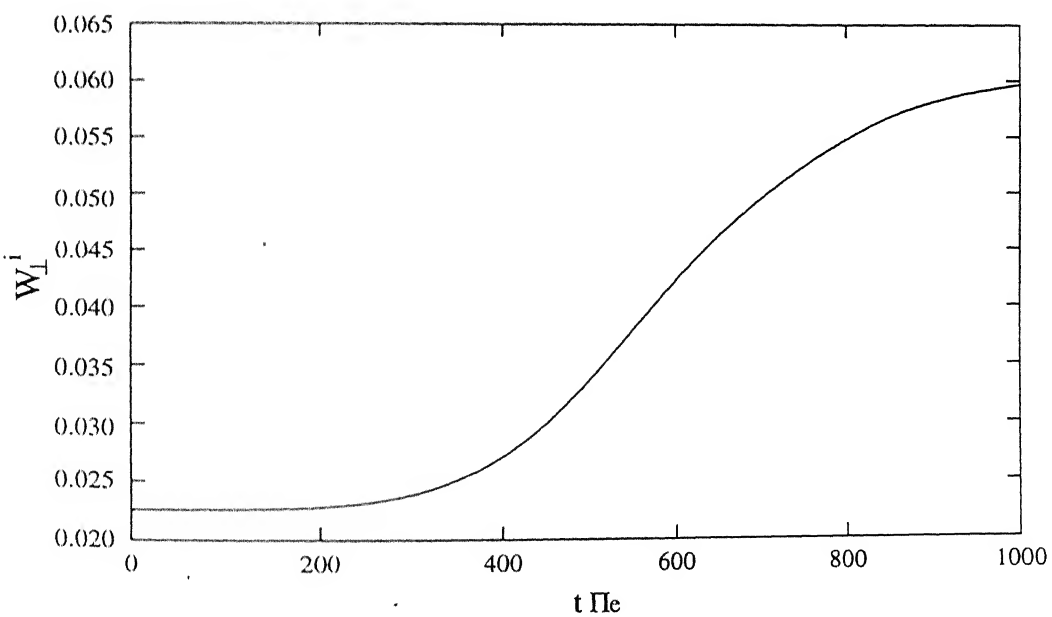

Figure 4.6: *(set II) Time evolution of the ion perpendicular kinetic energy ($W_{\perp}^{i}$) for m_i/m_e = 100.0, T_e/T_i = 16.0 and ω_0/ω_g = 1.0.*

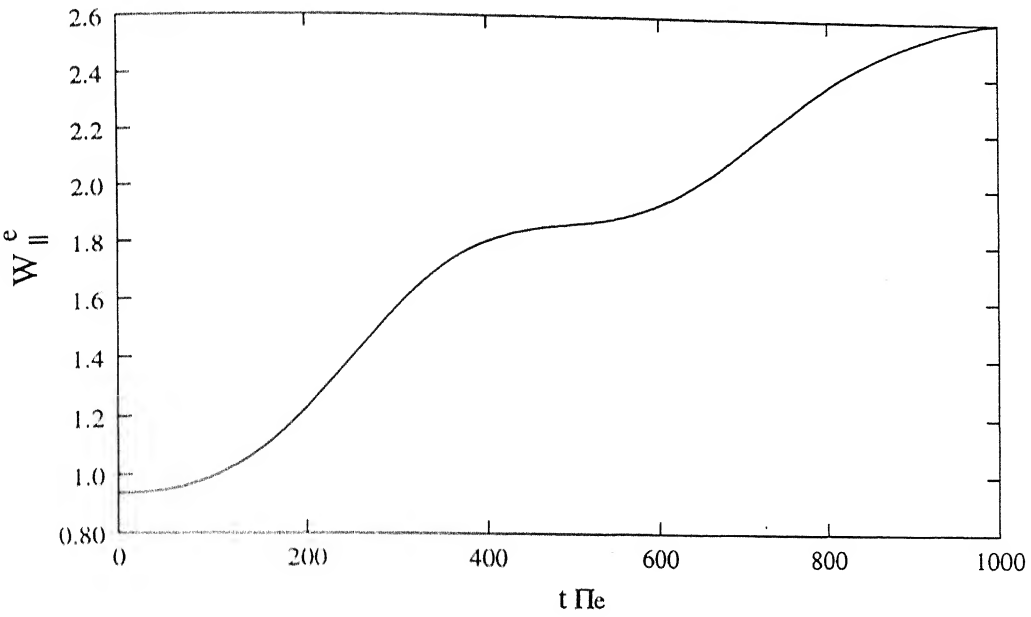

Figure 4.7: *(set II) Time evolution of the electron parallel kinetic energy ($W_{\parallel}^{e}$) for m_i/m_e = 100.0, T_e/T_i = 16.0 and ω_0/ω_g = 2.0.*

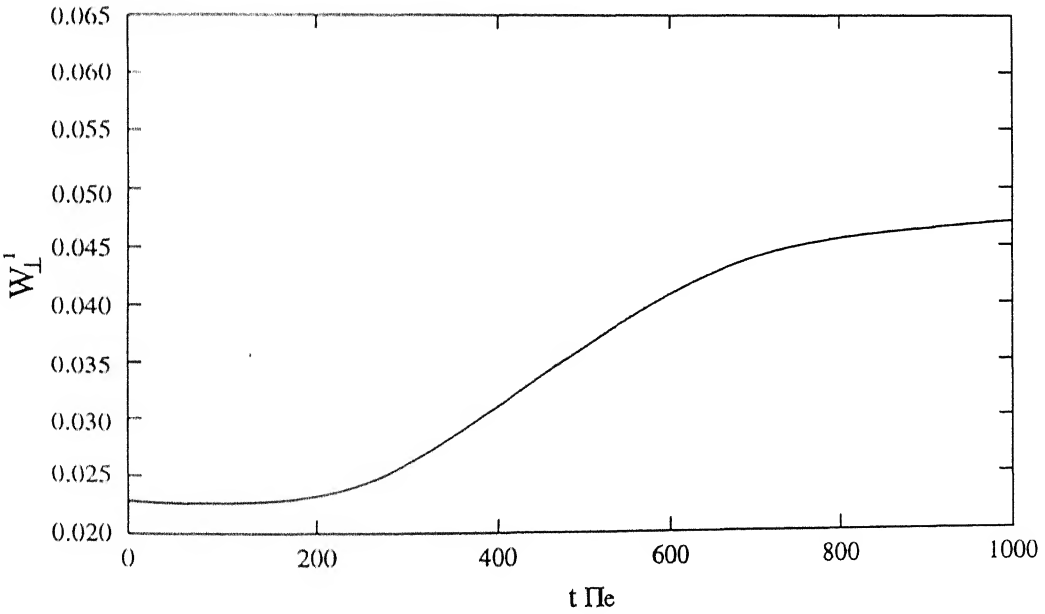

Figure 4.8: *(set II) Time evolution of the ion perpendicular kinetic energy ($W_{\perp}^{i}$) for m_i/m_e = 100.0, T_e/T_i = 16.0 and $\omega_0/\omega_g = 2.0$.*

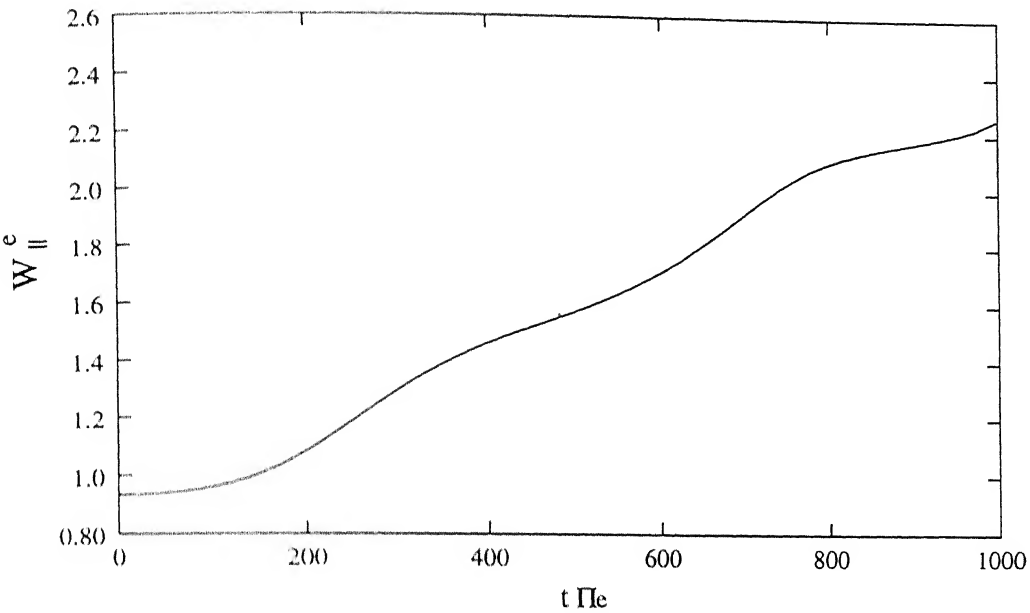

Figure 4.9: *(set III) Time evolution of the electron parallel kinetic energy* ($W_{\parallel}^{e}$) *for* $m_i/m_e = 100.0$ *and* $T_e/T_i = 16.0$.

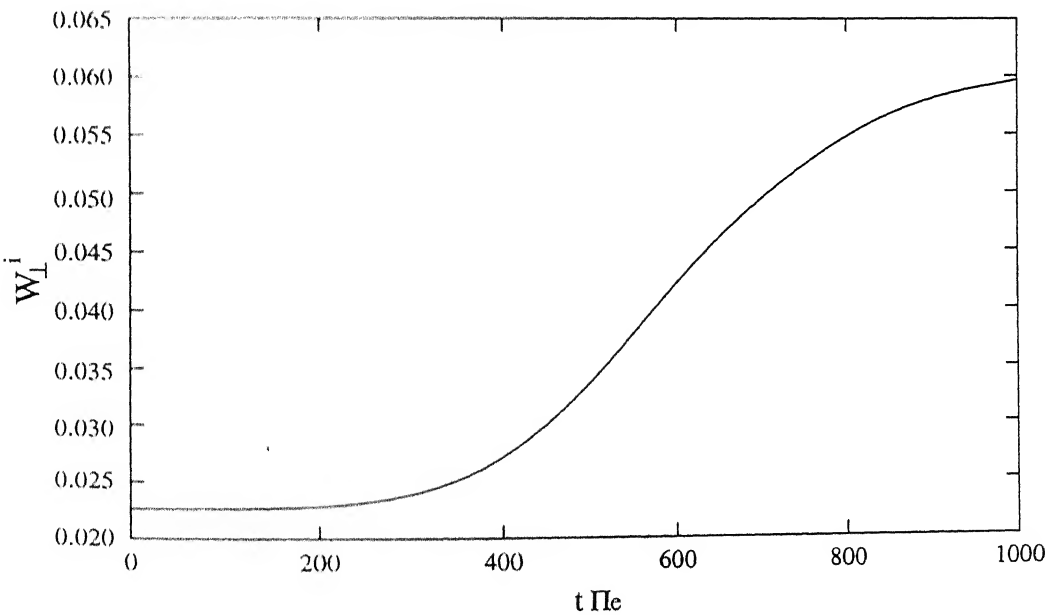

Figure 4.10: *(set III) Time evolution of the ion perpendicular kinetic energy* ($W_{\perp}^{i}$) *for* $m_i/m_e = 100.0$ *and* $T_e/T_i = 16.0$.

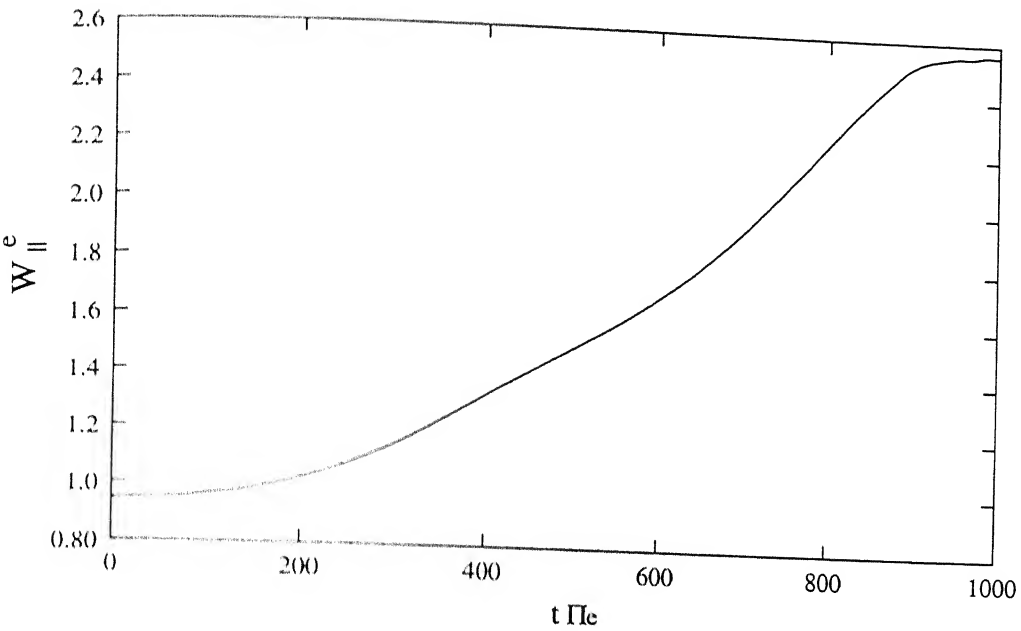

Figure 4.11: *(set III) Time evolution of the electron parallel kinetic energy* ($W^e_{\parallel}$) *for* $m_i/m_e = 100.0$ *and* $T_e/T_i = 100.0$.

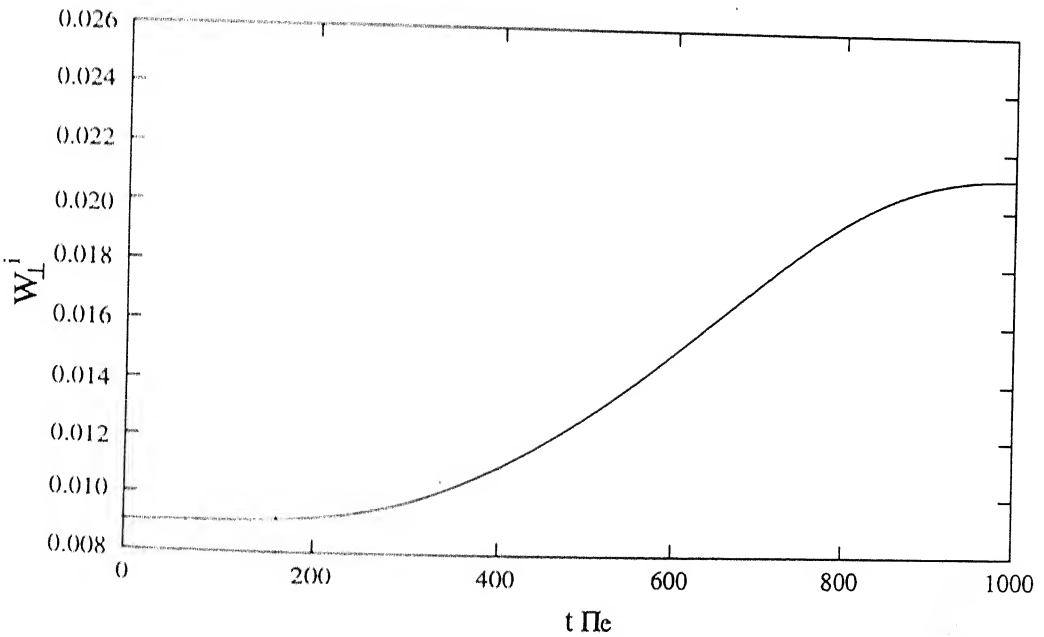

Figure 4.12: *(set III) Time evolution of the ion perpendicular kinetic energy* ($W^i_{\perp}$) *for* $m_i/m_e = 100.0$ *and* $T_e/T_i = 100.0$.

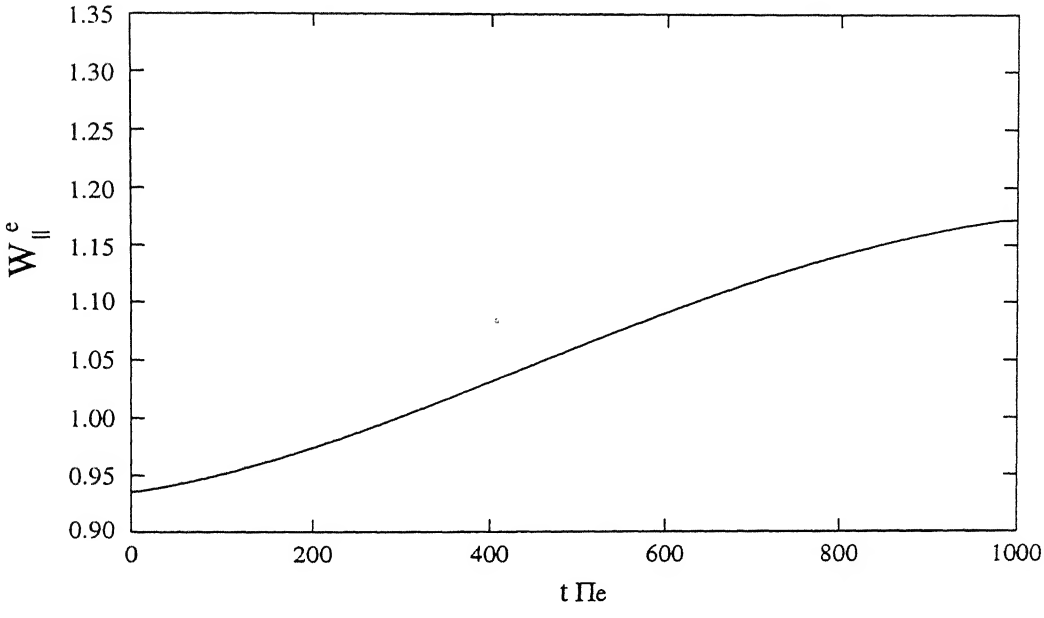

Figure 4.13: *(set IV) Time evolution of the electron parallel kinetic energy ($W_{\|}^{e}$) for a small external static magnetic field* $\mathbf{B}_0$.

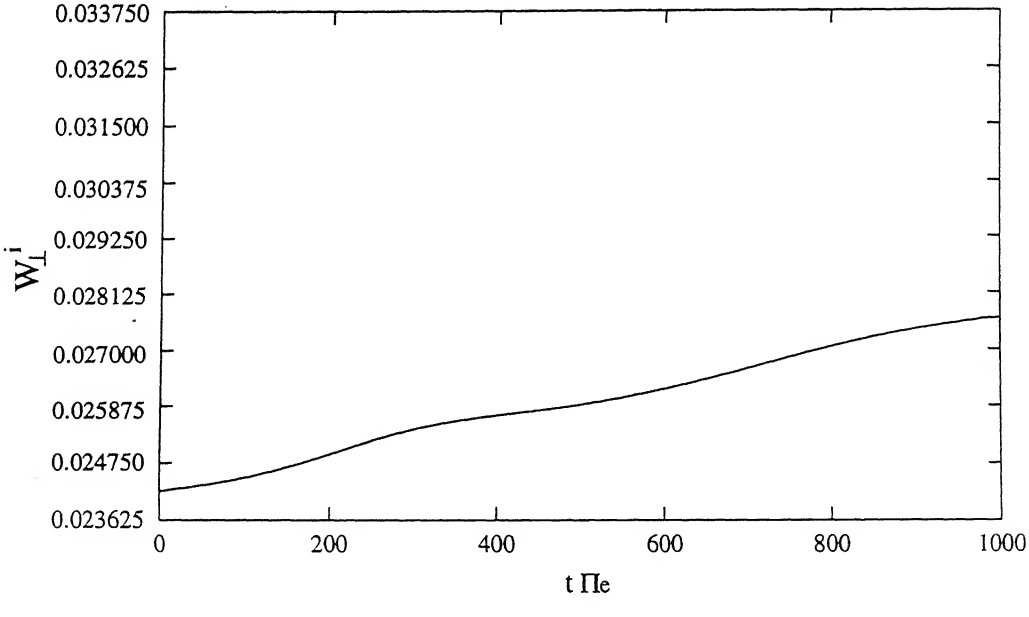

Figure 4.14: *(set IV) Time evolution of the ion perpendicular kinetic energy ($W_{\perp}^{i}$) for a small external static magnetic field* $\mathbf{B}_0$.

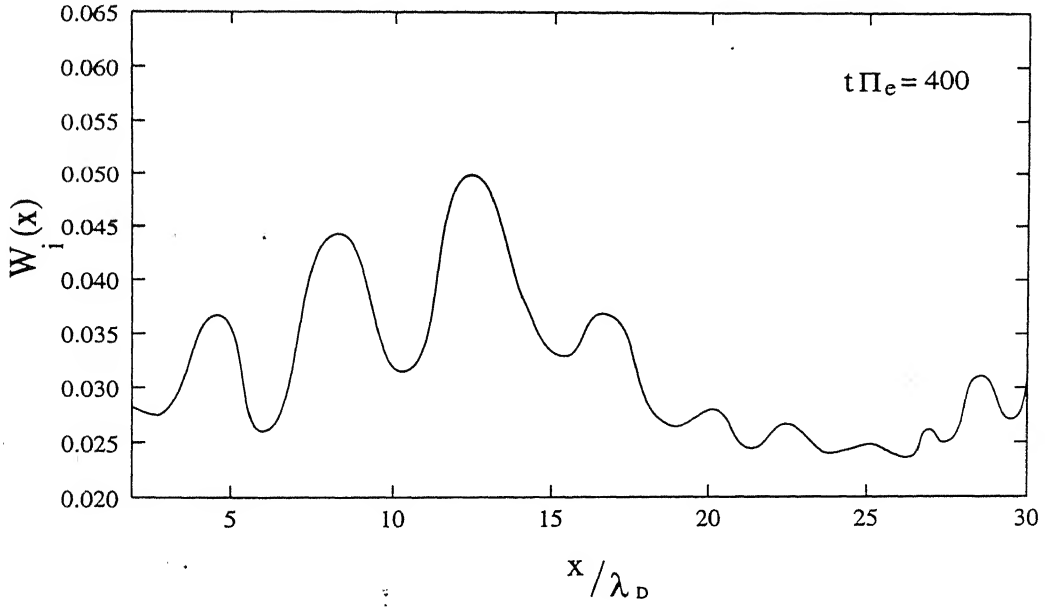

Figure 4.15: *(set V)Spatial dependence of ion kinetic energy perpendicular to magnitic field at 400^{th} (source at $x = 0$).*

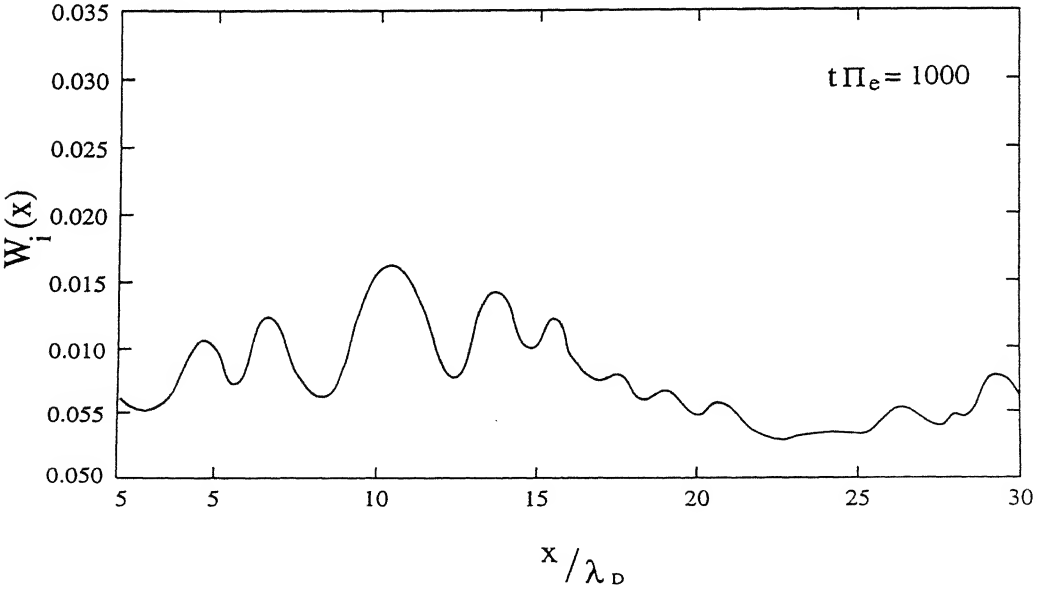

Figure 4.16: *(set V)Spatial dependence of ion kinetic energy perpendicular to magnitic field at 600^{th} time iteration (source at $x = 0$).*

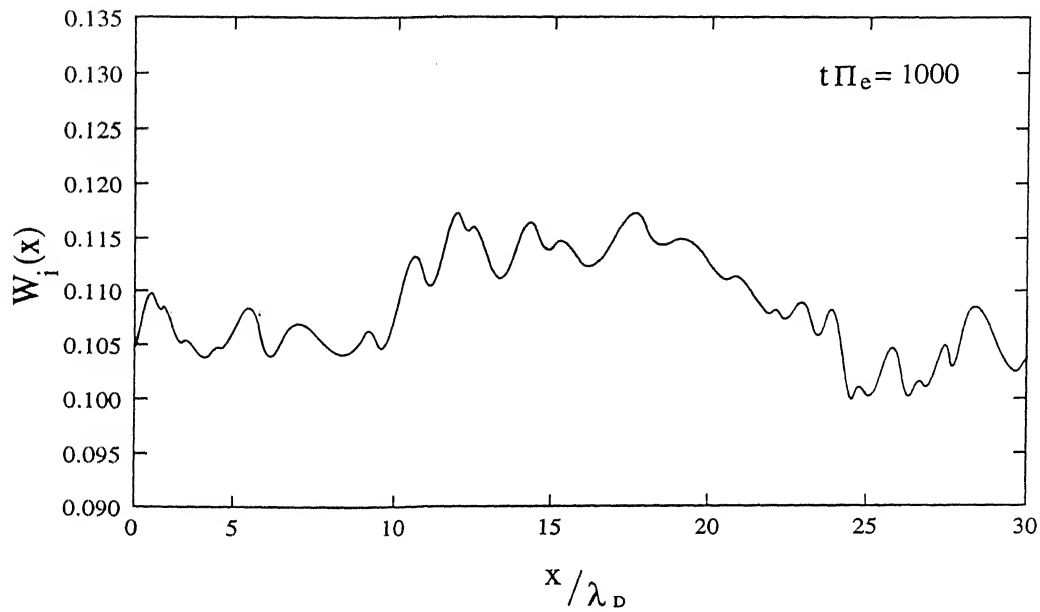

Figure 4.17: *(set V)Spatial dependence of ion kinetic energy perpendicular to magnitic field at 1000^{th} time iteration (source at $x = 0$).*

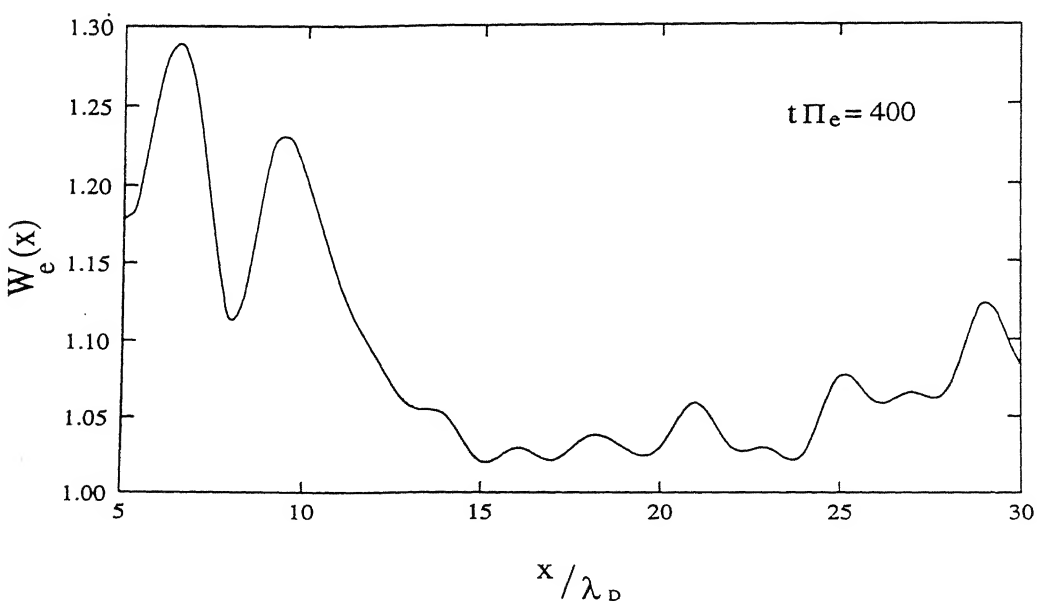

Figure 4.18: *(set V)Spatial dependence of electron kinetic energy parallel to magnitic field at 400^{th} time iteration (source at $x = 0$).*

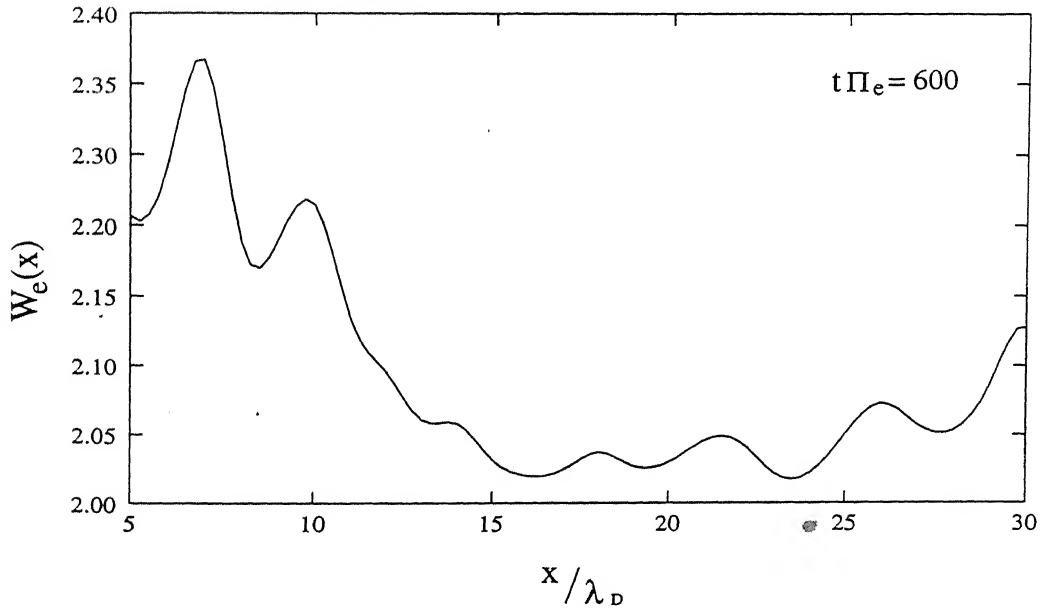

Figure 4.19: *(set V)Spatial dependence of ion kinetic energy perpendicular to magnitic field at 1000^{th} time iteration (source at $x = 0$).*

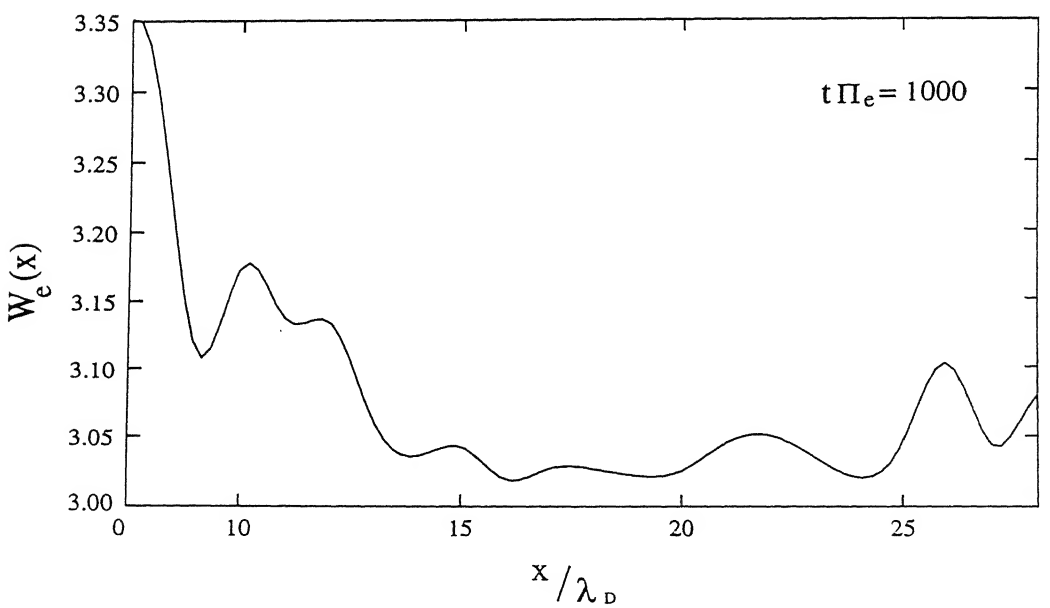

Figure 4.20: *(set V)Spatial dependence of electron kinetic energy parallel to magnitic field at 400^{th} time iteration (source at $x = 0$).*

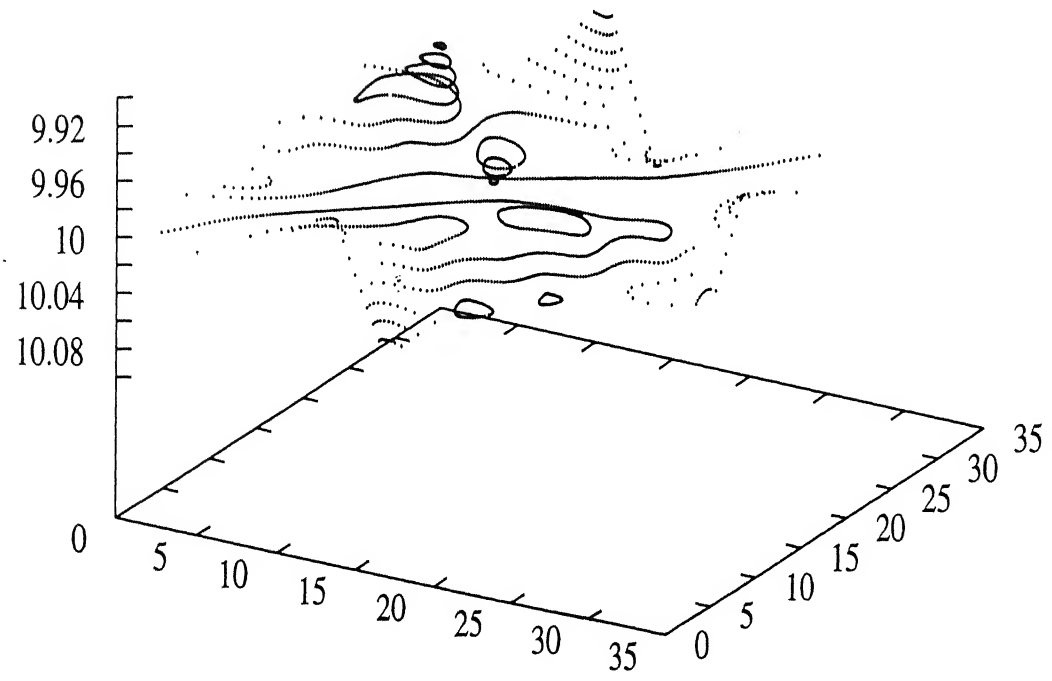

Figure 4.21: *Phase-space plots (isometric projection) for parallel velocity component of electrons at* $t\Pi_e = 400$

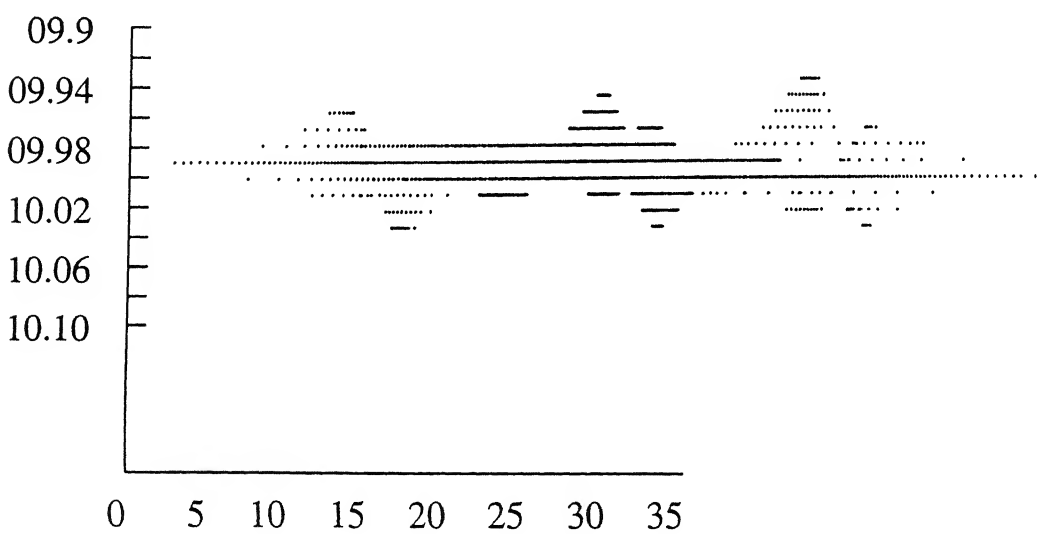

Figure 4.22: *Phase-space plots (orthographic projecion) for parallel velocity component of electrons at* $t\Pi_e = 400$

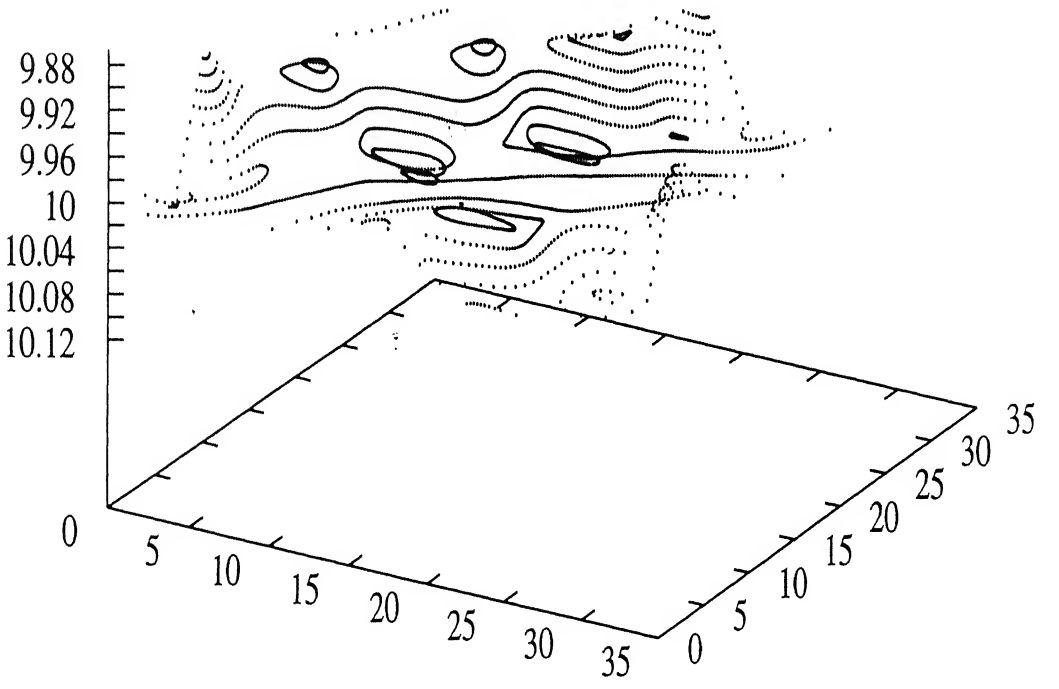

Figure 4.23: *Phase-space plots (isometric projection) for parallel velocity component of electrons at* $t\Pi_e = 800$

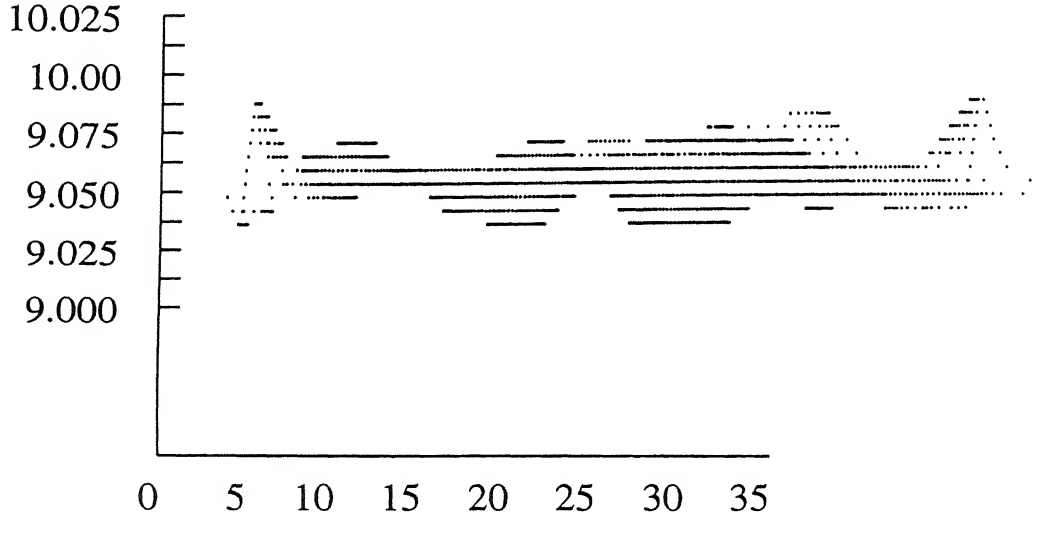

Figure 4.24: *Phase-space plots (orthographic projecion) for parallel velocity component of electrons at* $t\Pi_e = 800$

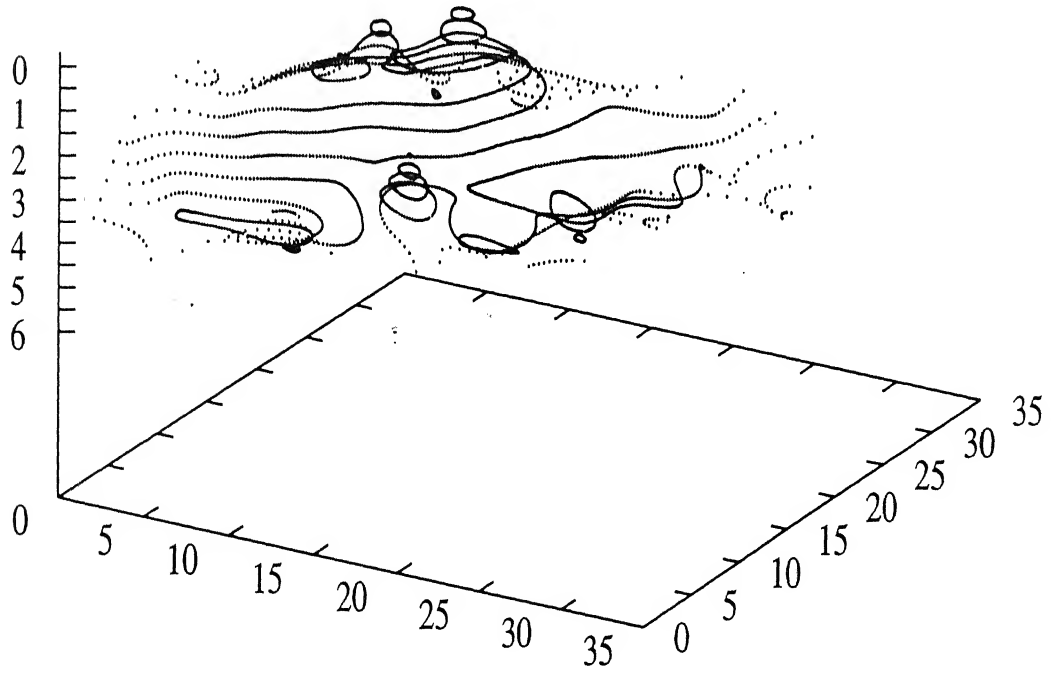

Figure 4.25: *Phase-space plots (isometric projecion) for perpendicular velocity component of ions at* $t\Pi_e = 400$

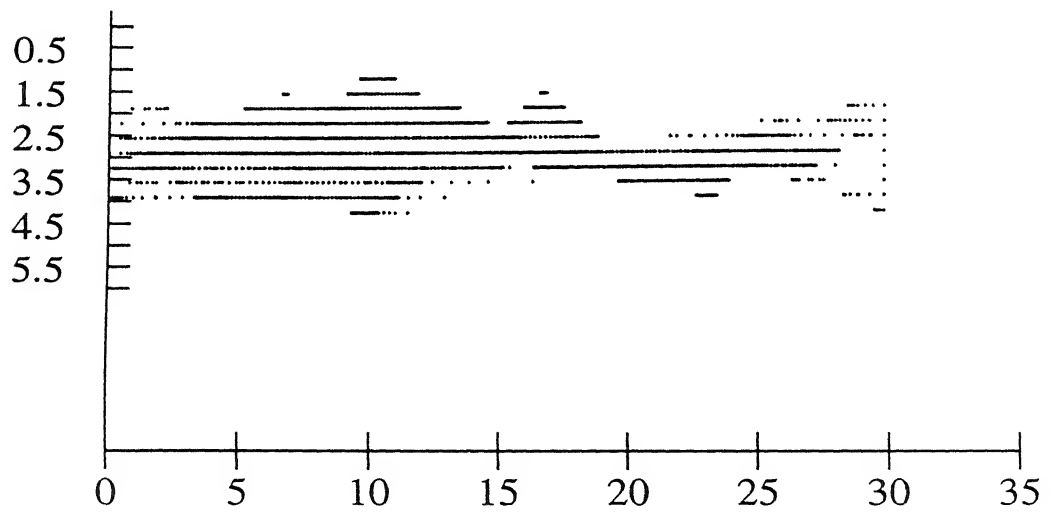

Figure 4.26: *Phase-space plots (orthographic projecion) for perpendicular velocity component of ions at* $t\Pi_e = 400$

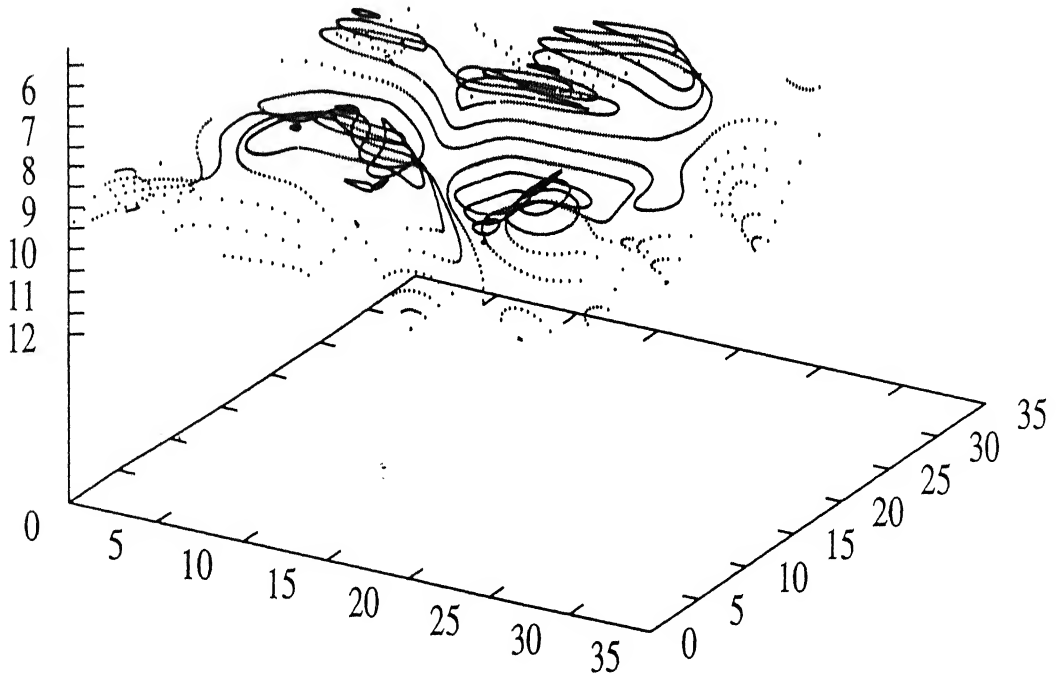

Figure 4.27: *Phase-space plots (isometric projecion) for perpendicular velocity component of ions at* $t\Pi_e = 800$

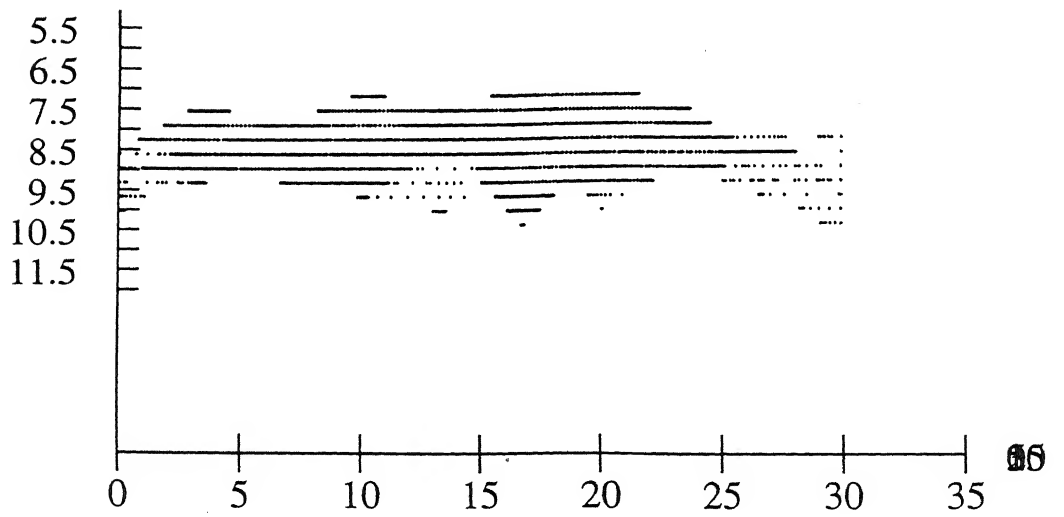

Figure 4.28: *Phase-space plots (orthographic projecion) for perpendicular velocity component of ions at* $t\Pi_e = 800$

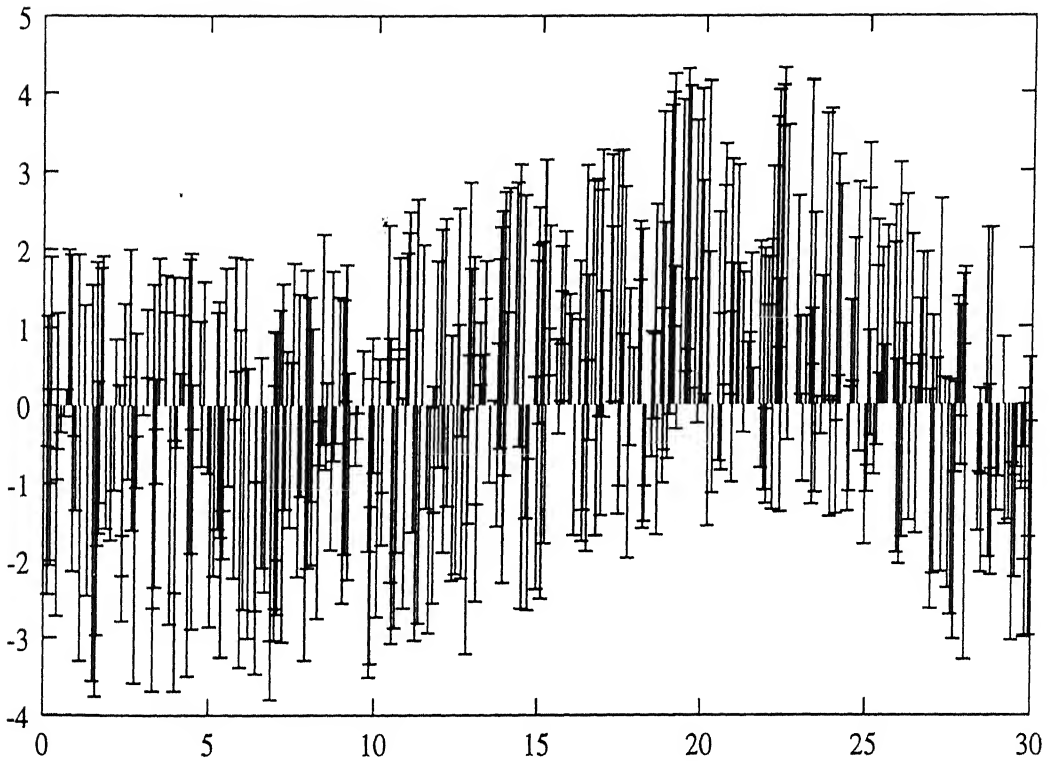

Figure 4.29: *$Y - V_y$ phase-space plots for perpendicular velocity component of ions at* $t\Pi_e = 800$

Chapter 5

Conclusions

With refrence to the results discussed in the previous chapter, following conclusions can be drawn:

1. Transformation of forward travelling 'E' wave into a plasma wave is necessary for heating the plasma. Continuous transformation of the electromagnetic 'E' wave into a plasma wave occurs only when the magnetic field exceeds a critical value.

2. Surface electron heating is observed which implies that the separation of the electromagnetic wave takes place at the lower density, as predicted. The 'E' wave having higher refractive index penetrates into the plasma, while, the 'H' wave is absorbed at the surface. Electrons having higher thermal speeds are responsible for damping of this wave, which results in electron surface heating.

3. As the resonant on heating is observed to take place after some plasma periods (i.e., almost after $t\Pi_e > 200$), it can be concluded that the heating is because of the resonance that takes place between the reflected electromagnetic wave and ions. This implies that a sufficient deceleration

of the electromagnetic wave is required so that the wave phase velocity almost matches the ion thermal speed.

4. It is observed that the transformation of lower hybrid waves to plasma waves is temperature dependent. The efficiency of the transformation is observed to decrease with increase in electron temperature.

This method of heating plasma near the plasma surface guarantees an efficient absorption of the plasma wave if an electromagnetic wave (of the electrostatic type) is generated at the plasma surface and sufficiently decelerated along the magnetic field, provided the magnetic field is more than the limit proposed by Glagolev [*Glagolev*(1972b)], and the exciter frequency is almost equal to the ion plasma frequency. Since the transformation condition for the waves depend only weakly on the plasma temperature (i.e., the ion temperature), this method dose not place any practical limitation on the ion temperature.

The electron heating takes place at the surface while the ion heating is observed at the inner regions of the plasma. The presence of the outer hot electron sheath shields out the hot ions from impurities coming from the walls. Moreover, the existance of 'H' waves on the surface skin-layer of plasma exerts a high frequency pressure on the plasma. This can, in particular, be useful in providing the required hydrodynamic stability of the plasma layer.

Appendix A

Algorithms Used in the Code to Solve the Poisson's Equations

Poisson's equation in the following form is used in the code:

$$\nabla^2\phi = -\frac{\rho}{\epsilon_0}. \tag{A.1}$$

One-dimensional case Eqn. A.1 can be written as

$$\frac{d^2\phi}{dx^2} = -\frac{\rho}{\epsilon_0}, \tag{A.2}$$

then, for any grid point 'i' the discretization (center space) is given by

$$\frac{\phi_{i+1} + \phi_{i-1} - 2\phi_i}{\Delta x^2} = -\frac{\rho_i}{\epsilon_0}. \tag{A.3}$$

Two-dimensional case Eqn. A.1 can be written as

$$\frac{\partial^2\phi}{\partial x^2} + \frac{\partial^2\phi}{\partial y^2} = -\frac{\rho}{\epsilon_0}. \tag{A.4}$$

then, for any grid point (i, j) the discretization (center space) is given by

$$\frac{\phi_{i+1,j} + \phi_{i-1,j} - 2\phi_{i,j}}{\Delta x^2} + \frac{\phi_{i,j+1} + \phi_{i,j-1} - 2\phi_{i,j}}{\Delta y^2} = -\frac{\rho_{ij}}{\epsilon_0}. \tag{A.5}$$

For the two cases considered above two different schemes are used. The one-dimensional case is solved by Gauss elimination using Thomas algorithm, while the two-dimensional case is solved using the Gauss-Seidel iterative technique.

A.1 Thomas Algorithm

The equation

$$\frac{d^2\Theta}{dx^2} = r, \tag{A.6}$$

which is of the form given by Eqn. A.2, is discretized by the center space approximation.

$$\frac{\Theta_{i+1} + \Theta_{i-1} - 2\Theta_i}{\Delta x^2} = r_i, \tag{A.7}$$

this discretization can also be written as

$$\frac{1}{\Delta x^2}\Theta_{i-1} - \frac{2}{\Delta x^2}\Theta_i + \frac{1}{\Delta x^2}\Theta_{i+1} = r_i. \tag{A.8}$$

The above equation cannot be applied for the boundary and is solvable only for the interior points. Then, if following is the boundary condition

$$d_1\Theta_1 = r_1,$$

the Eqn. A.8, written for all the grid points $i = 1, \ldots, N-1, N$, gives a set of equations which can be represented in the matrix form as

$$\begin{bmatrix} d_1 & 0 & 0 & 0 & \cdots & 0 \\ b_2 & d_2 & a_2 & 0 & \cdots & 0 \\ 0 & b_3 & d_3 & a_3 & \cdots & 0 \\ \vdots & \vdots & \vdots & \vdots & \ddots & \vdots \\ 0 & 0 & 0 & 0 & \cdots & d_N \end{bmatrix} \begin{bmatrix} \Theta_1 \\ \Theta_2 \\ \Theta_3 \\ \vdots \\ \Theta_N \end{bmatrix} = \begin{bmatrix} r_1 \\ r_2 \\ r_3 \\ \vdots \\ r_N \end{bmatrix}, \tag{A.9}$$

where a, b and d represent above-diagonal, below-diagonal and the diagonal elements of the matrix, respectively. This type of matrix is called a *tridiagonal matrix*. The algorithm used requires $O(N)$ folating point operations as

compared to $O(\frac{1}{3}N^3)$ operations generally required in other algorithms. Thus this technique is computationally very efficient.

The Thomas algorithm is divided into two steps:

1. Forward elimination.
2. Back substituation.

Forward elimination The following set of steps are repeated from $i = 1$ to $i = N - 1$

$$factor = b_{i+1}/d_i \tag{A.10}$$

$$d_{i+1} = d_{i+1} - factor \times a_i \tag{A.11}$$

$$r_{i+1} = r_{i+1} - factor \times r_i \tag{A.12}$$

Back substituation First the value of Θ at $i = N$ is calculated as

$$\Theta_N = r_N/d_n$$

then the following algebraic operation is repeated in a loop running from $i = N - 1$ down to $i = 1$ to calculate the values of rest of the Θ's:

$$\Theta_i = (r_i - a_i \times \Theta_{i+1})/d_i. \tag{A.13}$$

Solving by the above technique, the values Θ at all the grid points can be obtained, provided the initial condition is defined.

A.2 Gauss-Seidel Iterative Technique

Gauss-Seidel iterative technique, also called the GS-SOR (SOR stands for Sucessive Over Relaxation), which begins with a guess solutions and corrects the guess until the system of equations are solved to a sufficient accuracy.

Advantage : It can use the squarity of matrix efficiently (does not generate unecessay work as in Gauss elimination).

Disadvantage : Convergence is not guaranteed for all matrices and the rate of convergence depends on the given matrix; operation count is uncertain.

Consider the following set of equations

$$\begin{aligned} a_{11}x_1 + a_{12}x_2 \cdots + a_{1n}x_n &= b_1, \\ &\vdots \\ a_{n1}x_1 + a_{n2}x_2 \cdots + a_{nn}x_n &= b_n. \end{aligned} \tag{A.14}$$

Make an initial guess for all x_i:

$$\tilde{x}^0 = x_1^0, \cdots, x_n^0. \tag{A.15}$$

Then the new values of x_i are calculated as

$$x_i^{P+1} = x_i^P + r_i/a_{ii}, \tag{A.16}$$

where

$$r_i = \left[b_i - \sum_{j=1}^{i-1} a_{ij}x_j^P - \sum_{j=i+1}^{n} a_{ij}x_j^P \right].$$

r_i is called the *residual* of the t^{th} equation evaluated on the newest values.

The SOR technique involves the acceleration parameter 'ω' such that

$$x_i^{P+1} = x_i^P + \omega r_i/a_{ii}.$$

$1 < \omega \leq 2$ implies *over relaxation* and, $0 < \omega \leq 1$ means *under relaxation*. *Over relaxation* is used to accelerate the solution and *under relaxation* is used when convergence is not achieved by Gauss-Seidel. The algorithm of this technique is as follows:

1. assume an initial geuss for all x_i's,

2. for each x_i, $i = 1$ to N do

$$\begin{aligned} r_i &= b_i - \sum a_{ij} x_j \\ x_i &= x_i + r_i / a_{ii} \end{aligned}$$

3. repeate the above steps till convergence is achieved.

Convergence is given by $\mid RMS \mid \leq error$, where

$$RMS = \sqrt{\frac{\sum_{i=1}^{N} r_i \times r_i}{N}}$$

Convergence Criterion

Convergence is gauranteed only if the matrix has a diagonal dominance, defined as

1. for every row

$$\mid a_{ii} \mid \geq \sum_{j=1}^{n} \mid a_{ij} \mid$$

and $j \neq i$

2. for at least one row

$$\mid a_{ii} \mid > \sum_{j=1}^{n} \mid a_{ij} \mid$$

and $j \neq i$.

These conditions are sufficient conditions for convergence.

Bibliography

[*Abe et al.*(1980)] Abe, H., H. Mamota, R. Itatani, and A. Fukuyama, High energy tail formation by a monochromatic wave in magnetized plasma, *Physics of Fluids*, *23*, 2417, 1980.

[*Alder et al.*(1982)], Alder, B., S. Fernbock, and M. Rotenberg, *Methods in Computational Physics Vol -9 (Plasma Physics)*. Springer-Verlag, New York, 1982.

[*Appert et al.*(1986)] Appert, K., T. Hellstn, O. Sauter, S. Succi, and J. Vaclavik, Computing of rf heating and current drive in tokamak, *Journal of Cmputaional Physica Communications*, *43*, 125–141, Eighth EPS Conf. on Computational Physics – Computing in Plasmas, 1986.

[*Bekefi*(1966)] Bekefi, G., *Radiation Processes in Plasma*. John Wiley, New York, 1966.

[*Birdsall and Fuss*(1969)] Birdsall, C. K., and D. Fuss, The cloud-in-cloud and cloud-in-cell physics for many body simulation, *Journal of Computational Physics*, *3*, 494–511, 1969.

[*Birdsall and Langdon*(1986)] Birdsall, C. K., and A. B. Langdon, *Plasma Physics via Computer Simulation*. McGraw-Hill, New York, 1986.

[*Bonoli*(1983)] Bonoli, P., Linear theory of lower hybrid waves in tokamak plasmas, in *RF Heating and Current Drive in Magnetic Fusion Plasmas, IEEE International Conference on Plasma Science.* Compiled in book *Wave heating and Current Drive in Plasmas*, edited by V. L. Granatstein, etc., 1983.

[*Boris*(1970)] Boris, J. P., Reletevestic plasma simulation optemization of a hybrid code, in *Proceedings of Fourth Conference on Numerical Simulation of Plasmas*, pp. 3–67, Naval Research Lab., Washington D.C. 1970.

[*Brambilla*(1976)] Brambilla, M., Propagation and absorption of waves at lower hybrid reasonance, *Plasma Physics*, *18*, 669–674, 1976.

[*Chu et al.*(1976)] Chu, C., J. M. Dawson, and H. Okuda, Plasma heating at frequencies near lower hybrid, *Physics of Fluids*, *19*, 981–987, 1976.

[*Chu and Lee*(1971)] Chu, T. K., and Y. C. Lee, *Bulletin of American Physics Society*, 1971.

[*Dawson et al.*(1973)] Dawson, J. M., W. L., and B. Rosen, The dipole expanssion methods methods for plasma simulations, *Journal of Computational Physics*, *13*, 114–129, 1973.

[*Decyk*(1986)] Decyk, V. K., Partial simulation of rf heating and current drive, *Computer Physics Reports*, *4*, 245–263, 1986.

[*Decyk et al.*(1979)] Decyk, V. K., J. M. Dawson, and G. J. Morales, Excitation of lower hybrid waves in finite plasma, *Physics of Fluids*, *22*, 507–514, 1979.

[*Decyk et al.*(1980)] Decyk, V. K., G. J. Morales, and J. M. Dawson, Simulaton of lower hybrid heating in non-uniform plasma slab, *Physics of Fluids*, *23*, 826–833, 1980.

[*Dnestrovskii and Kostomarov*(1982)] Dnestrovskii, Y. N., and D. P. Kostomarov, *Numerical Simulation of Plasmas*. Springer-Verlag, New York, 1982.

[*Drecier et al.*(1971)] Drecier, H., D. B. Henderson, and J. C. Ingraham, Anamalous micro-wave absorption near plasma freqency, *Physical Review Letters*, *26*, 1616–1620, 1971.

[*DuBois and Goldman*(1967)] DuBois, D. F., and M. Goldman, Parametrically exited plasma fluctuations, *Physical Review*, *164*, 207–222, 1967.

[*Eklund*(1980)] Eklund, S., Twenty years of nuclear fusion. an overview of highlights in the evolution of controlled nuclear fusion research, *Nuclear Fusion*, *20*, 1980.

[*Glagolev*(1972a)] Glagolev, V. M., Propagation and absorption of ion hybrid waves in a weakly inhomogeneous plasma layer - I, *Plasma Physics*, *14*, 301–314, 1972a.

[*Glagolev*(1972b)] Glagolev, V. M., Propagation and absorption of ion hybrid waves in a weakly inhomogeneous plasma layer - II, *Plasma Physics*, *14*, 315–326, 1972b.

[*Harlow*(1964)] Harlow, F. H., The particle-in-cell computing method for fluid dynamics, *Mathematical and computational Physics*, *3*, 319–343, 1964.

[*Hawang and Wilson*(1981)] Hawang, D. H., and J. R. Wilson, Radio freqency wave application in magnetic fusion devices, *Proceedings of the IEEE*, *69*, 1030–1042, 1981.

[*Hook and Bernabai*(1971)] Hook, W. M., and S. Bernabai, *Physical Review Letters*, *28*, 407, Refrence from Kindel et. al., 1971.

[*Jackson*(1967)] Jackson, E. A., Parametric effect of radiation on plasma, *Physical Review*, *153*, 235–244, 1967.

[*Karney*(1978)] Karney, C. F. F., Stochastic ion heating by lower hybrid waves - I, *Physics of Fluids*, *21*, 1584, 1978.

[*Karney*(1979)] Karney, C. F. F., Stochastic ion heating by lower hybrid waves - II, *Physics of Fluids*, *22*, 2188, 1979.

[*Karney*(1986)] Karney, C. F. F., Fokker plank and quasi-linear code, *Computer Physics Reports*, *4*, 183–244, 1986.

[*Kettani and Hoyaux*(1973a)] Kettani, A. M., and M. F. Hoyaux, *Plasma Engineering*. Butterworths, London, 1973a.

[*Kettani and Hoyaux*(1973b)] Kettani, A. M., and M. F. Hoyaux, *Plasma Engineering*. Butterworths, London, 1973b.

[*Kindel et al.*(1972)] Kindel, J. M., H. Okuda, and J. M. Dawson, Parametric instabilities and anamolous heating of plasma near the lower hybrid frequency, *Physical Review Letters*, *29*, 995–997, 1972.

[*Krall and Trivelpiece*(1973)] Krall, N. A., and A. W. Trivelpiece, *Principles of Plasma Physics*. McGraw-Hill, New York, 1973.

[*Lewis*(1970)] Lewis, H. R., Energy conserving numerical approximations for vlasov plasmas, *Journal of Computational Physics*, *6*, 136–141, 1970.

[*Mamota*(1977)] Mamota, H., Radio-frequency heating stationary systems, in *Proceedings of the Workshop on Plasma Physics*, p. 213, Varenna, Italy. Compiled in book *Plasma Transport, Heating and MHD Theoy* , 1977.

[*Matsuda et al.*(1980)] Matsuda, K., Y. Matsuda, and G. E. Guest, Surface heating, density rippling and propagation cones in high power lower hybrid heating, *Physics of Fluids*, *23*, 1422, 1980.

[*Messian and Vandenplas*(1974)] Messian, A. M., and P. E. N. Vandenplas, Radio-frequency heating of large thermonuclear tori, in *Plasma Physics and controlled Nuclear Fusion Research*, p. 319, Tokyo, Japan. 1974.

[*Montgomery and Tidman*(1964)] Montgomery, D. C., and D. A. Tidman, *Plasma Kinetic Theory*. McGraw-Hill, New York, 1964.

[*Musil and Zacek*(1974)] Musil, J., and F. Zacek, Anomalous absorption of intense electromagnetic waves in plasma at high magnetic fields, *Plasma Physics*, *16*, 735–739, 1974.

[*Nakajima et al.*(1982)] Nakajima, N., H. Abe, and R. Itatani, Energy and momentum deposition in plasma due to the lower hybrid waves by finite source, *Physics of Fluids*, *25*, 2234, 1982.

[*Ott and McBride*(1972)] Ott, E., and J. B. McBride, Streaming instabilities and anomalous heating in plasma, in *1st Topical Conference on R.F heating of Plasma*, p. Paper A4, Lubbock, Texas. 1972.

[*Piliya*(1977)] Piliya, A. D., Radio-frequency heating stationary systems, in *Proceedings of the Workshop on Plasma Physics*, p. 203, Varenna, Italy. Compiled in book *Plasma Transport, Heating and MHD Theoy* , 1977.

[*Raimbault and Shohet*(1975)] Raimbault, P. A., and J. L. Shohet, Lower hybrid reasonance heating in a hot electron plasma, *Plasma Physics*, *17*, 327–344, 1975.

[*Stix*(1962)] Stix, T. H., *Theory of Plasma Waves*. McGraw–Hill, New York, 1962.

[*Stix*(1965)] Stix, T. H., Radiation and absorption via mode conversion in an inhomogenous collision-free plasma, *Physical Review Letters*, *15*, 878–882, 1965.

[*Takamura and Okuda*(1975)] Takamura, S., and T. Okuda, Heating of highly ionized plasma in the lower hybrid frequency range, *Plasma Physics*, *17*, 435–445, 1975.

[*Wong and Tang*(1976)] Wong, K. C., and T.-W. Tang, Rf coupling and mode conversions at the lower hybrid resonance, *Plasma Physics*, *18*, 921–928, 1976.